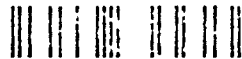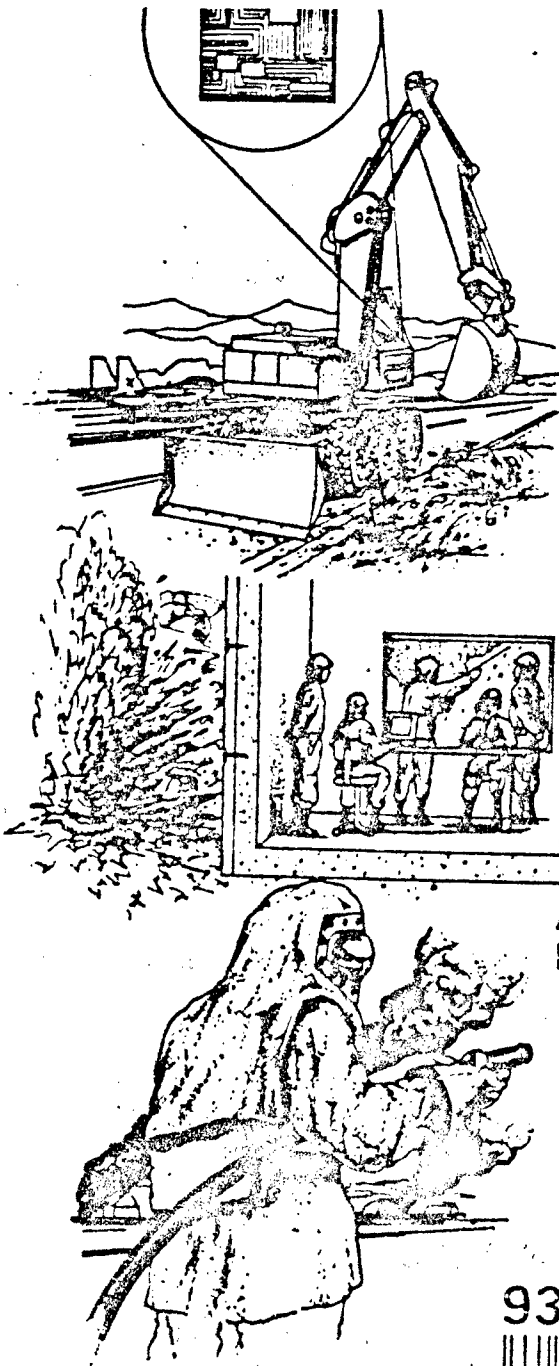AD-A273 704

ESL-TR-92-76

ADVANCED PANEL AND CONNECTION SYSTEM FOR REINFORCED SOIL

C. Y. TUAN, D. H. MERKLE

APPLIED RESEARCH ASSOCIATES, INC.
2101 SAN MATEO BLVD. NE, SUITE A220
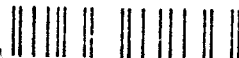ALBUQUERQUE NM 871110

MARCH 1993

FINAL REPORT

FEBRUARY 1991 - NOVEMBER 1992

APPROVED FOR PUBLIC RELEASE:
DISTRIBUTION UNLIMITED

DTIC
ELECTE
DEC 15
S
E

93-30290

93 12 14 041

REPORT DOCUMENTATION PAGE

1. AGENCY USE ONLY (Leave blank)	2. REPORT DATE March 1993	3. REPORT TYPE AND DATES COVERED Final report; From 91 02 To 92 11

4. TITLE AND SUBTITLE

Advanced Panel and Connection System for Reinforced Soil

5. FUNDING NUMBERS

F08635-88-C-0067

6. AUTHOR(S)

Tuan, C.Y.; Merkle, D.H.

7. PERFORMING ORGANIZATION NAME(S) AND ADDRESS(ES)

Applied Research Associates, Inc.
2101 San Mateo Blvd. NE, Suite A220
Albuquerque, NM 87110

8. PERFORMING ORGANIZATION REPORT NUMBER

9. SPONSORING / MONITORING AGENCY NAME(S) AND ADDRESS(ES)

U. S. Air Force Civil Engineering Support Agency
Tyndall Air Force Base, FL 32403-6001

10. SPONSORING / MONITORING AGENCY REPORT NUMBER

ESL-TR-92-76

11. SUPPLEMENTARY NOTES

12a. DISTRIBUTION / AVAILABILITY STATEMENT

This report has been reviewed by the Public Affairs Office
and is releasable to the National Technical Information
Service (NTIS). At NTIS, it will be available to general
public, including foreign nations.

12b. DISTRIBUTION CODE

13. ABSTRACT (Maximum 200 words)

The objective of this effort is to develop a dynamic reinforced soil design method that characterizes shock wave propagation through reinforced soil and the dynamic interaction with modular wall panel sections, and use this method to prepare a preliminary design for an anchored wall panel and soil-reinforcing system for an airbase protective shelter. Mathematical and finite element models were used for parametric studies to provide design guidance. Based on the results of extensive numerical analyses, a step-by-step procedure has been proposed for designing a reinforced soil and modular wall panel connection system to withstand the ground shock from a buried explosion. The design procedure consists of six major steps: (1) determine the geogrid volume ratio in the reinforced soil; (2) determine the peak value and time decay rate of the free-field normal stress in the reinforced soil due to a given explosion; (3) conduct limit analyses of the maximum pull-out resistance of the soil reinforcement; (4) conduct limit analyses of the maximum resistance of wall panel shear connectors; (5) determine the maximum wall panel displacement due to the given threat; and (6) design against breaching of a reinforced concrete wall panel. The preliminary design of an anchored wall panel and soil reinforcing system using this proposed procedure is illustrated in this report.

14. SUBJECT TERMS

Finite element models, Ground shock, Protective structures, Reinforced soil, Structural dynamics

15. NUMBER OF PAGES

106

16. PRICE CODE

17. SECURITY CLASSIFICATION OF REPORT	18. SECURITY CLASSIFICATION OF THIS PAGE	19. SECURITY CLASSIFICATION OF ABSTRACT	20. LIMITATION OF ABSTRACT
UNCLASSIFIED	UNCLASSIFIED	UNCLASSIFIED	UL

DTIC QUALITY INSPECTED 1

EXECUTIVE SUMMARY

A. OBJECTIVE

The objective of this effort is to develop a dynamic reinforced soil design method that characterizes shock wave propagation through reinforced soil and the dynamic interaction with modular wall panel sections, and use this method to prepare a preliminary design for an anchored wall panel and soil-reinforcing system for an airbase protective shelter.

B. BACKGROUND

Protective shelters for military applications are traditionally constructed with reinforced concrete. Most current hardened aircraft shelters are heavily reinforced, cast-in-place concrete barrel-vault structures. These types of construction are expensive, time consuming, and require skilled labor, equipment and large quantities of construction materials that may not be available on site. Therefore, it is not compatible with the US Air Force's Global Reach/Global Power concept of quickly constructing hardened aircraft shelters at colocated operating bases, using military personnel for labor.

The use of prefabricated, high-strength modular roof and wall panels, along with reinforced soil, will allow these shelter components to be pre-positioned in theater and rapidly erected by civil engineering labor as the need arises. Using modular wall panels anchored to a soil backfill reinforced with geosynthetics for hardened shelter construction could reduce construction cost by at least 30 percent, as opposed to the use of reinforced concrete. Over 80 percent of the volume of these shelters is soil, minimizing logistical demands for the construction. Furthermore, damage to the shelter from airblast and ground shock would be localized due to the modular wall construction. Thus, expedient repair methods can be applied to these prefabricated reinforced soil shelter facilities with little difficulty. It is expected that this innovative construction technique will increase the survivability of airbase shelters, while reducing construction and maintenance costs.

C. SCOPE

The scope of this effort included: (1) defining requirements for the airbase protective shelter anchored wall panel and soil reinforcing system to be designed; (2) a comprehensive review of the engineering literature and current research related to design of reinforced soil and anchored wall panels, with emphasis on dynamic loads; (3) airbase protective shelter anchored wall panel and soil reinforcing system design concept definition, screening, evaluation, and selection; (4) developing a mathematical model for explosive ground shock response of the selected anchored wall panel and soil reinforcing system design concept; (5) determining numerical values for the parameters of the developed mathematical model; (6) developing a computational procedure, using the developed mathematical model; (7) selecting or developing a computer code using the developed computational procedure; (8) performing parametric calculations to support development of a preliminary design method; (9) analyzing calculational results and developing a preliminary design method; and (10) executing a preliminary design satisfying the defined requirements, using the selected design concept and developed design method.

D. METHODOLOGY

Mathematical and finite-element models were developed to characterize shock wave propagation through reinforced soil and the dynamic interaction with modular wall panel sections. These models were used for parametric studies to provide design guidance.

E. TEST DESCRIPTION

No field or laboratory tests were conducted under this effort.

F. RESULTS

Based on the results of extensive numerical analyses, a step-by-step procedure has been proposed for designing a reinforced soil and modular wall panel connection system to withstand the ground shock from a buried explosion. The design procedure consists of six major steps: (1) determine the geogrid volume ratio in the reinforced soil; (2) determine the peak value and time decay rate of the free-field normal stress in the reinforced soil due to a given explosion; (3) conduct limit analyses of the maximum pull-out resistance of the soil

reinforcement; (4) conduct limit analyses of the maximum resistance of wall panel shear connectors; (5) determine the maximum wall panel displacement due to the given threat; and (6) design against breaching of a reinforced concrete wall panel. The preliminary design of an anchored wall panel and soil reinforcing system uses this proposed procedure. The design procedure is based on the "limit state" concept, which requires determination of the peak ground shock loading as well as the ultimate resistance of the structural system.

Three-dimensional (3D) finite element analyses using SAP90^{TM} were conducted to study the geometric effects of different wall panel configurations on the structural behavior of the connection system. Rectangular and hexagonal wall panels commonly used in highway construction, and a "masonry wall" type of construction were studied in detail. It was concluded that using 4-foot wide, 2-foot high, 8-inch thick wall panels or blocks, arranged in a masonry wall configuration, would minimize the joint forces and consequently maximize the wall's survivability.

G. CONCLUSIONS

Due to the impulsive nature of ground shock, the maximum response of the wall panel and reinforced soil system depends mainly on the capacity and rate of energy absorption and dissipation of the system. Therefore, the connection between wall panels and soil reinforcement and the soil reinforcement itself should be ductile beyond the proportional limit. Furthermore, the soil reinforcement should possess a high elastic tensile modulus to minimize the wall panel displacement.

H. RECOMMENDATIONS

The simplified design procedure proposed herein for a modular wall panel and reinforced soil connection system should be validated by conducting full-scale explosive tests or small-scale centrifuge tests. The design parameters to be varied in the tests should include panel geometry, geogrid mechanical properties, and shear connector design. These tests should be fully instrumented to provide data for design guidance. The transducers should include free-field pressure gages in soil, strain (or stress) gages on the geogrid, interface stress gages on wall panels, accelerometers on wall panels, and LVDT's to measure instantaneous as well as permanent displacement of wall panels.
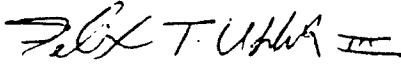
PREFACE

This report was prepared by Applied Research Associates, Inc., under Scientific and Engineering Technical Assistance (SETA) contract F08635-88-C-0067 with the Air Force Civil Engineering Support Agency, Engineering Research Division, (AFCESA/RAC). The work was performed between February 1991 and November 1992 as part of SETA Subtask 2.14, "Advanced Panel and Connection System for an Airbase Protective Shelter Employing Reinforced Earth."
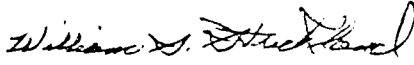
The project was initiated by Mr. William S. Strickland, Chief of the Airbase Survivability Branch. Major Jacob Gheriani of the Israeli Air Force was the Air Force Project Officer from February 1991 to August 1992, and Major Dan Shenbach of the Israeli Air Force was the Air Force Project Officer from September 1992 to November 1992.

This report has been reviewed by the Public Affairs Office and is releasable to the National Technical Information Service (NTIS). At NTIS, it will be available to the general public, including foreign nations.

This technical report has been reviewed and is approved for publication.

DAN SHENBACH, Maj, IAF
Project Officer

FELIX T. UHLIK, III, Lt Col, USAF
Chief, Airbase Systems Branch

WILLIAM S. STRICKLAND
Chief, Airbase Survivability Section

TABLE OF CONTENTS

x

LIST OF FIGURES

xiii

LIST OF TABLES

(The Reverse of this Page is Blank.)

SECTION I

INTRODUCTION

A. OBJECTIVE

The objective of this effort is to develop a dynamic reinforced-soil analysis method that characterizes shock wave propagation through reinforced soil and the dynamic interaction with modular wall panel sections, and use this method to prepare a preliminary design of an anchored wall panel and soil reinforcing system for an airbase protective shelter.

B. BACKGROUND

Protective shelters for military applications are traditionally constructed with reinforced concrete. For instance, most current hardened aircraft shelters are heavily reinforced, cast-in-place concrete barrel vault structures. There are three basic designs: (1) first generation (TAB-VEE and modified TAB-VEE), (2) second generation, and (3) third generation. All three designs are cast-in-place reinforced concrete arches with corrugated steel inner liners, but they differ in the arch span, height, overall length, and door and exhaust port design. The TAB-VEE shelter is a semi-circular arch with a span of 48 feet, a height of 24 feet, and a length of 100 feet. The doors are clamshell-shaped armor steel, hinged on a concrete collar recessed about 20 feet in from the front opening. The modified TAB-VEE door is also clamshell-shaped. However, the door halves are welded together and placed in front of the arch opening, rolling sideways for access. The second and third generation shelters are both double-radius arches, the major difference being the arch span (82 feet for the second generation and 72 feet for the third generation). The height and length are 28 and 120 feet, respectively. The two reinforced concrete doors roll sideways, and are supported by steel trusses that form an outrigger for stability. This type of construction is expensive, time-consuming, and requires skilled labor, equipment and large quantities of construction materials that may not be available on site. Therefore, it is not compatible with the US Air Force's Global Reach/Global Power concept of quickly constructing hardened aircraft shelters at colocated operating bases, using military personnel for labor.

The use of prefabricated, high-strength, modular roof and wall panels, along with reinforced soil, will allow these shelter components to be pre-positioned in-theater and rapidly erected by

1

civil engineering labor as the need arises. Using modular wall panels anchored to a soil backfill reinforced with geosynthetics for hardened shelter construction could reduce construction cost by at least thirty percent, as opposed to using reinforced concrete. Over 80 percent of the volume of these shelters is soil, thus minimizing logistical demands for construction. Furthermore, damage to the shelter from airblast and ground shock would be localized due to the modular wall construction. Thus, expedient repair methods can be applied to these prefabricated, reinforced soil shelter facilities with little difficulty. It is expected that this innovative construction technique will increase the survivability of airbase shelters, while at the same time reducing construction and maintenance costs.

C. SCOPE

The scope of this effort included: (1) defining requirements for the airbase protective shelter anchored wall panel and soil reinforcing system to be designed; (2) a comprehensive review of the engineering literature and current research related to design of reinforced soil and anchored wall panels, with emphasis on dynamic loads; (3) airbase protective shelter anchored wall panel and soil reinforcing system design concept definition, screening, evaluation, and selection; (4) developing a mathematical model for explosive ground shock response of the selected anchored wall panel and soil reinforcing system design concept; (5) determining numerical values for the parameters of the developed mathematical model; (6) developing a computational procedure, using the developed mathematical model; (7) selecting or developing a computer code using the developed computational procedure; (8) performing parametric calculations to support development of a preliminary design method; (9) analyzing calculational results and developing a preliminary design method; and (10) executing a preliminary design satisfying the defined requirements, using the selected design concept and developed design method.

2

SECTION II

LITERATURE REVIEW

A comprehensive review of the engineering literature and current research related to the design of reinforced soil and anchored wall panels, particularly for dynamic loads, has been conducted. Because of the large amount of technical information reviewed, the information is summarized under four categories: constitutive modeling and experiments, static analysis and design, dynamic behavior, and analytical and numerical modeling of reinforced soil.

A. CONSTITUTIVE MODELING AND EXPERIMENTS

One of the first examinations of the equivalent elastic properties of an "apparently homogeneous" reinforced soil medium was undertaken by Westergaard(1938). He assumed that a soft soil medium was reinforced by many thin horizontal layers of unstretchable sheets. Salamon(1968) related the elastic properties of the equivalent homogeneous material to those of its separate isotropic layers. Thus, the equivalent material is "cross-anisotropic" with a vertical axis of symmetry. Harrison and Gerrard(1972) studied the variation of the equivalent material properties due to limiting conditions, using Salamon's equations. They found that, for the Westergaard material, three of the five cross-anisotropic parameters are independent, and that, for the general material, four are independent. For both materials, the Poisson's ratio of the reinforcement has limited influence in determining the equivalent properties and the stress-deformation response of the materials. Gerrard(1982) later derived the elastic properties of an equivalent homogeneous material representing a soil mass reinforced by a series of parallel, equally spaced sheets in a single set or in two or three orthogonal sets.

Yang(1972) conducted triaxial tests to investigate the deformation and strength characteristics of sand reinforced with fiberglass nets. The results showed that the deformation modulus of reinforced sand was higher than that of the unreinforced sand, and that the strength of the reinforced sand could increase by several hundred percent, so that the applied deviator stress cannot fail the specimen without causing tensile failure in the reinforcement or crushing of the soil grains. Haliburton, et al.(1978) tested 27 commercially available geotextiles for tensile strength, creep behavior, soil-fabric frictional resistance, and the effects of immersion and water absorption on the developed tensile strength. Tumay, et al.(1979) conducted dry sand model retaining wall

3

tests to compare the performance of metal and non-woven fiber fabric reinforcement. He concluded that fiber fabric has advantages over metal reinforcement. Williams and Houlihan(1987) conducted experiments using a direct shear friction device, to evaluate the interface friction properties between seven soils and five geosynthetics. The results showed three primary modes of failure: sliding between the soil and the geosynthetic, sliding on a failure surface in the soil, and sliding between multiple layers of geosynthetics. All the tests were conducted at a constant strain rate, which was varied from 0.0001 to 0.01 in/min. The shear stress built up slowly until a peak shear stress was reached, at which point sliding occurred at a constant rate of strain along the weakest plane in the system. The slow stress buildup in the system made it possible to determine the peak stress, which corresponded to the static coefficient of friction, and the residual stress, which corresponded to the dynamic coefficient of friction. The results of friction analyses showed a wide range of variation of the dynamic coefficient of friction: from 0.26 between a sandy soil with 5% clay and a high-density polyethylene, to 0.99 between a Gulf Coast clay and a non-woven, continuous filament, polyester geotextile. O'Rourke, et al.(1990) summarized the results of over 450 direct shear tests on sand-polymer interfaces. The shear strength characteristics of a polymer interface can be conveniently expressed as the ratio of the interface friction angle and the direct shear soil friction angle.

Jewell, et al.(1984) identified three interaction mechanisms for soil and grid reinforcement. Theoretical expressions were developed to describe direct sliding resistance, bearing stress, and reinforcement bond strength, in terms of soil and reinforcement parameters.

Wu(1991) critically studied existing test methods for measuring geotextile load-extension properties when subjected to soil confining stress. He pointed out that, under most conditions, geotextiles deform with the confining soil, without inducing soil-geotextile interface adhesion. He also proposed a new test method, which measures the confined stiffness and strength of a geotextile independently of the reinforced-soil test specimen. The stiffness and strength obtained from this method are conservative if interface slippage occurs.

Ingold(1983) conducted undrained triaxial tests on fully or partially saturated clay with impermeable reinforcement and on saturated clay with permeable reinforcement. Results showed all failures were bond failures. Ingold and Miller(1983) conducted drained triaxial compression tests on reinforced clay. Their radiographic results showed that strength enhancement is due to

radial strain constraint, arising from shear stresses mobilized on the soil-reinforcement interface. A theoretical model was also proposed to predict this behavior.

Sawicki(1983) developed a rigid plastic model for the plastic behavior of soil unidirectionally reinforced by fibers. The soil is assumed to be a perfectly plastic Mohr-Coulomb material. When slippage occurs at the soil-reinforcement interface, the reinforcement is assumed to serve as a rigid constraint to inhibit the plastic flow of soil. Juran and Christopher(1989) conducted model tests to study the behavior and failure mechanisms of reinforced soil retaining walls using geotextiles and geogrids, and to measure the mobilized tension forces in the reinforcement.

Palmeira and Milligan(1989) identified the usual factors affecting reinforced soil pull-out test results. These include the influence of boundary conditions, the frictional characteristics and proximity of the shear box front wall, and the influence of scale. Goodings and Santamarina(1989) conducted 1-g centrifuge model tests to study the effects of foundation soil and retained backfill on the behavior of reinforced soil retaining walls.

B. STATIC ANALYSIS AND DESIGN

Lee, et al.(1973) discussed the failure mechanism of reinforced earth retaining walls. It was noted that both the soil shear strength and the bond strength between soil and reinforcing are frictional in nature, and thus directly dependent on the normal effective stress distribution. The reinforcing must be strong enough to prevent tension failure, and wide, long, and rough enough to prevent a pull-out failure. Simple analysis and design procedures were proposed for constructing reinforced earth retaining walls.

Schlosser and Long(1974) observed that, for reinforced earth retaining walls under gravity load, the points of maximum tension in the different layers of reinforcement lie on a parabolic curve, which separates the reinforced soil into an active zone and a passive zone. Thus, the tie force in the reinforcement at the wall is only a small fraction of the maximum reinforcement tension, which occurs at about one-third the length of the reinforcement from the wall. They showed that the interface friction is directly proportional to the gradient of tension per unit length of reinforcement. However, the shear stress is greater on the lower face of the reinforcement than on the upper face. Methods for calculating the reinforcement tie force are presented, and the predicted values were in close agreement with test data.

5

Chang and Forsyth(1977a) presented field data on the behavior of the first reinforced earth wall built in the United States. Design equations for soil reinforcement and face units were developed. They concluded that the active earth pressure should be used to calculate the stresses in the front portion of the reinforcement and its connection, and that the "at rest" earth pressure should be used for the middle portion of the reinforcement. Chang and Forsyth(1977b) compared the field soil stresses and horizontal movements of this wall with those predicted by the finite element analysis proposed by Romstad, et al.(1976).

Al-Hussaini and Perry(1978) conducted field tests on a retaining wall backfilled with sand and reinforced with galvanized steel ties. They found that the Rankine earth pressure theory provides a good approximation for the measured lateral pressure when the wall carries no surcharge load. However, the curve connecting the points where maximum tensile stresses occurred in the reinforcing ties did not coincide with the theoretical Rankine failure surface.

Giroud, et al.(1981) described the mechanism of geotextile reinforcement of unpaved roadways, and developed a method to determine the required thickness of an aggregate layer. Rowe(1984) developed a numerical technique for the analysis of geotextile-reinforced embankments. The technique considers soil-reinforcement interaction, slip at the soil-fabric interface, and plastic failure within the soil. A design procedure using design charts was proposed.

Juran and Chen(1989) proposed a working stress design method for reinforced earth walls, based on the fundamental understanding of constitutive behavior of soil and reinforcement, and of the soil-reinforcement interaction. They pointed out that the response of reinforced soil to loading is highly dependent upon the initial state of stress and strain in the soil. deBuhan, et al.(1989) proposed a limit state design method for reinforced earth walls, treating reinforced earth as an anisotropic and homogeneous material. The strength criterion used was of an anisotropic frictional type.

Juran, et al.(1990), based on the requirements of strain compatibility between soil and reinforcement, proposed a new design method for geosynthetic-reinforced earth walls. The soil-reinforcement load-transfer model used in this analysis incorporates the effects of soil dilatancy and reinforcement extensibility on reinforcement tension and the probable failure surface location .

6

C. DYNAMIC BEHAVIOR

Richardson and Lee(1975) developed seismic design procedures for reinforced earth retaining walls, based on small scale shake table tests. Soil reinforcement interface friction data under static and vibratory loading were also given. The required size and spacing of reinforcement can be determined from the design procedures. Richardson, et al.(1977) instrumented a 20-foot high reinforced earth wall, subjected to low-strain-level forced vibration using mechanical vibrators, and to high-strain-level explosive tests. The tie force distribution in the soil reinforcement was presented. The reinforced earth structure showed nonlinear, strain-dependent stiffness and damping properties. There was a significant decrease in the first mode frequency with increasing dynamic strain excitation. The explosive test damping values approximate the upper limit of the Seed-Idriss curve(1970), which applies only to material hysteretic damping.

Segrestin and Bastick(1988) used seismic test data of reduced- and full-size reinforced soil retaining walls to validate dynamic finite element analyses.

D. ANALYTICAL AND NUMERICAL MODELING

Romstad, et al.(1976) incorporated the "equivalent material" concept into a standard finite-element procedure to model the behavior of soil with extensible strip reinforcement. Analysis results showed that the ratio of reinforcement stiffness to soil stiffness has a significant effect on the reinforcement force. Shen, et al.(1976) conducted a finite-element analysis of an instrumented reinforced earth wall, using the "equivalent material" approach, and proposed design procedures based on several possible modes of failure for determining the size, spacing, and length of reinforcing strips.

Andrawes, et al.(1980) developed a finite-element model to study the behavior of a model embankment reinforced with tension-resistant inclusions. Nonlinear, stress-dependent models are used to represent the stress-strain relations of soil and inclusions, as well as to represent the shear stress-deformation characteristics at the soil-inclusion interface. The analysis results were compared against test data.

Leshchinsky and Reinschmidt(1985) used a limit state equilibrium condition to obtain a closed-form solution for the stability of membrane-reinforced embankment slopes. Leshchinsky and

7

Boedeker(1989) developed a stability analysis approach for geosynthetic-reinforced earth structures over firm foundations. Both internal and external stability conditions were included.

Drake, et al.(1987,1989) developed a simplified "Structure Medium Interaction" (SMI) model to predict ground shock loads on buried structures. Analytical solutions for the particle displacement and interface stress are given. This model, however, considers an extended medium, and therefore does not accommodate the merging of reflected shocks. Furthermore, a velocity boundary condition, rather than a stress boundary condition, was imposed on the model.

Juran, et al.(1988a, 1988b) developed a model for load-transfer in reinforced soils. The model assumes elasto-plastic strain-hardening soil and elastic-perfectly plastic reinforcement. The effects of soil dilatancy, reinforcement extensibility, and reinforcement inclination with respect to the failure surface, on the reinforcement tension were evaluated.

Yogendrakumar, et al.(1992) evaluated and compared two finite-element methods for the dynamic response analysis of reinforced-soil retaining wall structures. The analysis results were compared against the wall response under blast loading reported by Richardson, et al.(1977).

SECTION III

DESIGN REQUIREMENTS

A. CONFIGURATION

The design shall focus on bermed, aboveground shelters, including those with balanced cut and fill. The geometry of the shelter structure shall be box-shaped for rapid construction and repair purposes.

B. PERFORMANCE CRITERIA

The shelters shall be rapidly erectable during wartime. However, they shall be readily convertible to permanent structures during peacetime.

The design shall survive a single attack event with possible local failure. Although the major function of these shelters is to protect aircraft and munitions, the shelter shall also protect personnel and sensitive equipment whenever applicable. Shock response spectra (SRS), commonly employed in earthquake engineering, may be used as a measure of merit to evaluate structural performance, and to assess structural damage and hazards to equipment and personnel.

C. DESIGN LOADS

The design threat shall be a 500-pound, general-purpose (GP) bomb detonated at a standoff of 10 feet from an interior wall. Airblast load due to a surface burst, as well as ground shock due to a detonation within the berm shall be considered for shelter design. The "worst case" blast effects from the given threat shall be used as design loads.

D. SOIL BACKFILL

Cohesionless, granular materials, such as sand, should be used for soil backfill. The backfill shall be free draining, or have provisions for free drainage. Furthermore, it is assumed there will be no blast-induced excess pore water pressure in the backfill. Both the soil shear strength and the bond strength between soil and reinforcing elements are frictional in nature, and thus depend on the normal stress distribution between the soil and reinforcing layers. On the other hand, it is

9

desirable to allow slippage between reinforcing and soil to relieve stress concentrations at panel connections. Therefore, the normal stress distribution shall be optimized to accomodate these effects. Additional normal stress can be achieved by building a soil surcharge on top of reinforcing layers.

E. SOIL REINFORCING

Soil reinforcing elements are generally strips, bars, sheets, or nets, which interact with the soil by means of frictional resistance. The fundamental function of soil reinforcing is to restrict tensile strain in the soil parallel to the reinforcing. The soil reinforcing shall have a high tensile modulus to limit or reduce large soil displacement, and high tensile strength to develop full soil frictional strength without reinforcement rupture.

Reinforcing elements in the form of meshes, available as geogrids, shall be used to restrict tensile strain in the soil parallel to the geogrids. In addition, the reinforcing, and panel/connector system shall be designed to distribute high local loads to more than one wall panel.

F. WALL PANELS

The wall panels shall be designed to minimize interior shock response, and to prevent panel failure. These panels may be constructed with lightweight concrete reinforced with wire mesh.

The connections of soil reinforcing to wall panels shall be designed to have adequate tensile strength, while the interconnections between panels shall be designed to have adequate shear and flexural strength.

G. AMBIENT ENVIRONMENTAL CONDITIONS

Most construction materials are subject to a number of diverse service environmental conditions. Often such environments impair a material's usefulness by degrading its mechanical properties.

Polymeric soil reinforcing can experience physical property degradation due to temperature fluctuations, underground moisture, chemicals, and radiation exposure.

Metallic parts and connectors used in the wall panel/soil reinforcing system are subject to

10

corrosion in a moist environment. It is essential to provide free drainage in the reinforced soil backfill, to prevent soil saturation due to rain. Furthermore, reinforced soil shelters shall be built above the water table.

These protective shelters shall have a design service life of 15 years. The adverse effects of ambient temperature fluctuations, soil moisture, and other environmental factors, shall be considered in the design.

H. OPERATIONAL REQUIREMENTS

Reinforced soil shelter construction will be accomplished using existing Air Force personnel and equipment. Only ordinary equipment, such as front-end loaders, bulldozers, and dump trucks, is required. This technology can be implemented with current construction practice. However, some on-site training might be needed for troop labor.

I. LOGISTIC CONSTRAINTS

A number of materials have been commonly used for modular wall panel construction. These include plastics, fabrics, lightweight steel, and precast concrete; among these precast concrete panels are the most widely used. A typical panel is about 5 feet-5 inches wide and 5 feet high, weighing about 2,500 pounds. Geogrids are available world-wide, and are shipped in rolls.

These panels could be either cast in place on the site or delivered via ground transportation. Airlift is not considered as the most desirable transport method.

J. CONSTRUCTIBILITY CRITERIA

The construction technique and structural components employed in the reinforced soil airbase protective shelter concept permit rapid deployment, and require no specialized construction facilities or skills. The construction can be carried out by troop labor and local workers.

A number of construction guidelines have been published since the introduction of geogrids and geotextiles in pavement and embankment construction. These include the United States Federal Highway Administration (FHWA) design guidelines (Christopher 1990), and the United States Army Corps of Engineers Technical Manual TM 5-818-8. These guidelines should be used

to ensure internal as well as external stability of reinforced earth berm shelters under gravity and seismic loads. The guidelines proposed in this study are additional requirements intended for designing shelters to survive conventional weapon effects.

SECTION IV

ANALYTICAL MODELING OF PANEL CONNECTION SYSTEM

A. ONE-DIMENSIONAL MATHEMATICAL MODEL

As shown in Figure 1, a typical wall can be constructed with interlocking modular panels or blocks connected to the soil reinforcement. The soil reinforcement is assumed to be layers of geogrid running parallel to the direction of wave propagation. Figure 2 shows a wall panel with a layer of reinforced soil attached to it. It is assumed in this model that the soil and geogrid undergo the same longitudinal strain, and that the soil and wall panel stay bonded at the interface. Furthermore, the shear and bending resistance from connections between the panels has been left out to simplify the analysis.

The elastic behavior of sheet-reinforced soil can be modeled as that of a composite material. Jones(1975) showed that the "macromechanical" behavior of a composite material can be described in terms of the mechanical properties of its constituents and their volume ratios in the composite construction. Harrison and Gerrard (1972) treated reinforced soil as a cross-anisotropic (or transversely isotropic) material consisting of layers of stiff and soft isotropic materials with a vertical axis of symmetry. If the reinforcement volume ratio in a reinforced soil is denoted as V_g, the apparent constrained modulus of the reinforced soil in the x-direction, is

$$K_x = \frac{E_s(1-v_s)}{(1+v_s)(1-2v_s)}(1-V_g) + \frac{E_g(1-v_g)}{(1+v_g)(1-2v_g)}(V_g)$$

$$-V_g(1-V_g)\frac{\left[\dfrac{E_s v_s}{(1+v_s)(1-2v_s)} - \dfrac{E_g v_g}{(1+v_g)(1-2v_g)}\right]^2}{\dfrac{E_s(1-v_s)}{(1+v_s)(1-2v_s)}(V_g) + \dfrac{E_g(1-v_g)}{(1+v_g)(1-2v_g)}(1-V_g)} \qquad (1)$$

13
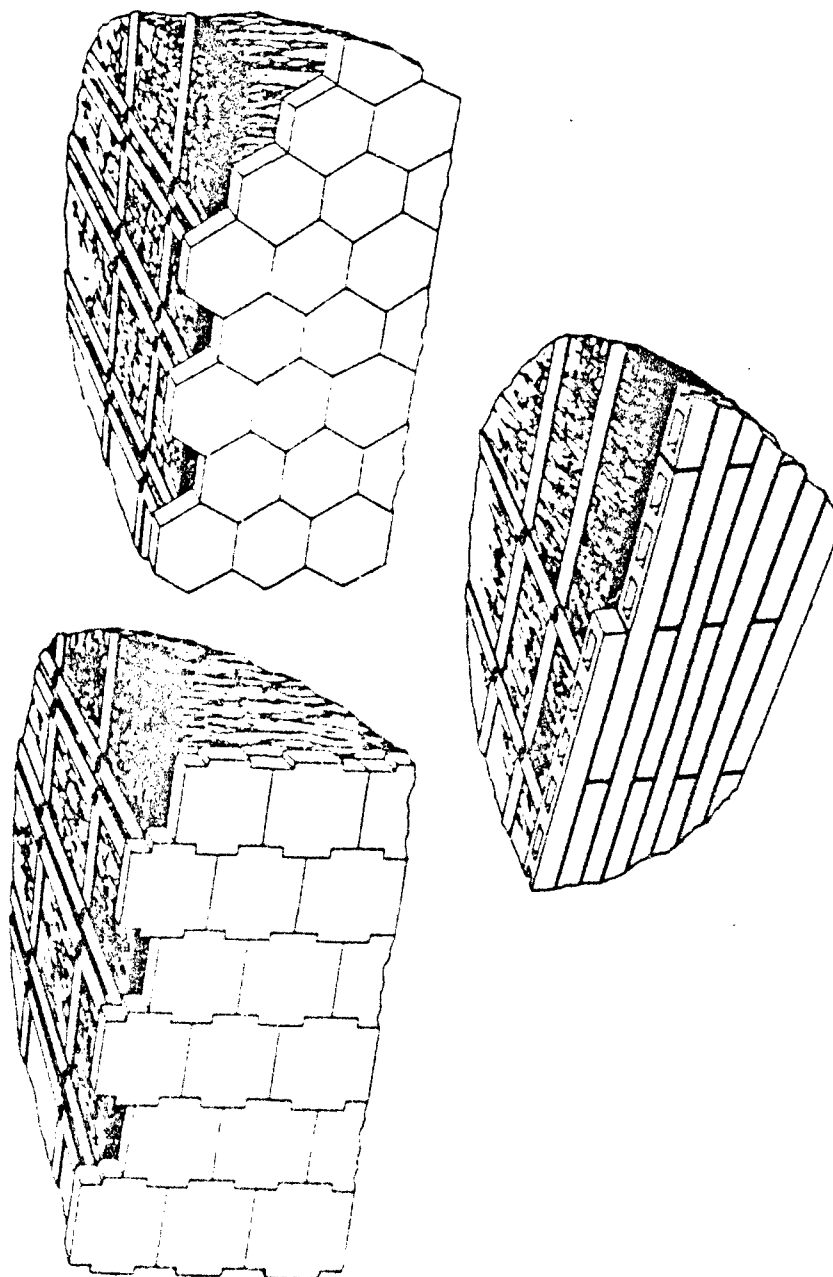
Figure 1. Interlocking Modular Wall Panels and Blocks

14
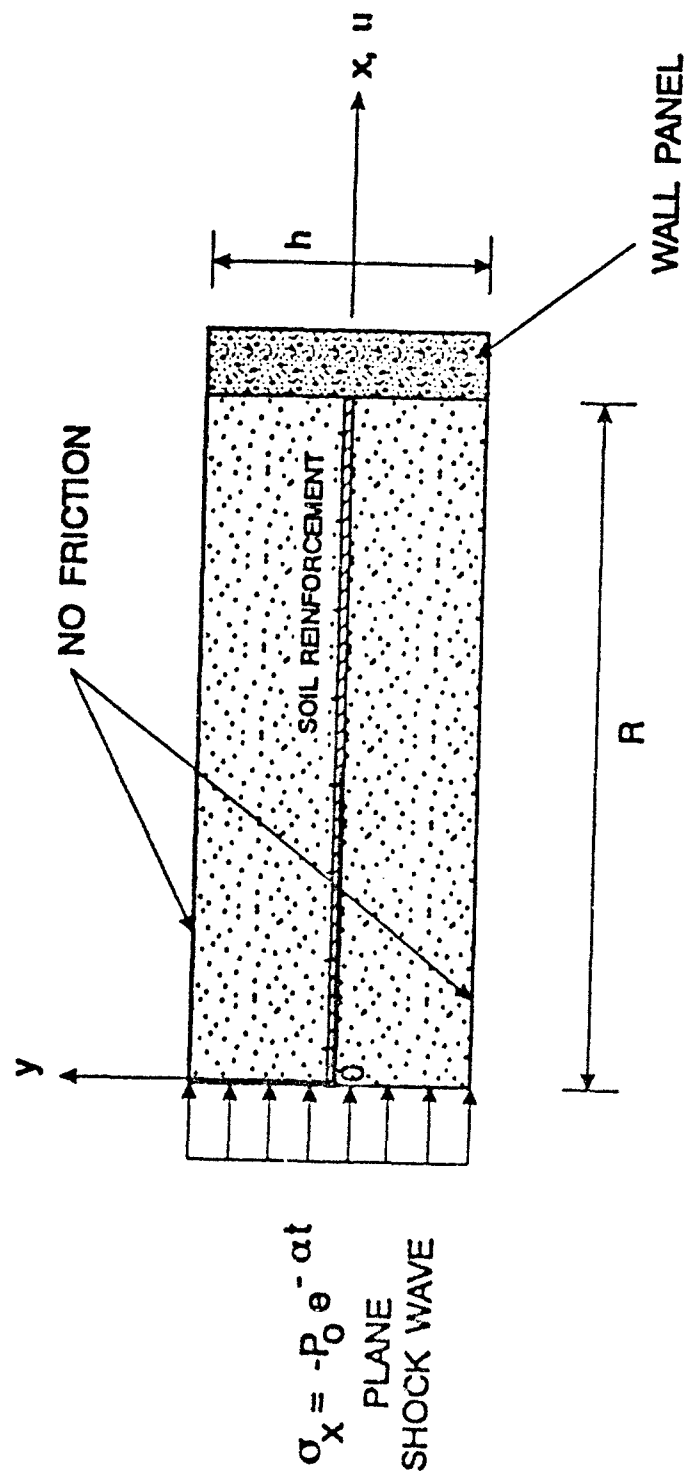
Figure 2. One-dimensional Model of Wall Panel and Soil Reinforcement Connection System

15

where E_s and E_g, and v_s and v_g are, respectively, the Young's moduli and Poisson's ratios of the soil and reinforcement.

Governing equation   The 1D wave equation for the particle displacement, $u(x,t)$, in a homogeneous medium is

$$\frac{\partial^2 u}{\partial t^2} = c^2 \frac{\partial^2 u}{\partial x^2} \qquad (2)$$

where c, the wave propagation velocity of reinforced soil, is given by

$$c \approx \sqrt{\frac{K_x}{\rho_o}} \qquad (3)$$

and ρ_o is the mass density of the reinforced soil.

Boundary conditions   At $x = 0$, the shock wave front, having an initial particle velocity, v_o, arrives at time $t = 0$ and decays exponentially, so that

$$\frac{\partial u}{\partial t}(0,t) = v_o \exp(-\alpha t) \qquad (t > 0) \qquad (4)$$

where α is the decay rate. The shock front pressure, P_o, is the product of the soil impedance, ρc, and the initial particle velocity, v_o.

At $x = R$, the equation of motion of the wall panel is

$$M \frac{\partial^2 u}{\partial t^2} = -\sigma_x h b - T_g \qquad (5)$$

where M is the wall panel mass, h is the panel height, b is the panel width, and T_g is the geogrid tension at the wall-soil interface. Casting this geogrid tension in terms of the interface displacement, Equation (5) becomes

$$\mu \frac{\partial^2 u}{\partial t^2} + \frac{\partial u}{\partial x} = 0 \qquad (6)$$

where

$$\mu = \frac{M}{K_s h b + E_g A_g} \qquad (7)$$

16

and K_s is the soil constrained modulus, and E_g and A_g are the Young's modulus and cross-sectional area of the geogrid, respectively.

<u>Initial conditions</u>   The wall panel/reinforced soil system is at rest before the shock front arrives, and thus the initial conditions are:

$$u(x,0) = 0 \qquad (0 \leq x \leq R) \qquad (8)$$

$$\frac{\partial u}{\partial t}(x,0) = 0 \qquad (0 \leq x \leq R) \qquad (9)$$

<u>Solution</u>   Equation (2), together with the boundary and initial conditions, was solved by the Laplace transform method. Taking the Laplace transform of Equations (2), (4), and (6) yields the transformed wave equation

$$\frac{\partial^2 U(x,s)}{\partial x^2} - \frac{s^2}{c^2} U(x,s) = 0 \qquad (10)$$

and the transformed boundary conditions

$$U(0,s) = \frac{v_o}{s(s+\alpha)} \qquad (11)$$

$$\frac{\partial U(R,s)}{\partial x} = -\mu s^2 U(R,s) \qquad (12)$$

where s is a complex variable, and x is held fixed throughout the transformation. The solution of Equations(10)-(12) is

$$U(x,s) = \frac{v_o}{s(s+\alpha)} \left[\cosh\theta - \left(\frac{\sinh\beta + \mu sc \times \cosh\beta}{\cosh\beta + \mu sc \times \sinh\beta} \right) \sinh\theta \right] \qquad (13)$$

where

$$\beta = \frac{sR}{c} \qquad (14)$$

and

$$\theta = \frac{sx}{c} \tag{15}$$

The particle displacement, u(x,t), was obtained by taking the inverse transform of Equation (13), for which purpose Equation (13) is rewritten in the form of

$$U(x,s) = \frac{v_o}{s(s+\alpha)}\left(e^{\theta} - \frac{e^{\theta} - e^{-\theta}}{1+\eta}\right) \tag{16}$$

where

$$\eta = \left(\frac{1 - \mu sc}{1 + \mu sc}\right)e^{-2\beta} \tag{17}$$

Because $\eta < 1$,

$$\frac{1}{1+\eta} = \sum_{j=0}^{\infty}(-1)^j \eta^j \tag{18}$$

and

$$U(x,s) = \frac{v_o}{s(s+\alpha)}\left[e^{\theta} - \left(e^{\theta} - e^{-\theta}\right)\sum_{j=0}^{\infty}(-1)^j \eta^j\right] \tag{19}$$

Keeping only the first three terms of the infinite series yields the solution for u(x,t) in the form

$$u(x,t) = \sum_{1}^{5} u_i \tag{20}$$

where, using the variables,

$$t1 = t - \frac{x}{c} \tag{21}$$

$$t2 = \left(t + \frac{x}{c}\right) - 2T \tag{22}$$

18

$$t3 = \left(t - \frac{x}{c}\right) - 2T \tag{23}$$

$$t4 = \left(t + \frac{x}{c}\right) - 4T \tag{24}$$

$$t5 = \left(t - \frac{x}{c}\right) - 4T \tag{25}$$

$$T = \frac{R}{c} \tag{26}$$

$$m = \mu \alpha c \tag{27}$$

$$p = m + 1 \tag{28}$$

$$q = m - 1 \tag{29}$$

$$\gamma = \frac{1}{\mu c} \tag{30}$$

the terms on the right hand side of Equation (20) take the form

$$u1 = 0 \qquad (t1 < 0)$$
$$= \frac{v_o}{\alpha}\left(1 - e^{-\alpha \cdot t1}\right) \qquad (t1 > 0) \tag{31}$$

$$u2 = 0 \qquad (t2 < 0)$$
$$= -\frac{v_o}{\alpha q}\left[p\left(1 - e^{-\alpha \cdot t2}\right) - 2m\left(1 - e^{-\gamma \cdot t2}\right)\right] \qquad (t2 > 0) \tag{32}$$

$$u3 = 0 \qquad (t3 < 0)$$
$$= \frac{v_o}{\alpha q}\left[p\left(1 - e^{-\alpha \cdot t3}\right) - 2m\left(1 - e^{-\gamma \cdot t3}\right)\right] \qquad (t3 > 0) \tag{33}$$

$$u4 = 0 \qquad (t4 < 0)$$

19

$$= -\frac{v_o}{\alpha q^2}\left\{p^2\left(1-e^{-\alpha \cdot t4}\right) - 4m^2\left(1-e^{-\gamma \cdot t4}\right) + 4mq\left[1-(1+\gamma \cdot t4)e^{-\gamma \cdot t4}\right]\right\} \quad (t4 > 0) \quad (34)$$

$$u5 = 0 \qquad\qquad (t5 < 0)$$

$$= \frac{v_o}{\alpha q^2}\left\{p^2\left(1-e^{-\alpha \cdot t5}\right) - 4m^2\left(1-e^{-\gamma \cdot t5}\right) + 4mq\left[1-(1+\gamma \cdot t5)e^{-\gamma \cdot t5}\right]\right\} \quad (t5 > 0) \quad (35)$$

The expressions for longitudinal normal stress, particle velocity, and particle acceleration can be readily derived from Equation (20). Although higher order terms could be added to the solution, the transient response of the reinforced soil system due to shock loading will have been damped out before they become effective. The model treats reinforced soil as a linearly elastic, homogeneous medium, and as such cannot model the hysteretic compaction or other plastic behavior of soil under stress wave propagation.

For the parameters given in Table 1, the wave propagation speed of the reinforced soil was computed to be 1780 fps. The displacement, velocity and acceleration time-histories of the wall panel are shown in Figures 3 to 5, respectively. The time-history of the interface stress between the soil and the wall panel is shown in Figure 6.

B. DYNA2D FINITE ELEMENT MODELS

DYNA2D, a public domain program developed by the Methods Development Group of the Lawrence Livermore National Laboratory (LLNL), is a nonlinear, explicit, finite element code for analyzing the transient dynamic response of two-dimensional structures. The only element formulation available in DYNA2D is a four-node continuum element that handles geometric as well as material nonlinearitites. Many material models are available to represent various material behavior, including elasticity, plasticity, composites, thermal effects and rate dependence. A diverse equation of state library allows accurate modeling of the hydrodynamic behavior of many materials, including propellants and high explosives. DYNA2D has a sophisticated contact interface capability, including frictional sliding, tie interfaces and single surface contact, to handle arbitrary mechanical interactions between independent bodies or between two portions of one body. In addition, DYNA2D contains a rezoner to allow nodes to be repositioned and a new mesh to be generated when the finite element mesh becomes excessively distorted during a

20

TABLE 1.   MODEL PARAMETERS FOR THE 1D ANALYSIS

Young's Modulus of Soil	37,000 psi
Poisson's Ratio of Soil	0.35
Dry Unit Weight of Soil	110 pcf
Geogrid Modulus	29,000 ksi
Poisson's Ratio of Geogrid	0.3
Volume Ratio of Geogrid	0.05%
Pressure at Shock Front	670 psi
Ground Shock Decay Rate	300 sec^{-1}
Standoff Distance	120 in.
Weight of Wall Panel	2430 pounds

Wall Panel Displacement
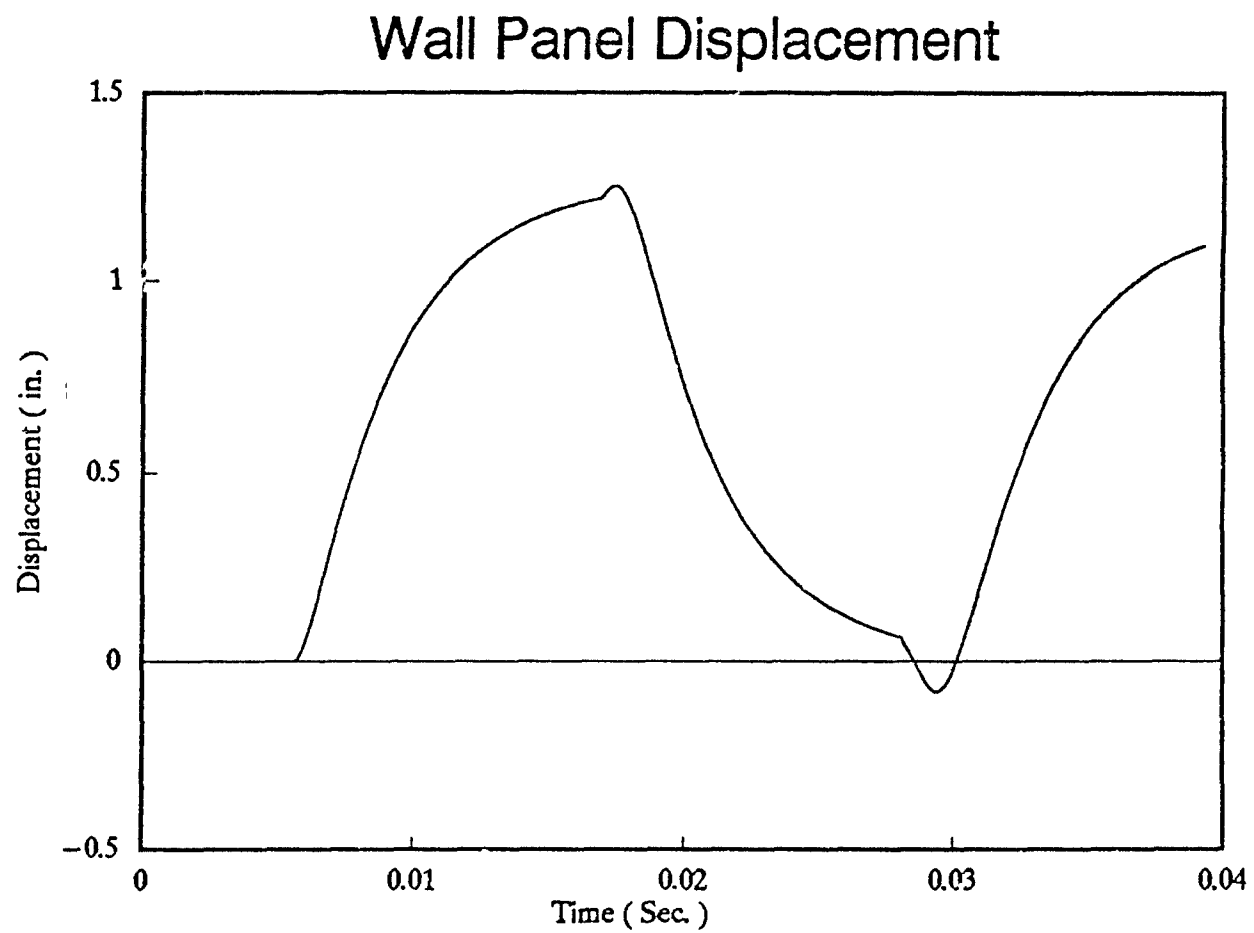
Figure 3.   Displacement Time-History of Wall Panel

22

Wall Panel Velocity
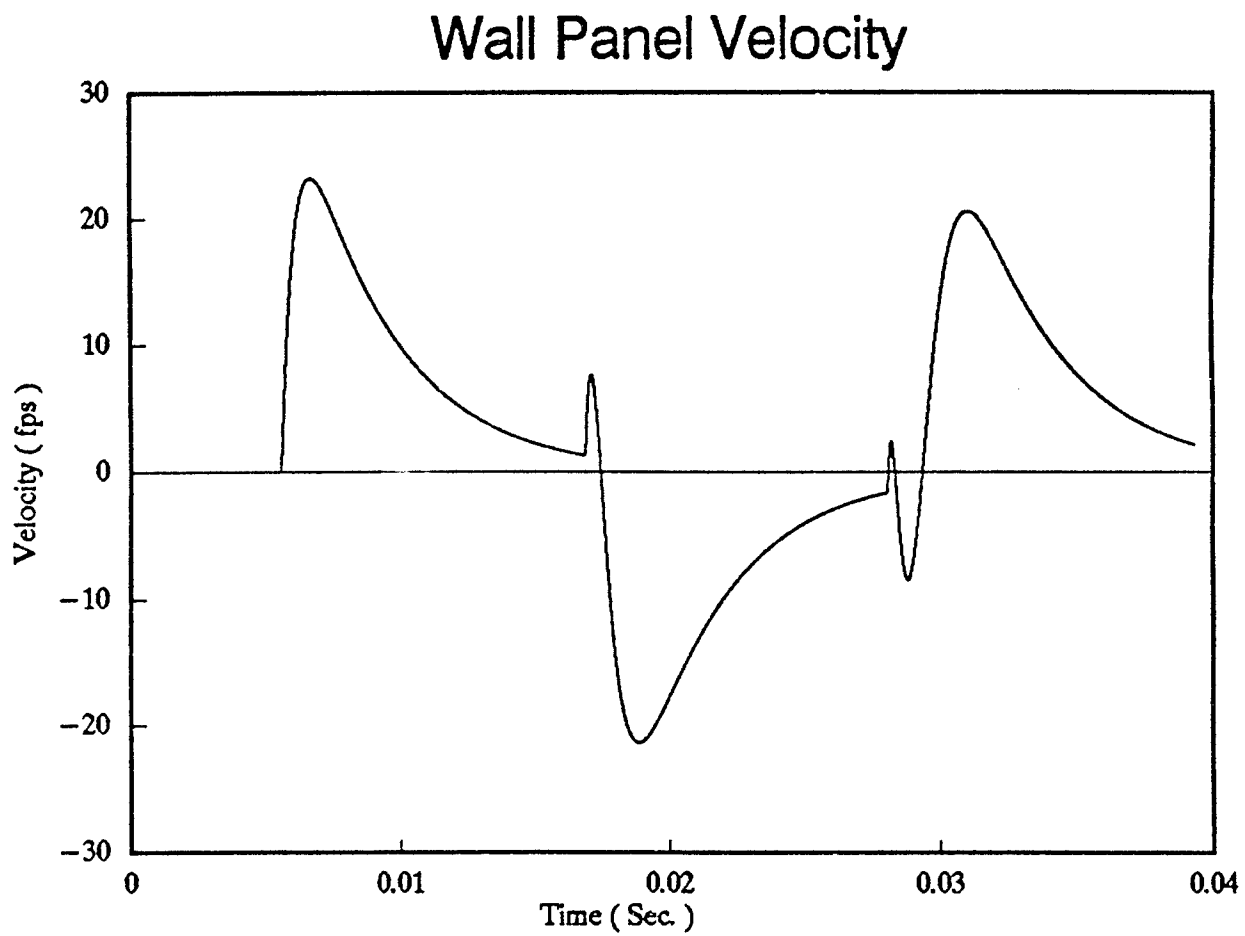
Figure 4.   Velocity Time-History of Wall Panel

Wall Panel Acceleration

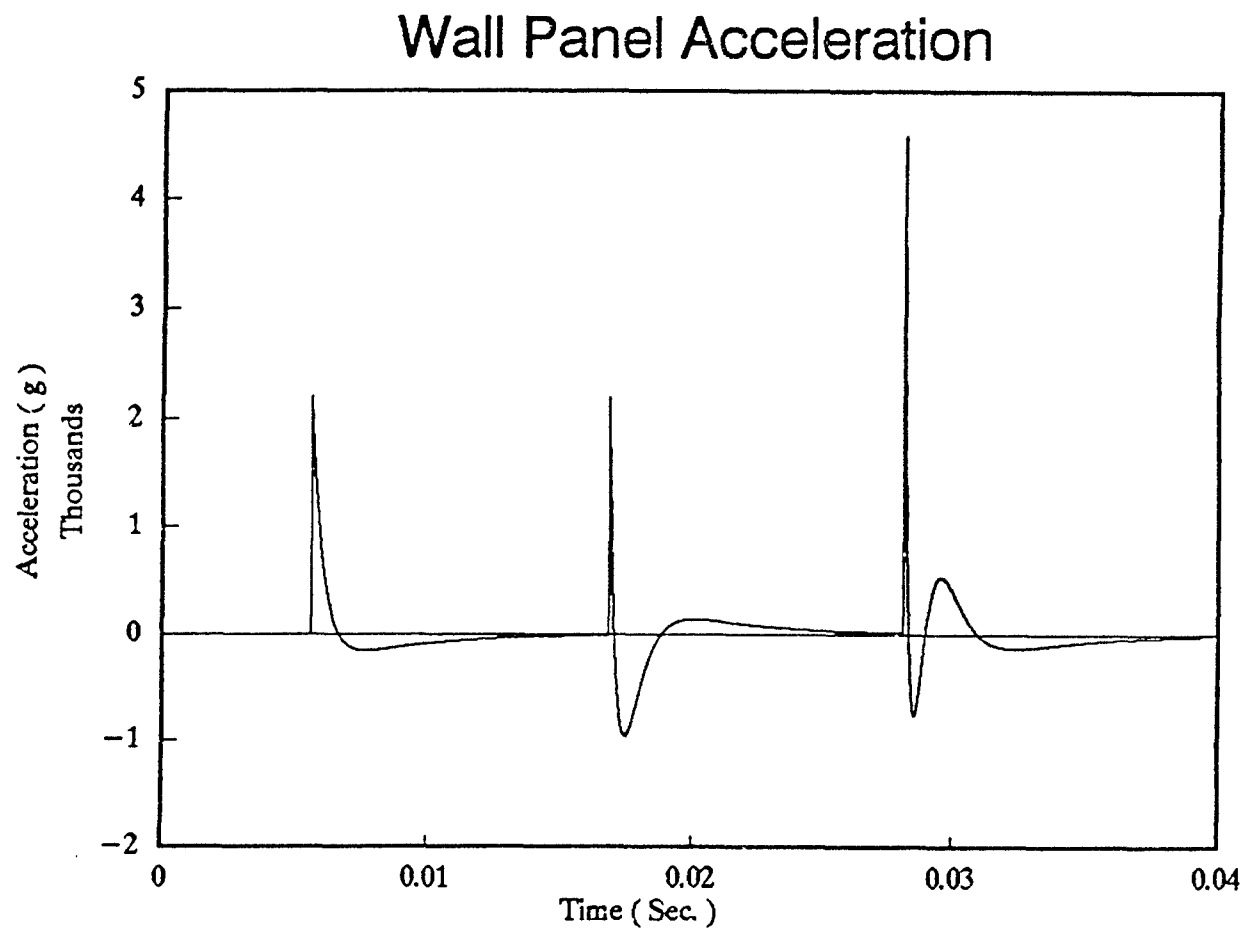Figure 5. Acceleration Time-History of Wall Panel

24

Interface Stress
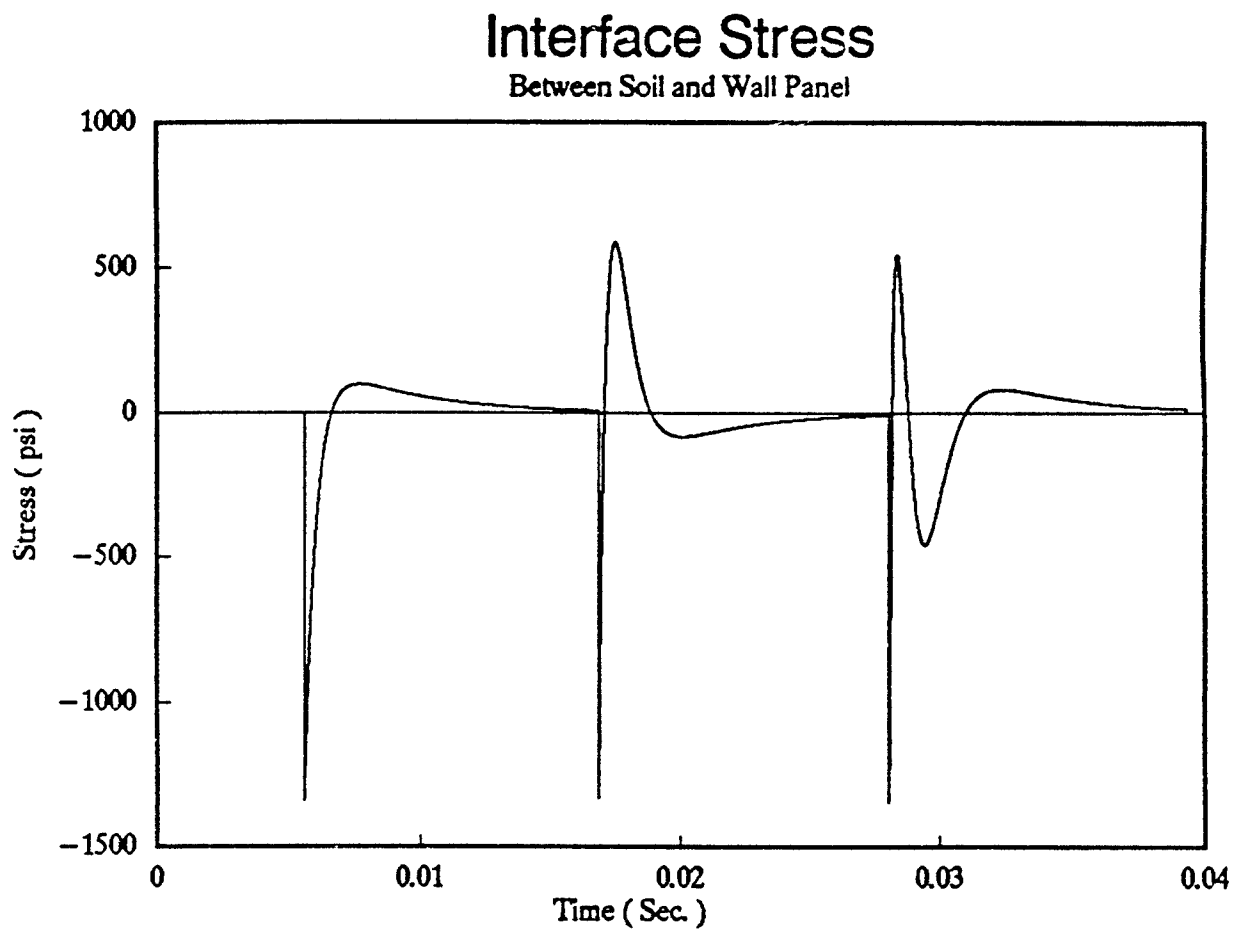### Between Soil and Wall Panel

Figure 6.   Time-History of Interface Stress Between Reinforced
Soil and Wall Panel

calculation. These features make DYNA2D particularly suitable for the transient response analysis of shelter walls with reinforced soil backfill under ground shock.

The reinforced soil ammunition magazine recently tested in Israel (Raudanski, et al. 1990; Reid 1990) was selected for DYNA2D finite-element simulation. The configuration and overall dimensions of this structure are shown in Figure 7(Reid 1991). The walls were built with cruiciform panels whose construction detail and dimensions are shown in Figure 8. These patented panels were made of concrete with compressive strength of 5000 psi and stacked on edge with a tongue-and-groove type of connection. Each panel was reinforced with four galvanized steel strips in two layers. The strips were approximately 2 inches wide and 0.25 inches thick. The embedment length of these strips in the backfill was 13 feet.

A plane strain DYNA2D model of one side wall (Wall A) of the test magazine was constructed to study the dynamic response of the wall under the ground shock due to a 500-pound GP bomb detonated at a standoff of 13.6 feet from the wall and at its midheight. As shown in Figure 9, the reinforced backfill as well as the wall was included in the finite element mesh. The soil backfill was assumed to be silty gravel having a unit weight of 112 pcf, a shear modulus of 670 ksi, and a bulk unloading modulus of 4200 ksi. Figure 10 shows the pressure versus volumetric strain curve for the soil's behavior. It was assumed that soil cannot carry tensile stresses. Figure 11 shows the relationship of soil yield stress with respect to pressure up to 1000 psi. It is of a Mohr-Coulomb frictional type, which is normally used for granular soils. The tongue-and-groove connections between the panels, and the strip-soil interfaces were modeled with frictional slidelines. The wall was simply supported at the top and the bottom, such that the top and bottom panels were free to rotate toward the inside of the shelter. The vertical displacement of the base was also constrained.

The geostatic stress distribution in the reinforced soil due to gravity was created by using the "dynamic relaxation" technique. This was achieved by simply applying the gravity loads slowly, and integrating the equations of dynamics until all significant transients had died out. Then the radial particle velocity profile due to the detonation of the bomb was imposed on the mesh at the bomb boundary surface. The particle velocity profile was obtained using the hydrodynamic code SABER-PC (Zimmerman 1991), which is described in detail in Section V of this report. As shown in Figure 12, the middle panel was pushed out by the ground shock at about 20 ms after detonation. This failure mechanism was observed on the video taped during the full-scale test.

26
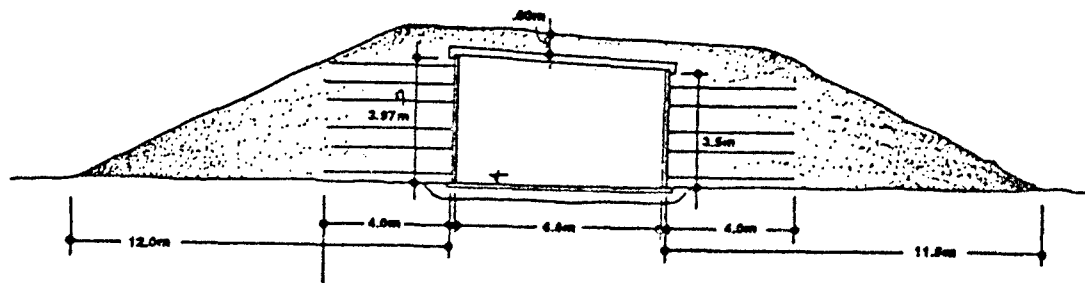
(a)
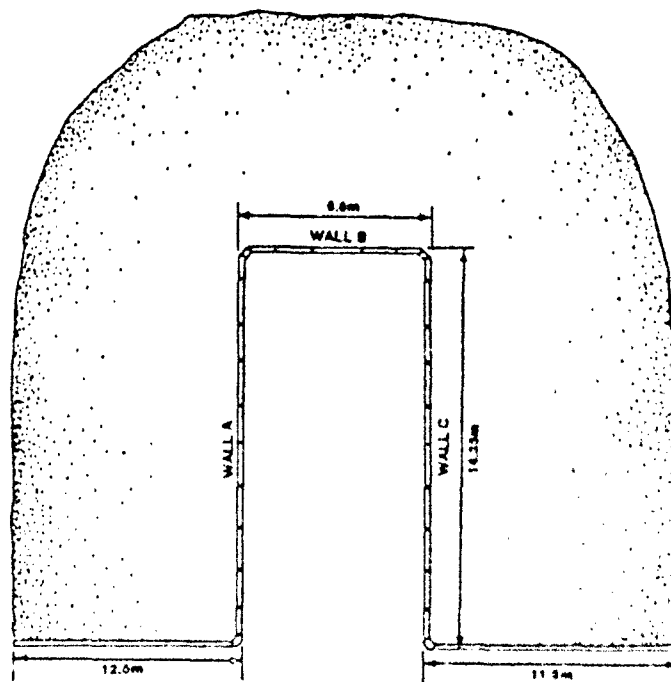
(b)

Figure 7. Full-Scale Test Munition Magazine
(a) Section View (b) Plan View
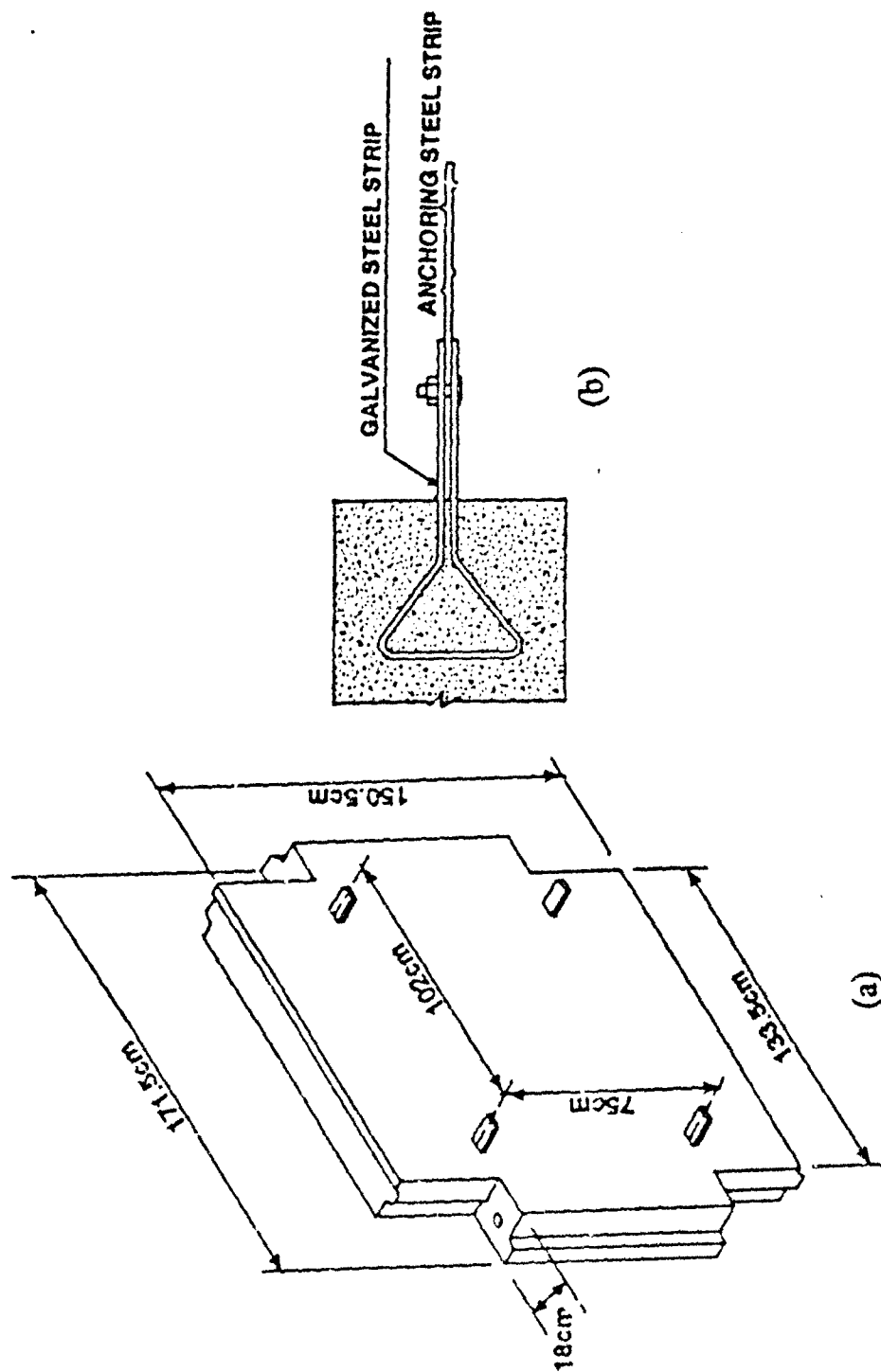
Figure 8. Concrete Wall Panel (a) Dimensions (b) Soil Reinforcing Strip

GALVANIZED STEEL STRIP

ANCHORING STEEL STRIP

(b)

150.5cm

102cm

75cm

133.5cm

171.5cm

18cm

(a)
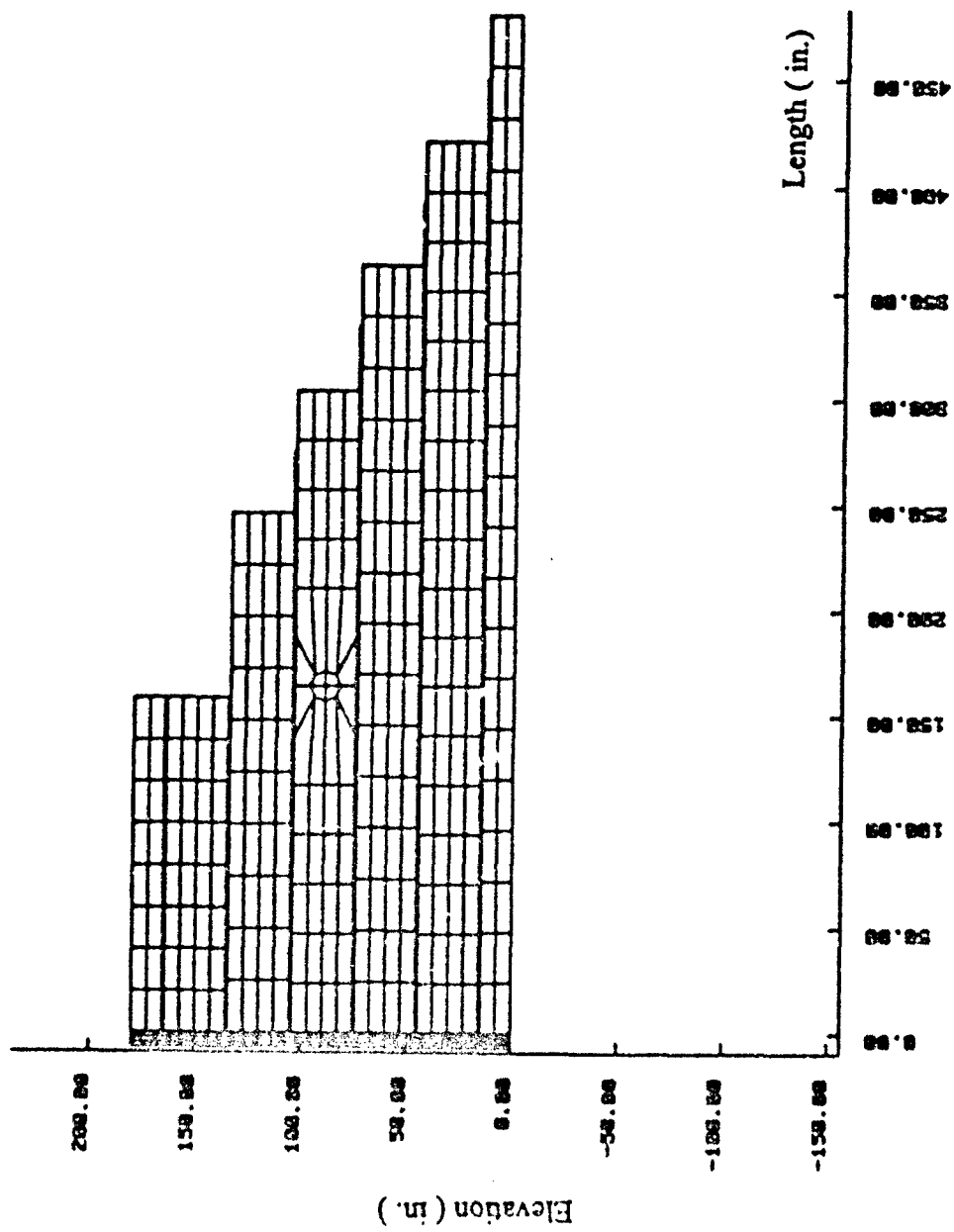
Figure 9. DYNA2D Finite-Element Mesh of Test Reinforced Earth Shelter

29
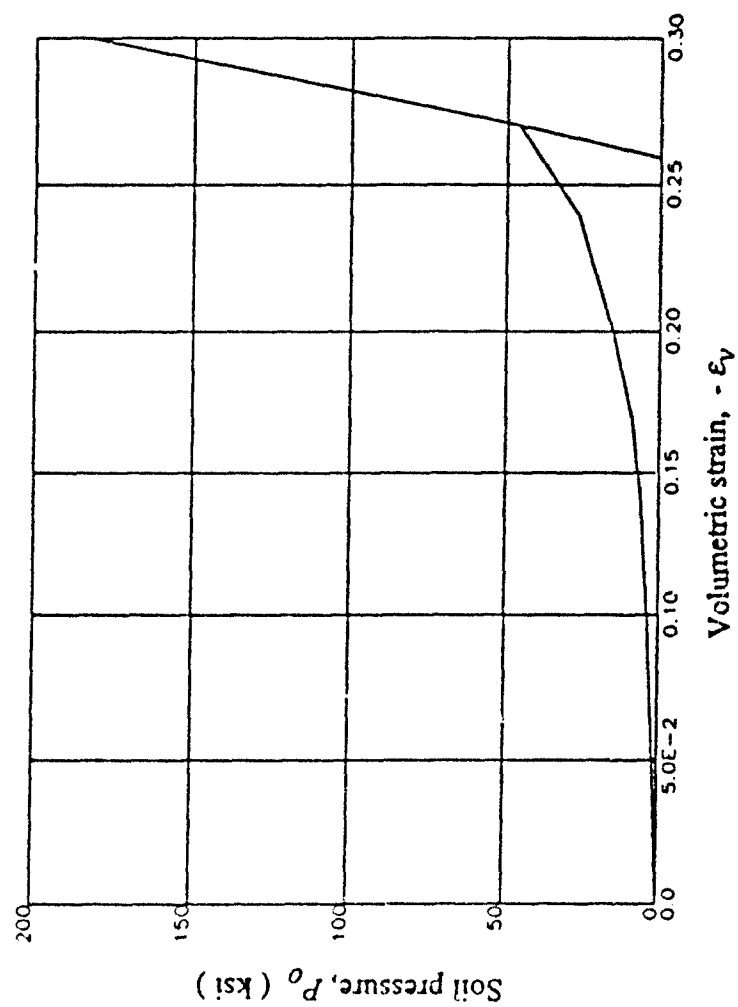
Figure 10. DYNA2D Constitutive Model for Soil Backfill

30

Yield Surface

(or Failure Surface)
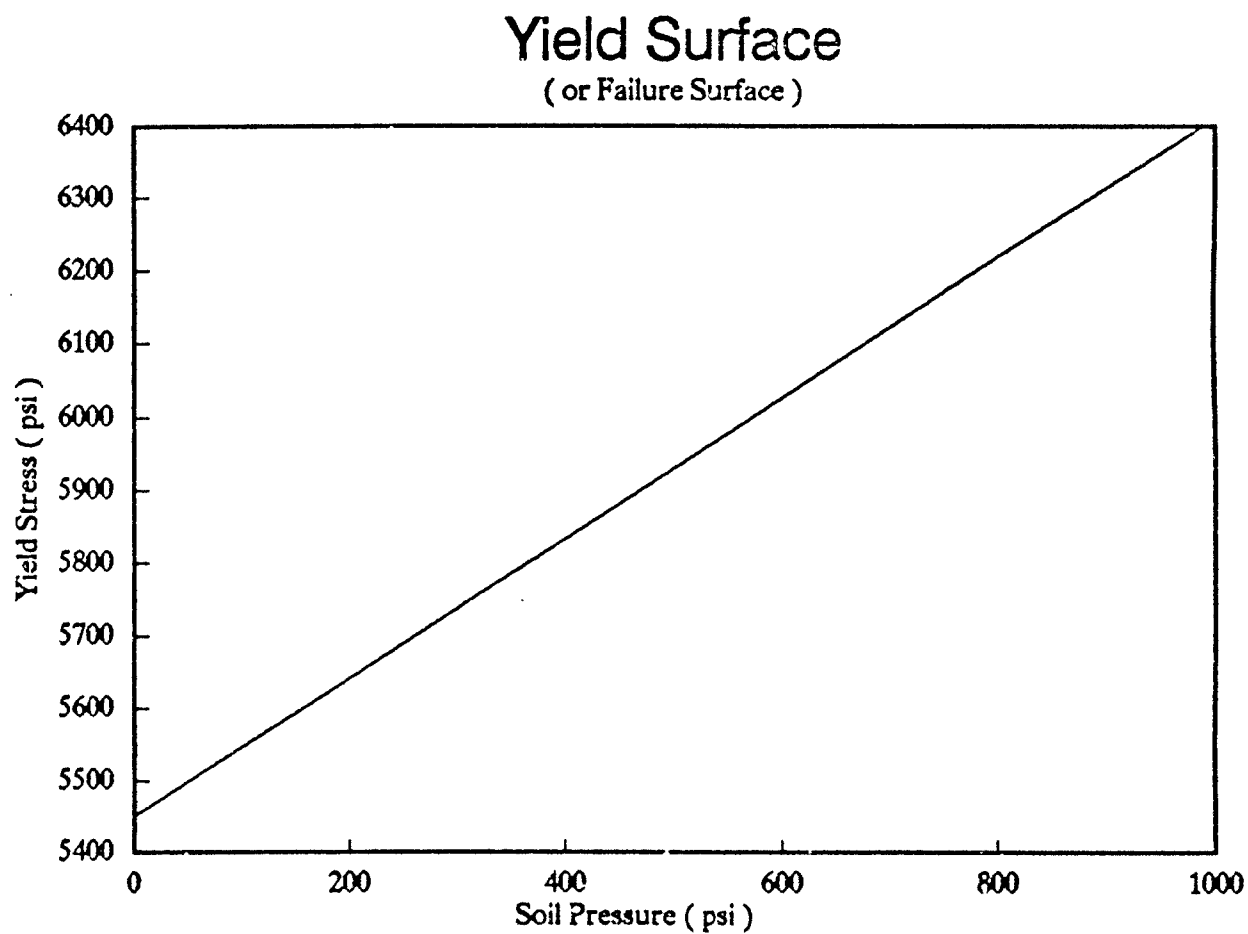
Figure 11. Soil Yield Surface
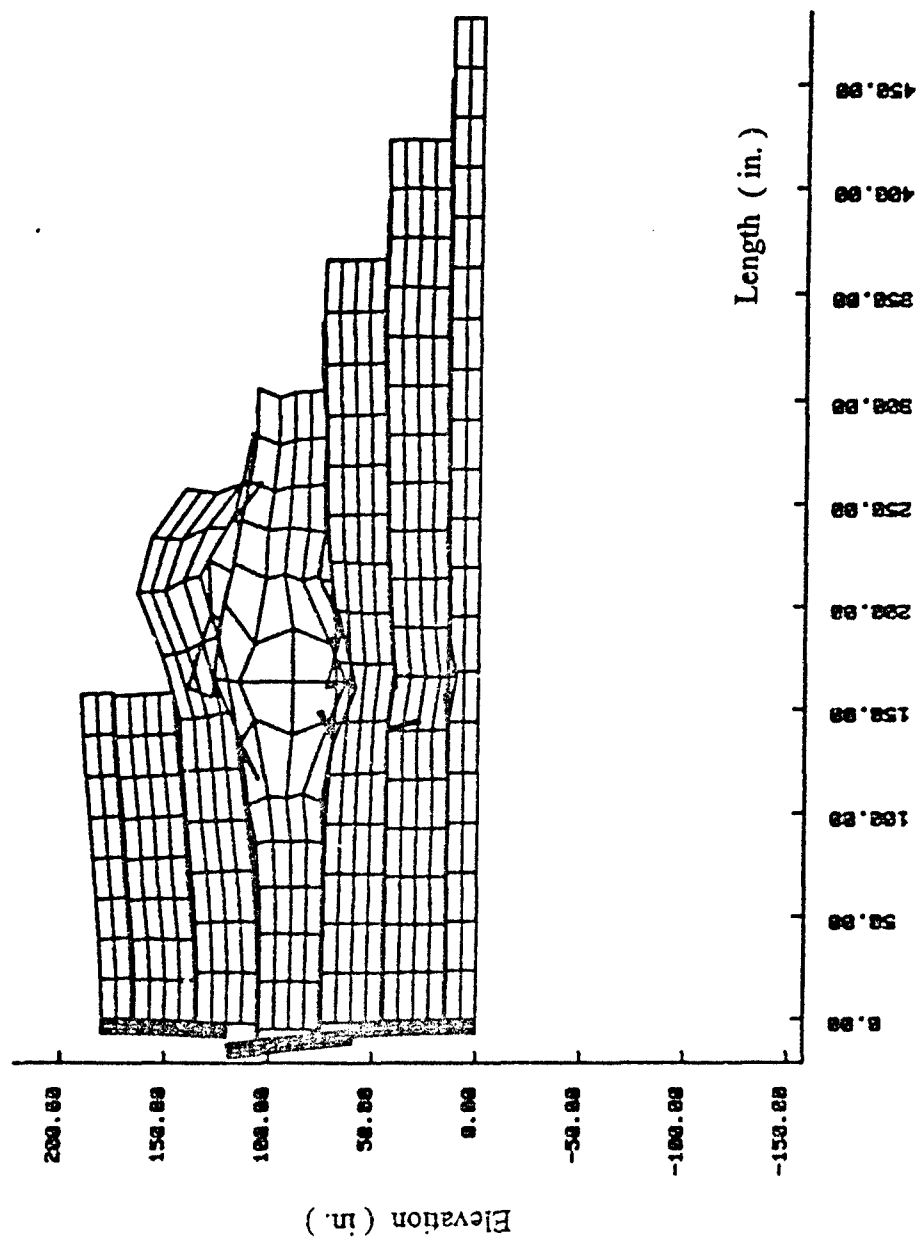
Figure 12. Deformation of Reinforced Earth 20 ms After Detonation

Thus, the finite element model closely simulated the dynamic behavior of the wall in the full-scale test. The model predicted that the maximum soil-panel interface stress was 710 psi and the maximum wall panel displacement was 7 inches. The time-histories of these parameters are shown in Figures 13 and 14, respectively.
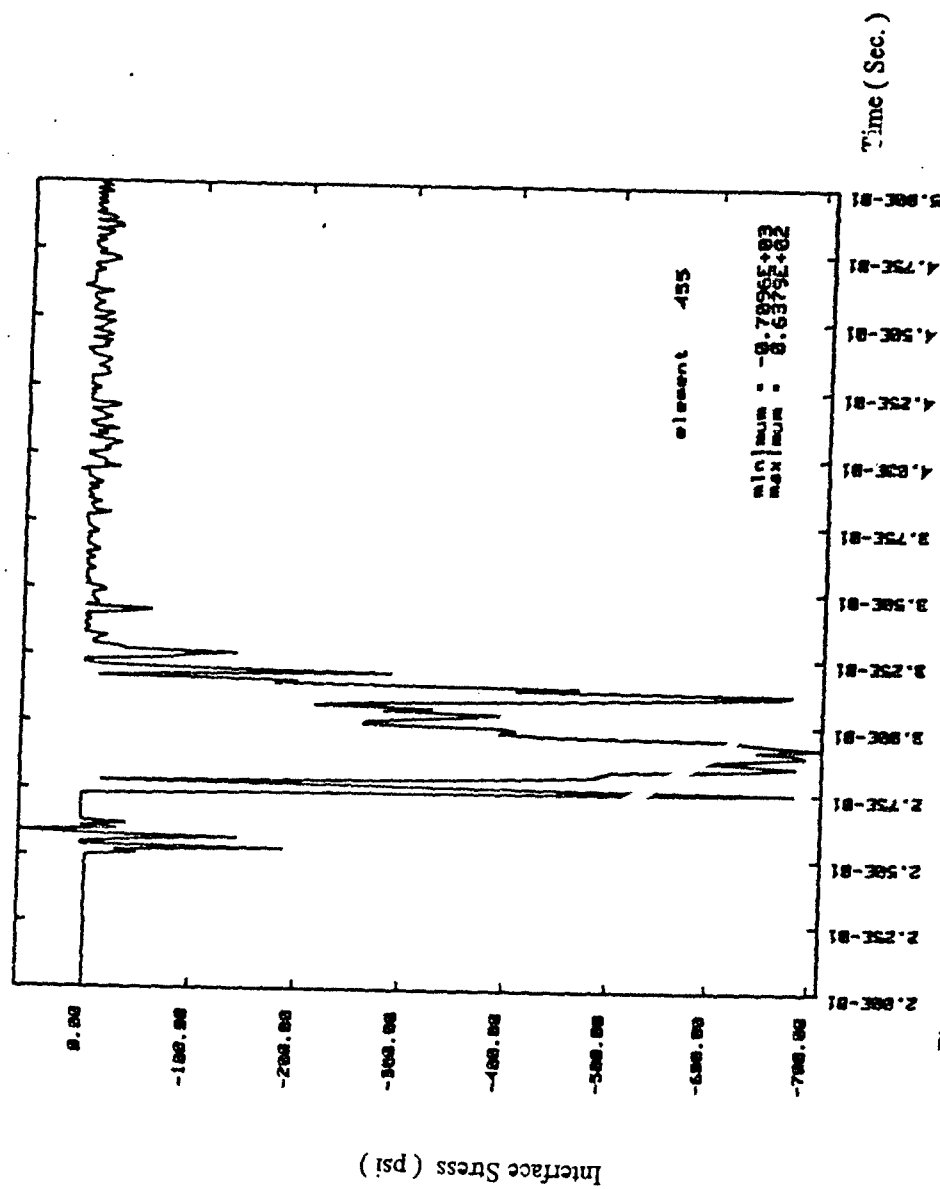
Figure 13. Time-history of Interface Stress at Mid-height of Wall

34
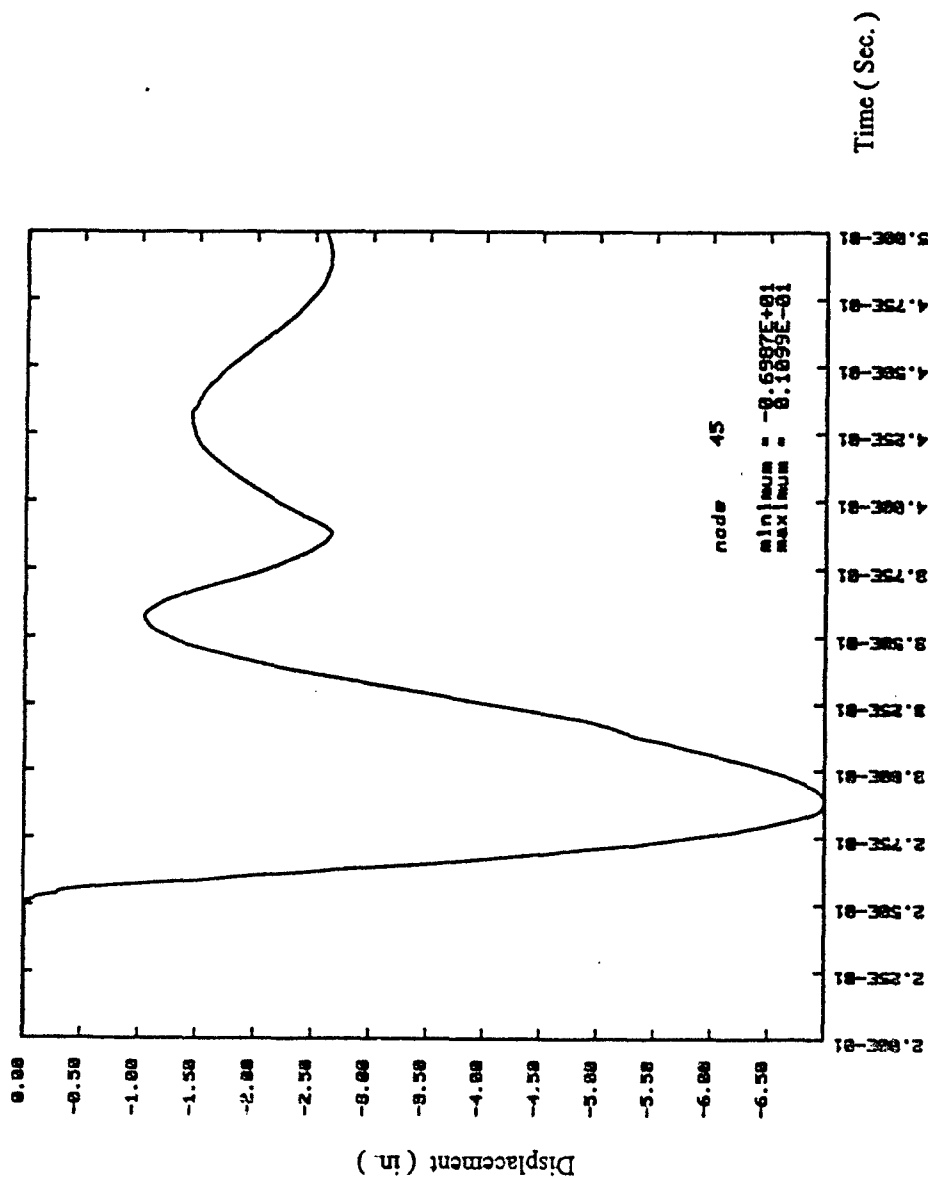
Figure 14. Displacement Time-history of Middle Wall Panel

SECTION V

PARAMETRIC STUDIES

A. GROUND SHOCK PREDICTIONS

Given a weapon yield and standoff, along with soil properties, the ground shock parameters can be estimated by using protective construction design manuals, such as Air Force Design Manual (ESL-TR-87-57) and the Department of Energy Design Manual (DOE/TIC-11268), or by running more comprehensive hydrodynamic codes. Most design manual procedures for ground shock prediction are based on empirical fits of field test data. Due to the scatter of data and the lack of a theoretical basis, ground shock predictions by design manual procedures are generally unreliable. Windham et al.(1991) compared hydrocode and design manual predictions against measurements of ground shock produced by shallow-buried MK83 bombs, and showed that current design manual procedures are inadequate. On the other hand, the hydrocode prediction based on in-situ soil backfill properties compared very well with measured data.

The free-field stress and ground motion due to the design threat specified in Section III are predicted by using the hydrocode SABER-PC as well as design manual procedures. These predictions are then compared in Table 2.

The net explosive weight of a 500-pound GP bomb is equivalent to 242 pounds of TNT. The backfill material, selected from SABER-PC's soil model library, is a dense, dry sand having a dry unit weight of 105 pcf, solids specific gravity of 2.67, 4 percent water content at 18.3 percent saturation, and 30 percent of air-voids content. The porosity of this sand is 0.369 and the bulk unit weight is 109.5 pcf. The subsurface detonation is assumed to be fully-contained. This means that the depth of burial of the weapon is sufficiently large that relief waves from the free surface will not significantly alter the subsurface stress waves.

SABER-PC is a one-dimensional, spherically symmetric, large strain, explicit finite element hydrocode. Common explosives and many predefined soil models are available for use in a ground shock calculation. Profiles of the velocity and stress waves due to 242 pounds of TNT detonating in dry sand are shown in Figures 15 and 16, respectively. The peak velocity and stress attenuation with range are shown in Figures 17 and 18. The attenuation curves fall off more

36

TABLE 2. COMPARISON OF GROUND SHOCK PREDICTION ALGORITHMS

QUANTITY	SABER-PC	CONWEP	AF Manual	Westine	Drake et al.
Peak V_o (fps)	24.7	48	37.7	42.5	40
Peak P_o (psi)	670	2114	1520	105	1666
Peak d_o (in.)	1.4	11.3	8.3	9.6	2.8
Peak a_o (g)	—	2402	2020	—	20079
Attenuation n	2.37	2.5	2.5	3.42	2.1

37

242 lb TNT in Dry Sand
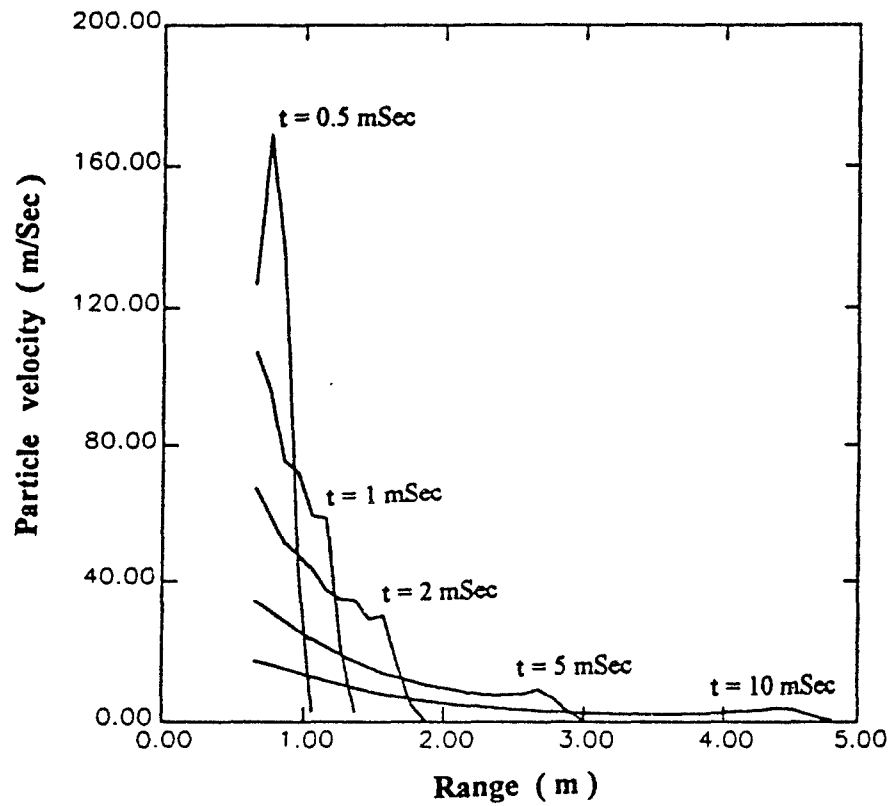
Figure 15. Radial Velocity Profile

242 lb TNT in Dry Sand
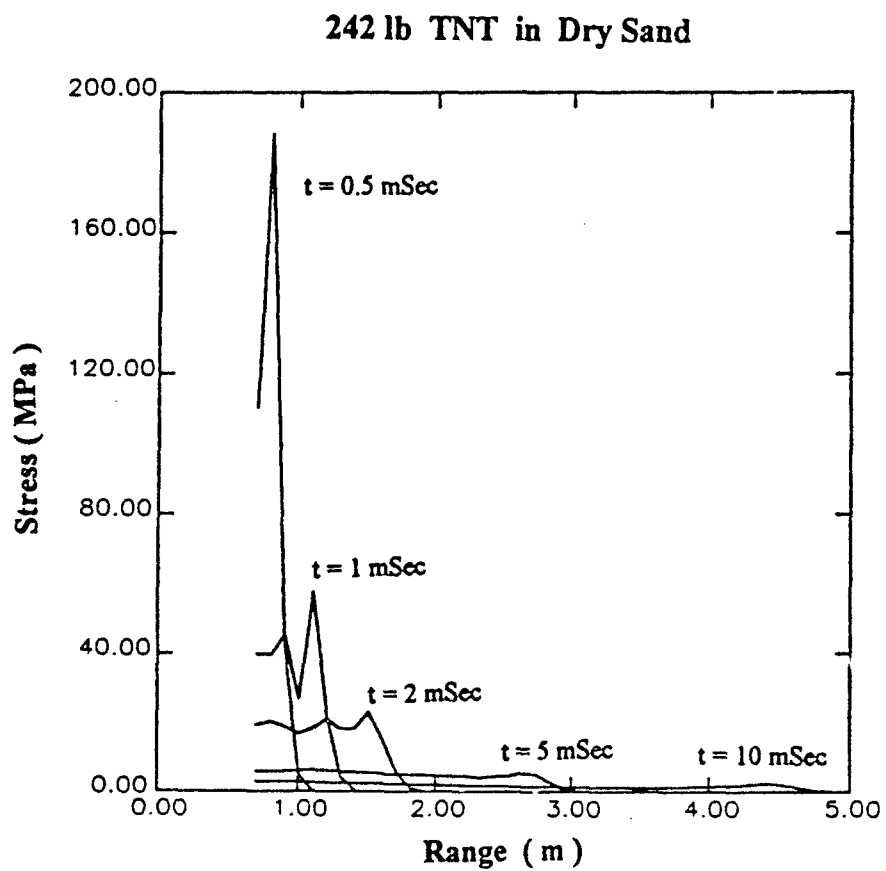
Figure 16.   Radial Stress Profile

39

242 lb TNT in Dry Sand
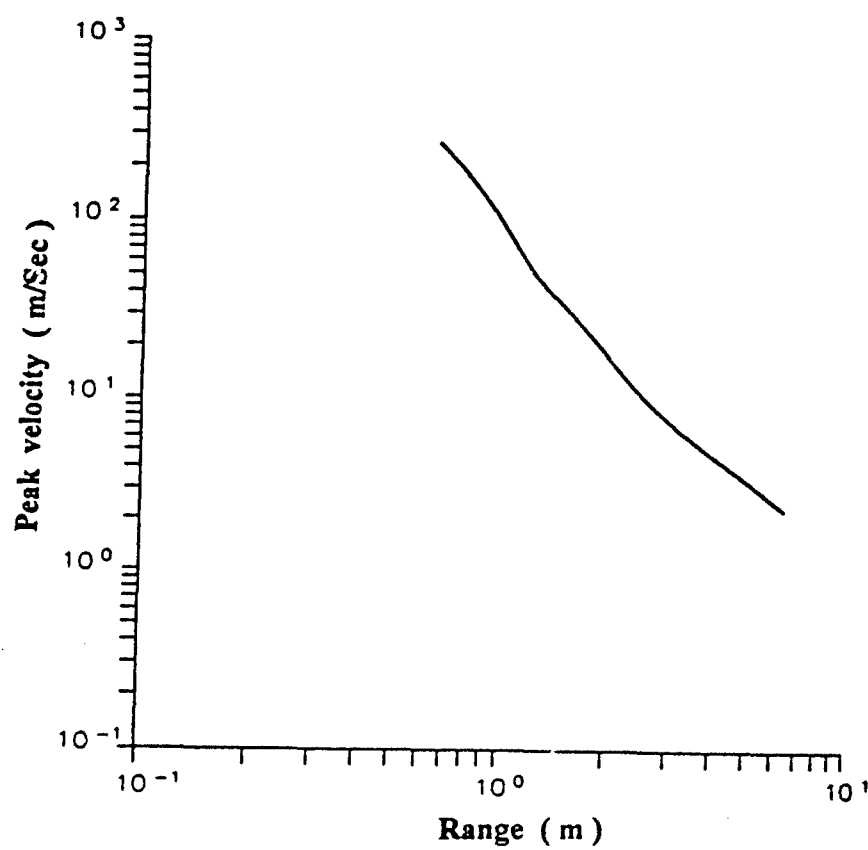
Figure 17. Radial Velocity Attenuation

242 lb TNT in Dry Sand
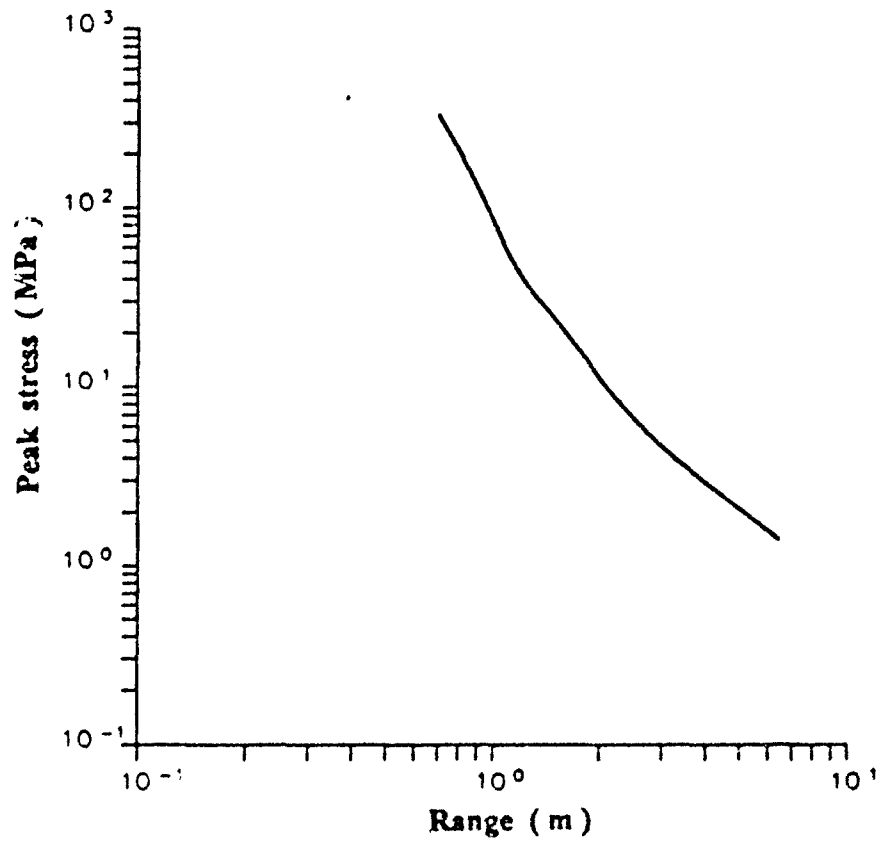
Figure 18. Radial Stress Attenuation

41

rapidly in the region near the explosion than in the region further away from the explosion. Time-histories of the free-field radial ground displacement, particle velocity and normal stress produced by the detonation at a standoff of 10 feet are shown in Figures 19, 20 and 21, respectively.

The Air Force Protective Construction Design Manual provides the following equations for predicting free-field stresses and ground motions from a bomb detonating on or within burster layers, or in the soil near a structure:

$$P_o = \rho_o c_L V_o = f \cdot \rho_o c_L \cdot \frac{160}{144} \cdot \left(\frac{R}{W^{1/3}} \right)^{-n}$$

$$V_o = f \cdot 160 \cdot \left(\frac{R}{W^{1/3}} \right)^{-n}$$

$$a_o \cdot W^{1/3} = f \cdot 50 \cdot c_L \cdot \left(\frac{R}{W^{1/3}} \right)^{-n-1}$$

$$\frac{d_o}{W^{1/3}} = f \cdot 500 \cdot \frac{1}{c} \cdot \left(\frac{R}{W^{1/3}} \right)^{-n+1}$$

$$\frac{I_o}{W^{1/3}} = f \cdot \rho_o \cdot \frac{c_L}{c} \cdot 1.1 \cdot \left(\frac{R}{W^{1/3}} \right)^{-n+1}$$

where P_o is the peak pressure in psi; f is the coupling factor for near-surface detonations; c_L is the loading wave velocity in fps; c is the seismic velocity in fps; R is the distance to the explosion in feet; W is the charge weight in pounds of C-4, V_o is the peak particle velocity in fps; a_o is the peak acceleration in g's; d_o is the peak displacement in feet; I_o is the peak impulse in lb-sec/in^2; ρ_o is the mass density of soil in lb-sec^2/ft^4 = γ / g; and n is the attenuation coefficient.

Typical soil properties are given in the Air Force Design Manual. For the dry sand under consideration, the seismic velocity c = 1600 fps, and the attenuation coefficient n = 2.5. The equivalent charge factor for converting TNT to C-4 is 0.73. Thus the charge weight W = 242 × 0.73 = 177 pounds of C-4. The ground shock coupling factor f is 1.0 for a fully-contained explosion, and the peak particle velocity is computed as:

Free−field Radial Displacement

(Range = 10 feet)
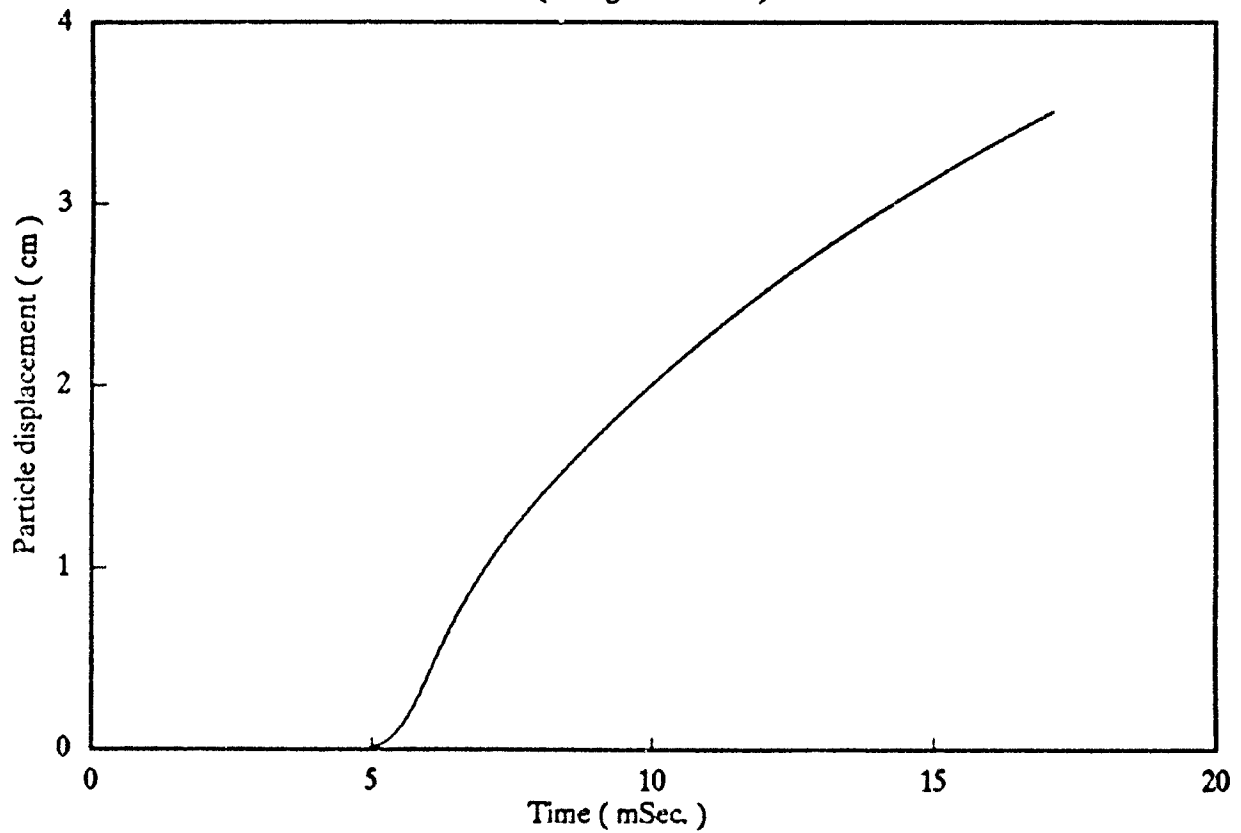
Figure 19. Free-Field Soil Radial Displacement

43

Free-field Particle Velocity
(Range = 10 feet)
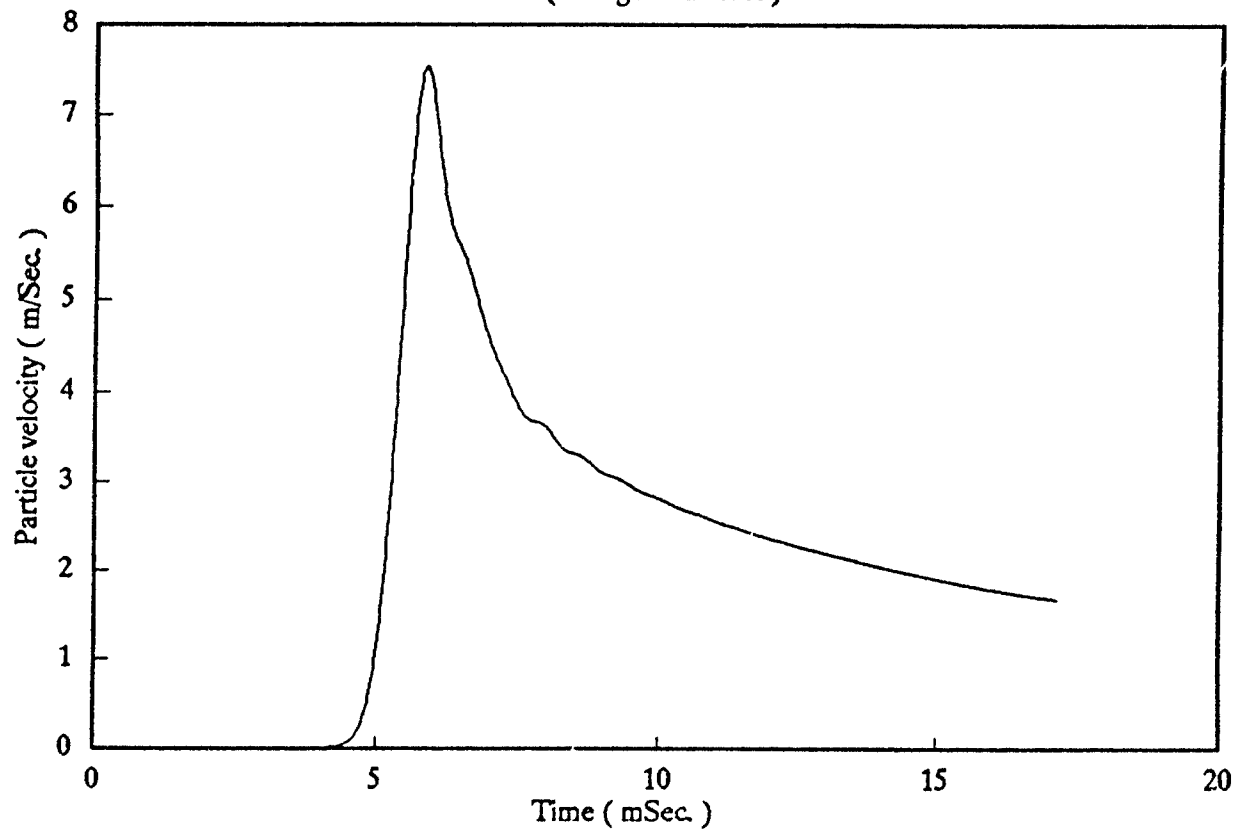
Figure 20.   Free-Field Soil Particle Velocity

44

Free-field Radial Stress
(Range = 10 feet)
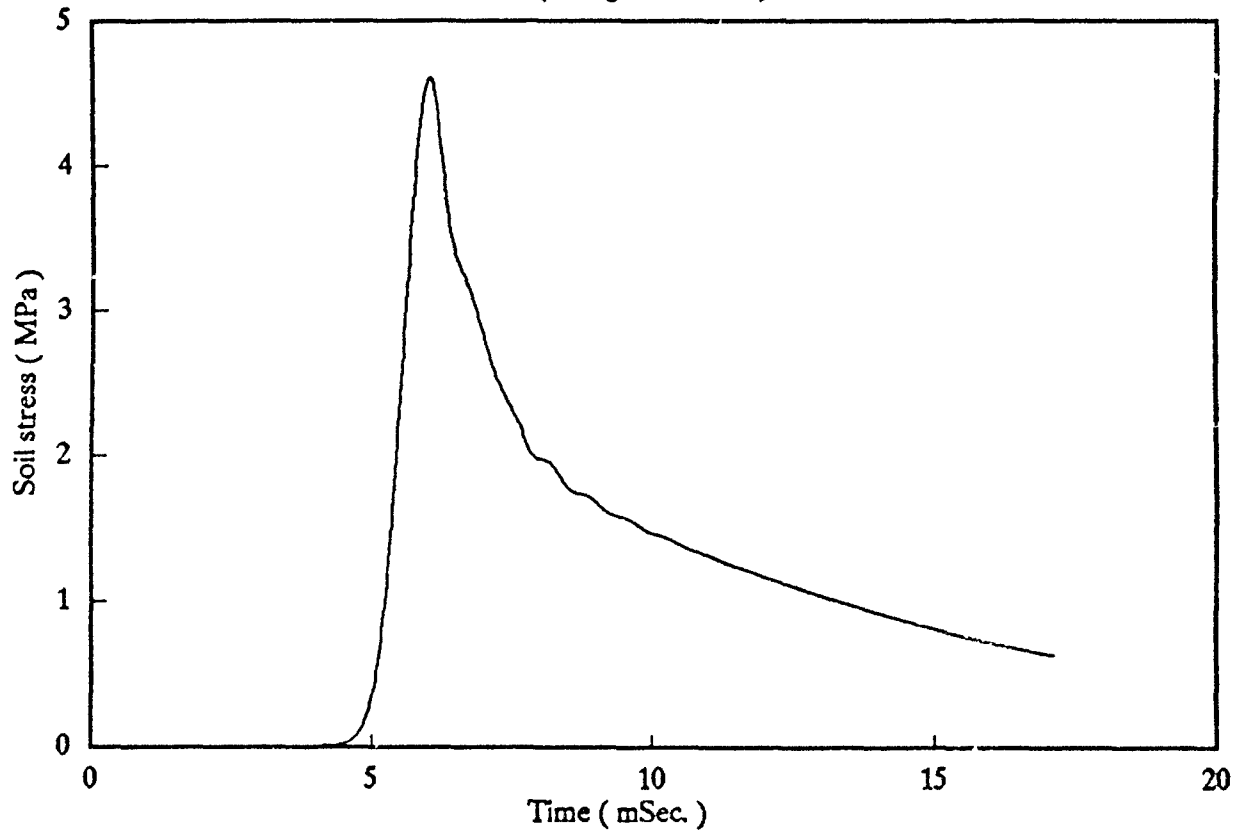
Figure 21.   Free-Field Soil Radial Stress

$$V_o = (1.0)(160)\left(\frac{10}{177^{1/3}}\right)^{-2.5} = 37.7 \quad \text{fps}$$

The loading wave velocity was estimated to be $c_L = 1713$ fps. The peak free-field stress is computed as:

$$P_o = (1.0)\left(\frac{109}{32.2}\right)(1713)\left(\frac{160}{144}\right)\left(\frac{10}{177^{1/3}}\right)^{-2.5} = 1520 \quad \text{psi}$$

The peak free-field ground acceleration is computed as:

$$a_o = (1.0)(50)(1713)\left(\frac{10}{177^{1/3}}\right)^{-3.5}(177)^{-1/3} = 2020 \quad \text{g}$$

The peak free-field ground displacement is computed as:

$$d_o = (1.0)(500)\left(\frac{1}{1713}\right)\left(\frac{10}{177^{1/3}}\right)^{-1.5}(177)^{1/3} = 0.69 \quad \text{feet}$$

The peak impulse is computed as:

$$I_o = (1.0)\left(\frac{109}{32.2}\right)\left(\frac{1713}{1600}\right)(1.1)\left(\frac{10}{177^{1/3}}\right)^{-1.5}(177)^{1/3} = 9.4 \quad \text{lb-sec/in}^2$$

The ground shock prediction procedures in the Department of Energy Protective Design Manual (DOE/TIC-11268) are based on the work of Westine(1978). Two equations are proposed to determine the radial displacement and radial particle velocity for buried explosive point sources:

$$\frac{X}{R}\left(\frac{P_o}{\rho_s c_p^2}\right)^{1/2} = \frac{0.04143\left(\frac{E}{\rho_s c_p^2 R^3}\right)^{1.105}}{\tanh^{1.5}\left[18.24\left(\frac{E}{\rho_s c_p^2 R^3}\right)^{0.2367}\right]} \tag{36}$$

46

$$\frac{U}{c_p}\left(\frac{P_o}{\rho_s c_p^2}\right)^{1/2} = \frac{6.169\times10^{-3}\left(\dfrac{E}{\rho_s c_p^2 R^3}\right)^{0.8521}}{\tanh\left[26.03\left(\dfrac{E}{\rho_s c_p^2 R^3}\right)^{0.30}\right]} \qquad (37)$$

where, using consistent units, X is the maximum radial soil displacement; U is the peak radial soil particle velocity; P_o is the atmospheric pressure; R is the standoff distance from the explosive; E is the explosive energy release; ρ_s is the mass density of the soil or rock; and c_p is the seismic P-wave velocity in the soil or rock.

Westine and Friesenhahn (1982) proposed an empirical equation for predicting free-field ground shock pressure from the detonation of a buried ordnance:

$$\frac{\left(\dfrac{P}{\rho c^2}\right)}{\left(4.35+\dfrac{Y}{d}\right)\left[0.25+0.75\tanh\left(0.48\cdot\dfrac{\rho^{1/3}c^{2/3}d}{E^{1/3}}\right)\right]} = 0.0175\left(\frac{\rho^{1/3}c^{2/3}R_{eff}}{E^{1/3}}\right)^{-3.42} \qquad (38)$$

where P is the maximum pressure; ρ is the soil's mass density; c is the speed of sound in the soil; d is the depth of burial of the weapon's center of gravity (C.G.); Y is the depth of the point of interest below the weapon's C.G.; E is the weapon's energy release; and R_{eff} is the effective slant range which accounts for weapon geometry and orientation. The effective standoff distance, R_{eff} is the distance at which a point explosive charge of the same weight will yield the same peak free-field pressure as the weapon at some angle. This effective range is given by

47

$$\frac{R_{eff}}{l} = \left[\frac{M - N^2 - \dfrac{1}{4}}{\dfrac{N+1/2}{(M+N)^{1/2}} - \dfrac{N-1/2}{(M-N)^{1/2}}} \right]^{1/3} \tag{39}$$

$$M = \left(\frac{Z}{l}\right)^2 + \left(\frac{X}{l}\right)^2 + \left(\frac{Y}{l}\right)^2 + \frac{1}{4} \tag{40}$$

$$N = \left(\frac{Y}{l}\right)\cos\theta + \left(\frac{Z}{l}\right)\sin\theta \tag{41}$$

where Z is the distance from the weapon C.G. to a vertical plane containing the point of interest; X and Y are the horizontal and vertical coordinates, measured in that vertical plane, from the point of interest to the point nearest the weapon C.G.; l is the weapon length; and θ is the weapon axis vertical inclination ($\theta = 0°$ corresponds to a vertical weapon axis).

The energy release per unit weight of TNT is 1.51×10^6 $ft \cdot lb / lb$. For the case under consideration, $E = 1.51 \times 10^6 \times 242 = 3.65 \times 10^8$ $ft \cdot lb$; $R_{eff} = 10$ feet; $\rho = 109/32.2 = 3.385$ $lb \cdot Sec^2 / ft^4$; $c = 1600$ fps; $Y = 0$; and $d = 8$ feet. The maximum radial ground displacement and particle velocity are computed to be 9.6 inches. and 42.5 fps, respectively, using Equations (36) and (37). The peak free-field ground shock pressure is calculated to be 105 psi using Equation (38).

Empirical fits were also made by Drake et al.(1989) to peak ground motion and stress data obtained from contained high explosive (HE) detonations in soil and to results of finite difference calculations in various soil and rock geologies. The resulting expressions are

$$a_p = \frac{2 \cdot v_p}{g \cdot t_r} \qquad r \leq 0.155 \cdot W^{1/3} \tag{42}$$

48

$$v_p = \begin{cases} \dfrac{606.2}{\sqrt{\rho_o}} \left(\dfrac{r}{W^{1/3}} \right)^{-3/2} & r \le 0.155 \cdot W^{1/3} \\[3mm] \dfrac{9906}{\sqrt{\rho_o}} \left(\dfrac{r}{r_c} \right)^{-n} & r > 0.155 \cdot W^{1/3} \end{cases} \tag{43}$$

$$\frac{d_p}{W^{1/3}} = \frac{3.31}{c_i} \left(\frac{r}{W^{1/3}} \right)^{-2} \qquad r > 0.155 \cdot W^{1/3} \tag{44}$$

$$\sigma_p = \rho_o \cdot c_L \cdot v_p \tag{45}$$

where

$$r_c = 0.155 \cdot W^{1/3} \tag{46}$$

$$c_L = c_o + s \cdot v_p \tag{47}$$

$$t_r = \left(\frac{c_i}{c_L} - 1 \right) \frac{r}{c_i} \qquad c_i > c_L \tag{48}$$

Here W is the contained yield of the weapon in *kg of TNT*; v_p is the peak particle velocity in *m/s*; a_p is the peak radial acceleration in *g's*; d_p is the peak displacement in *meters*; σ_p is the peak stress in *Pa*; r is the radial distance from the explosion in *meters*; g is gravitational acceleration ($9.8 \ m/s^2$); n is the peak velocity attenuation exponent; s is an equation of state factor (≈ 1.5 for geologic media); and t_r is the rise time in *sec*.

For the case under consideration, $r = 3.048$ *meters*, and $W = 109.8$ *kg of TNT*. Therefore, $r > 0.155 \cdot W^{1/3}$. The in-situ soil density is $\rho_o = 1750 \ kg/m^3$, which is equivalent to a unit weight of 109 *pcf*. For this dense, dry sand, the initial loading wavespeed is $c_o = 520 \ m/s$, the seismic wavespeed is $c_i = 550 \ m/s$, and the velocity attenuation exponent is $n = 2.1$. The peak particle velocity is computed using Equations (43) and (46):

49

$$v_p = \frac{9906}{\sqrt{1750}} \left(\frac{3.048}{0.155 \times 109.8^{1/3}} \right)^{-2.1} = 12.2 \ m/s$$

Applying Equation (47), the loading wavespeed is

$$c_L = 520 + 1.5 \times 12.2 = 538 \ m/s.$$

Applying Equation (48), the rise time of the shock wave is

$$t_r = \left(\frac{550}{538} - 1 \right) \frac{3.048}{550} = 1.24 \times 10^{-4} \ sec$$

Applying Equation (42), the peak ground acceleration is

$$a_p = \frac{2 \times 12.2}{9.8 \times 1.24 \times 10^{-4}} = 20079 \ g$$

Applying Equation (44), the peak ground displacement is

$$d_p = \frac{3.31}{550} \left(\frac{3.048}{109.8^{1/3}} \right)^{-2} \times 109.8^{1/3} = 0.07 \ m$$

Applying Equation (45), the peak stress is

$$\sigma_p = 1750 \times 538 \times 12.2 = 11.49 \times 10^6 \ Pa$$

CONWEP, a computer program based on the Army Protective Design Manual (TM 5-855-1), was also used to predict the ground shock parameters for comparison. These results are summarized in Table 2.

B. SAP90™ FINITE ELEMENT PROGRAM

A series of computer programs for structural analysis has been developed by Professor Edward L. Wilson and co-workers at the University of California, Berkeley, over the past twenty-five years. The name SAP, standing for Structural Analysis Package, was coined in 1970 with the release of the first SAP program for mainframe computers. In the years that followed, further research and development in the area of finite element formulation and numerical solution techniques resulted in the release of SOLIDSAP, SAP3 and SAP IV. Since the release of SAP IV, major advances have occurred in the fields of numerical analysis, structural mechanics and

computer technology. These advances led to the release of SAP80, the first microcomputer version of SAP, and to the release of SAP90^{TM}.

SAP90^{TM} has static and dynamic analysis options. The finite element library consists of four elements: a three-dimensional frame element, a shell element, a two-dimensional solid element and a three-dimensional solid element. The two-dimensional frame, truss, membrane, plate bending, axisymmetric and plane strain elements are available as degenerated elements. A boundary element, in the form of spring supports, is also included. All material behaviors are linearly elastic. Dynamic loading can be in the form of a base acceleration response spectrum, or time-varying loads and base accelerations.

C. GEOMETRIC EFFECTS OF WALL PANEL CONFIGURATIONS

Three-dimensional finite-element analyses using SAP90^{TM} have been conducted to study the effects on the structural behavior of the panel connection system due to different panel configurations. In this study, the only attribute varied was the panel geometry.

A 15.7 feet wide by 13.5 feet tall segment of a retaining wall, made with interlocking modular panels commonly used in highway construction, was selected for comparative studies. The patented rectangular panel used in the full-scale reinforced soil bunker test (Reid 1991) was selected as the baseline configuration. The construction detail and dimensions of this panel were previously shown in Figure 8. Hexagonal panels having the same facial area, and rectangular blocks staggered in a masonry construction configuration were also included in the studies. These configurations were previously illustrated in Figure 1.

The wall segment was assumed to be simply supported at the top and bottom, and the edge effects due to its finite width were ignored. The modular wall panels and blocks were assumed to be 7 in. thick, and made of reinforced concrete having a unit weight of 150 pcf. Each panel or block was modeled with shell elements having membrane as well as bending stiffness. The panels were pinned together at certain boundary nodes where shear connectors were located. Boundary elements in the form of spring supports were used to model the soil reinforcement, which was kept the same in all cases. Figures 22 to 24 show the finite element meshes of these panel configurations, where the dots denote locations of soil reinforcement. The soil reinforcement was assumed to have a spring constant of 500 *lb/in.* and all the structural systems were assumed to have 5% critical damping.

51

Y → **X**
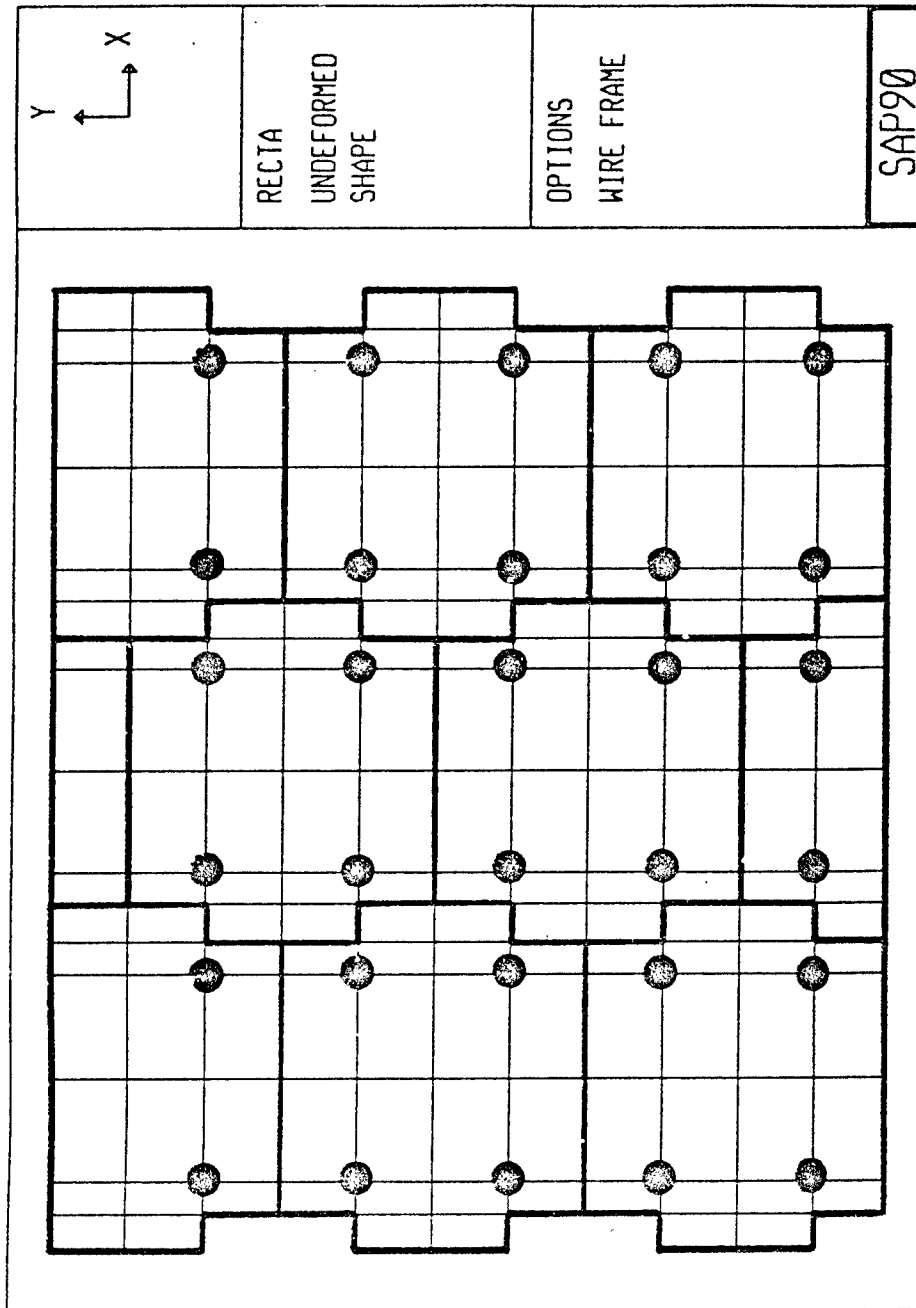
RECTA
UNDEFORMED
SHAPE

OPTIONS
WIRE FRAME

SAP90

Figure 22. SAP90™ Finite Element Mesh of Rectangular Wall Panel Configuration
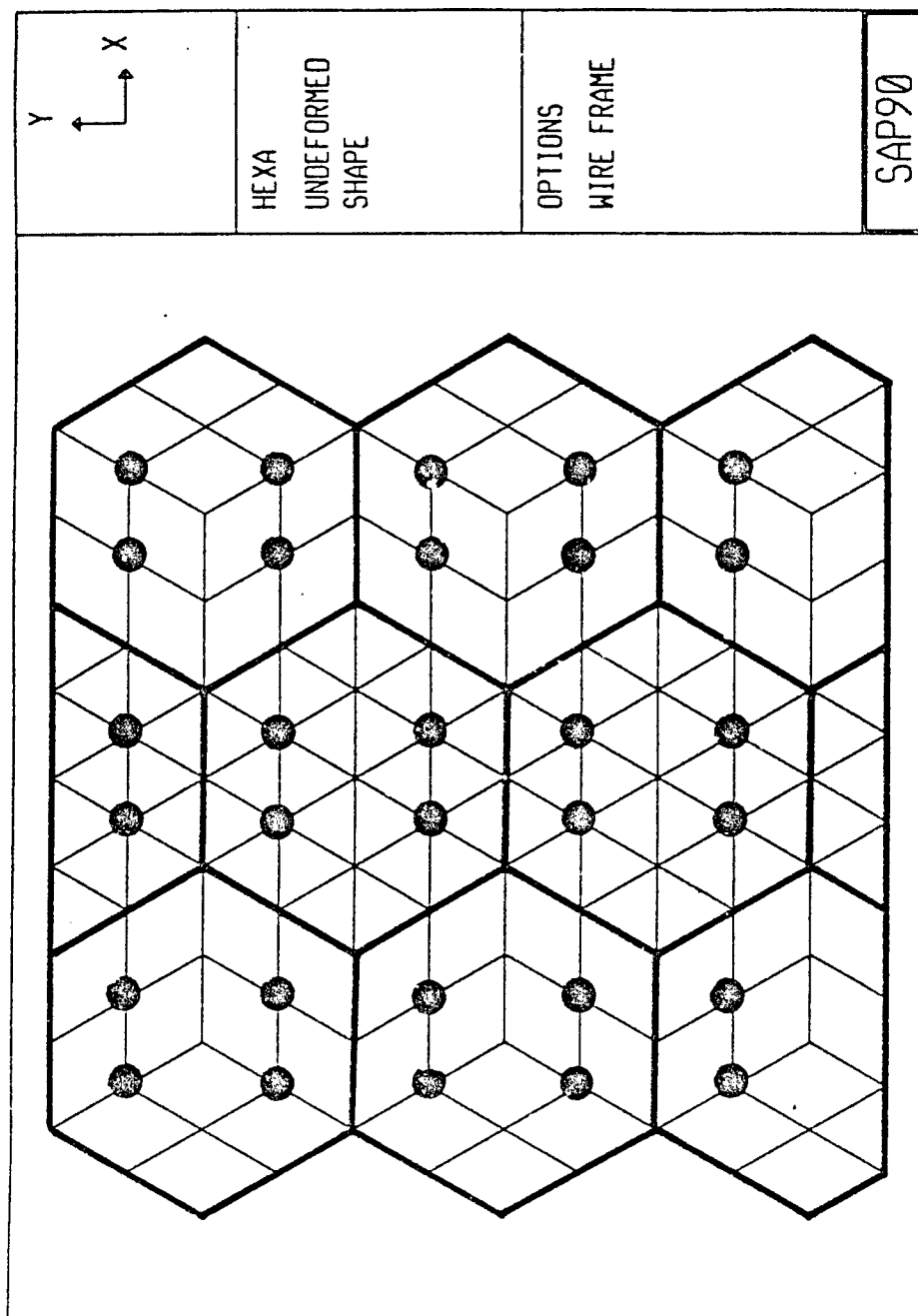
Figure 23. SAP90™ Finite Element Mesh of Hexagonal Wall Panel Configuration
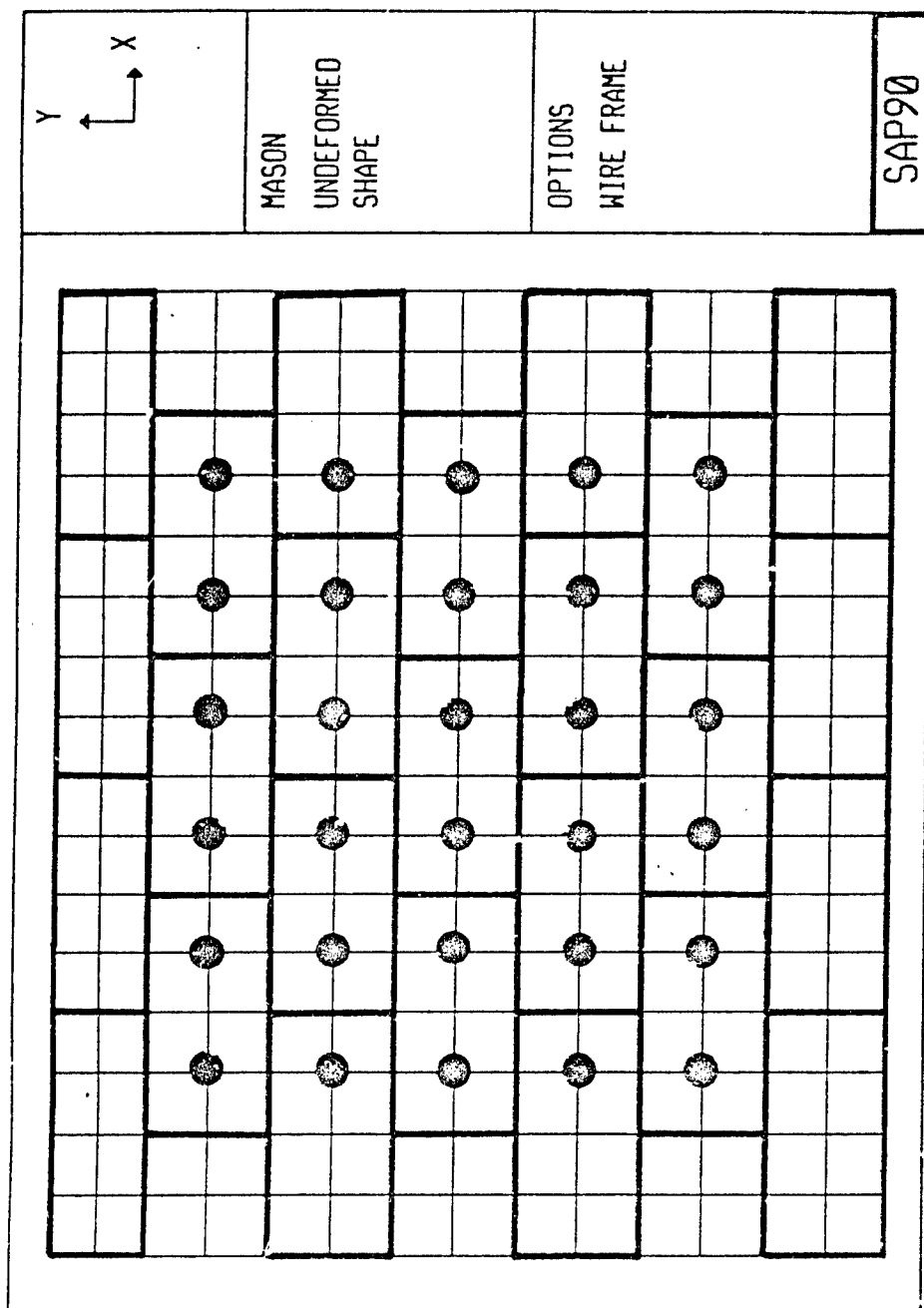
Figure 24. SAP90™ Finite Element Mesh of Masonry Wall Configuration

The transient dynamic structural responses of these configurations under the ground shock loading due to the specified threat were obtained for a duration of 200 ms. The ground shock was modeled as time-varying pressure loading on the panels. Both the spatial and temporal variations of the pressure distribution were considered. The point of detonation was assumed to be at midheight of the wall segment, at a standoff of 10 feet from the wall. The shock front had a peak pressure of 813 psi, arriving at 3.9 ms and decaying to 495 psi when it reached the edges of the wall at 5.6 ms. These ground shock parameters were obtained using SABER-PC and then adjusted for the presence of soil reinforcement.

Since only the peak response parameters of these structural systems are of concern, the analyses were carried out for a short duration. It was assumed that the panels stayed in contact with the soil during the loading phase, and that the peak response occurred shortly after the panels became separated from the soil. Figures 25 to 33 display the displacement, velocity and acceleration time histories for the rectangular panel, hexagonal panel and masonry block configurations, respectively. Figures 34 to 36 display the deformed shapes of these configurations. A summary of the geometric effects of these connection systems on the peak response parameters is given in Table 3.

Rectangular blocks arranged in a masonry wall configuration can significantly reduce the joint forces and moments, and consequently enhance the survivability of the wall. Further analyses of a 16 feet wide by 16 feet tall retaining wall segment were conducted to determine the optimum aspect ratio and thickness of the blocks in order to minimize the shear and moment at the connection points. The aspect ratio (height to width) of the blocks was varied at 1:1, 1:2 and 1:3. The thickness of the blocks was varied from 3 inches to 12 inches in increments of 1 inch. All other parameters were kept unchanged. The blocks were assumed to be 4-foot wide, pin-connected at the joints along each course or horizontal layer. Each block had two vertical reinforcing bars running through horizontal layers to provide shear and moment resistance. These reinforcing bars were assumed to be placed at the quarter points so that they were spaced at 2-foot intervals.

Figures 37 and 38 illustrate the influence on the peak shear and moment at critical panel connection points due to variations of the panel aspect ratio and thickness. Figure 37 clearly shows that the optimum panel should have an aspect ratio of 1:2 and a thickness of 8 inches to
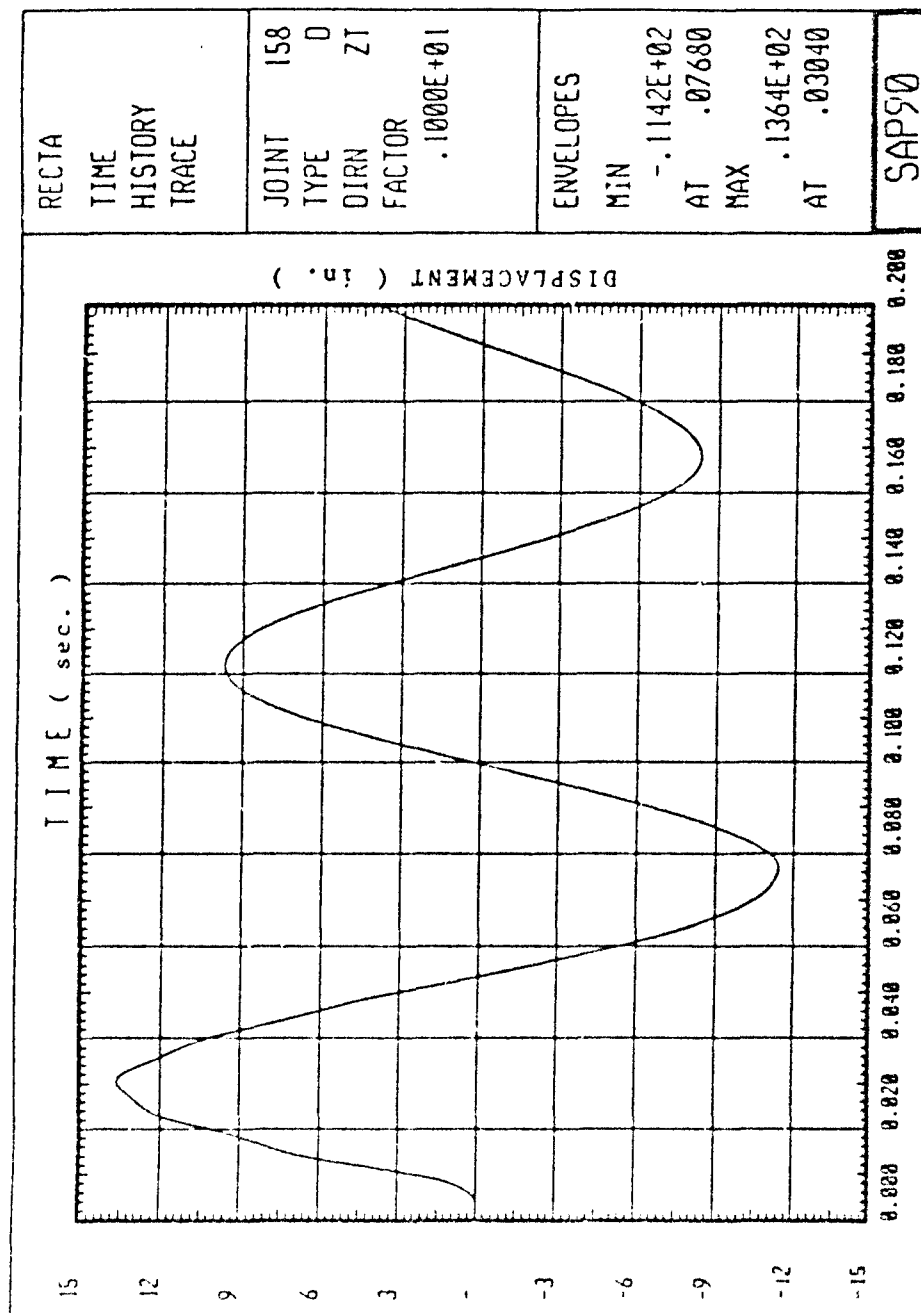
Figure 25. Displacement Time-history at the Center of Rectangular Wall Configuration

56
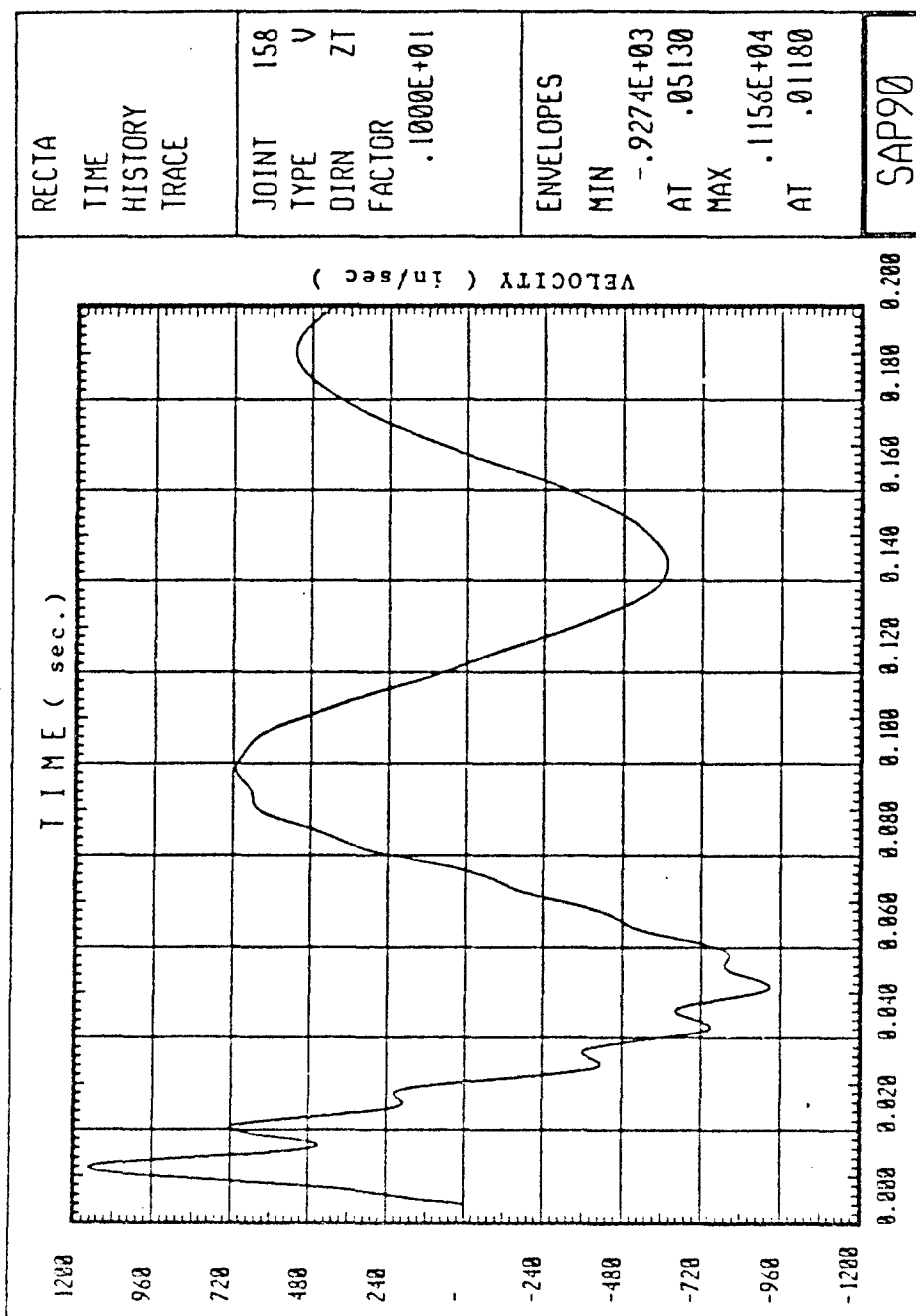
Figure 26. Velocity Time-history at the Center of Rectangular Wall Configuration

57
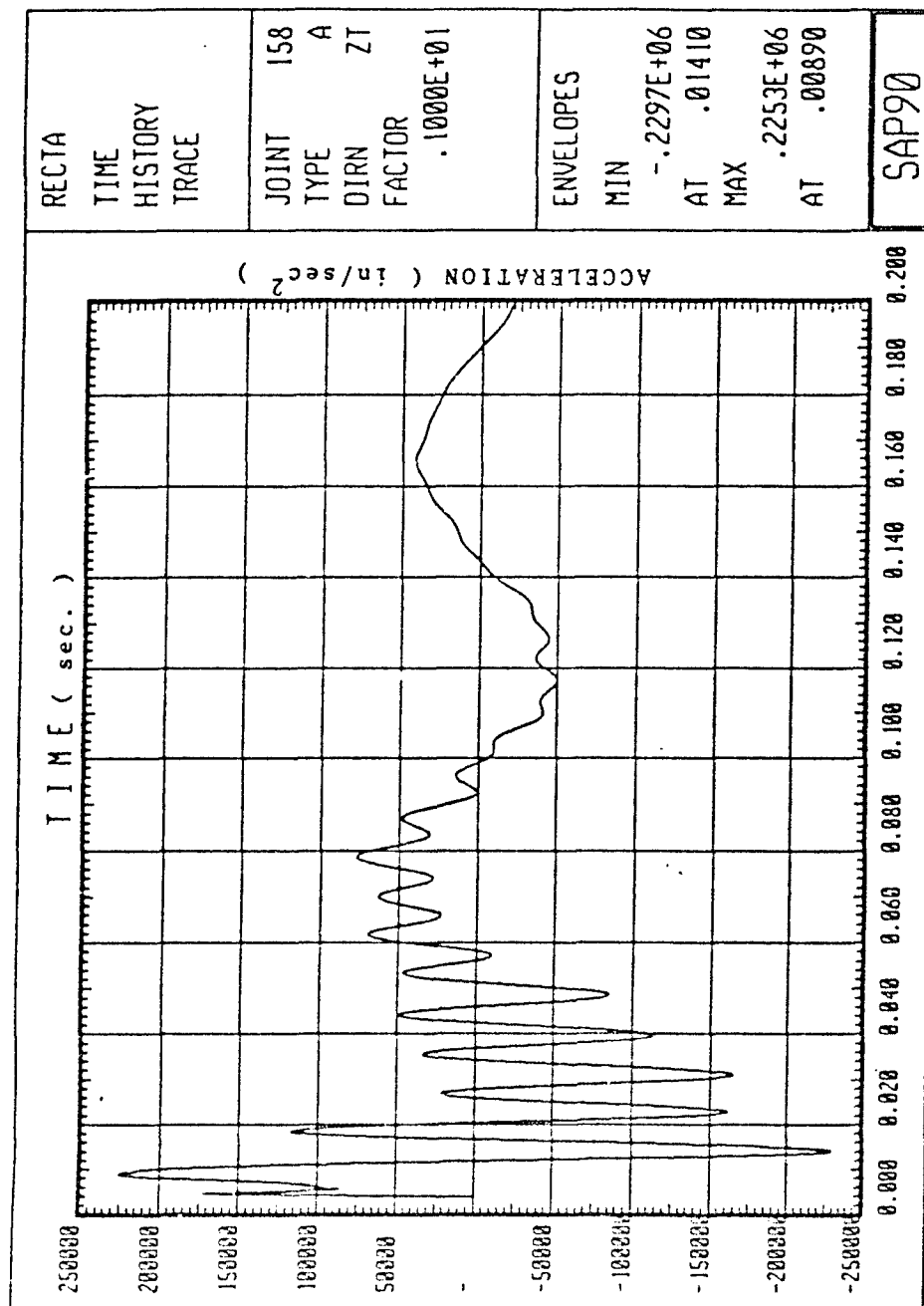
Figure 27. Acceleration Time-history at the Center of Rectangular Wall Configuration
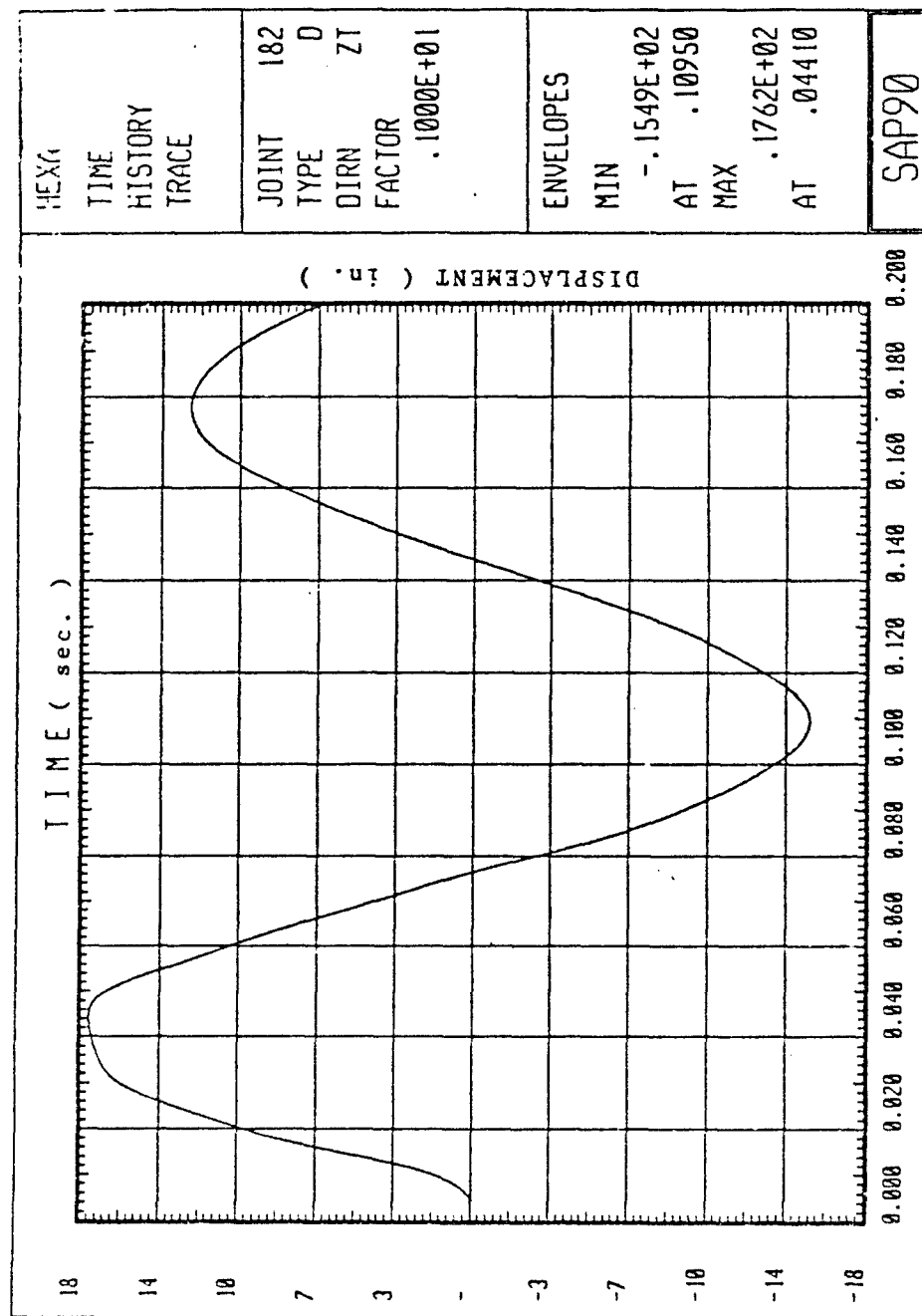
Figure 28. Displacement Time-history at the Center of Hexagonal Wall Configuration

HEXA
TIME
HISTORY
TRACE

JOINT 182
TYPE   V
DIRN   ZT
FACTOR .1000E+01

ENVELOPES
MIN   -.8414E+03
AT   .07920
MAX   .1055E+04
AT   .01470

SAP90

VELOCITY (in/sec)

TIME (sec.)

1200 960 720 480 240 - -240 -480 -720 -960 -1200

0.000 0.020 0.040 0.060 0.080 0.100 0.120 0.140 0.160 0.180 0.200
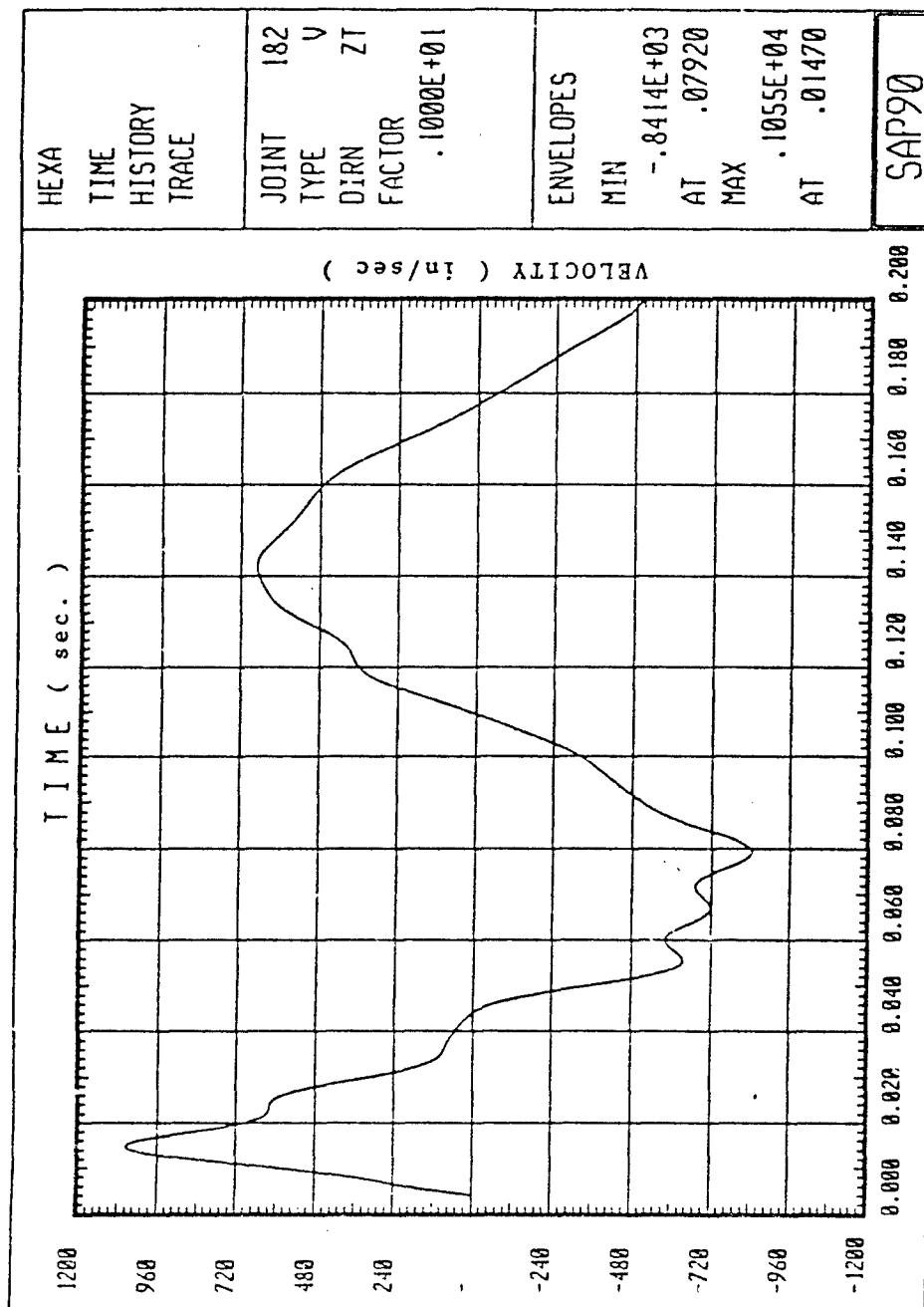
Figure 29. Velocity Time-history at the Center of Hexagonal Wall Configuration
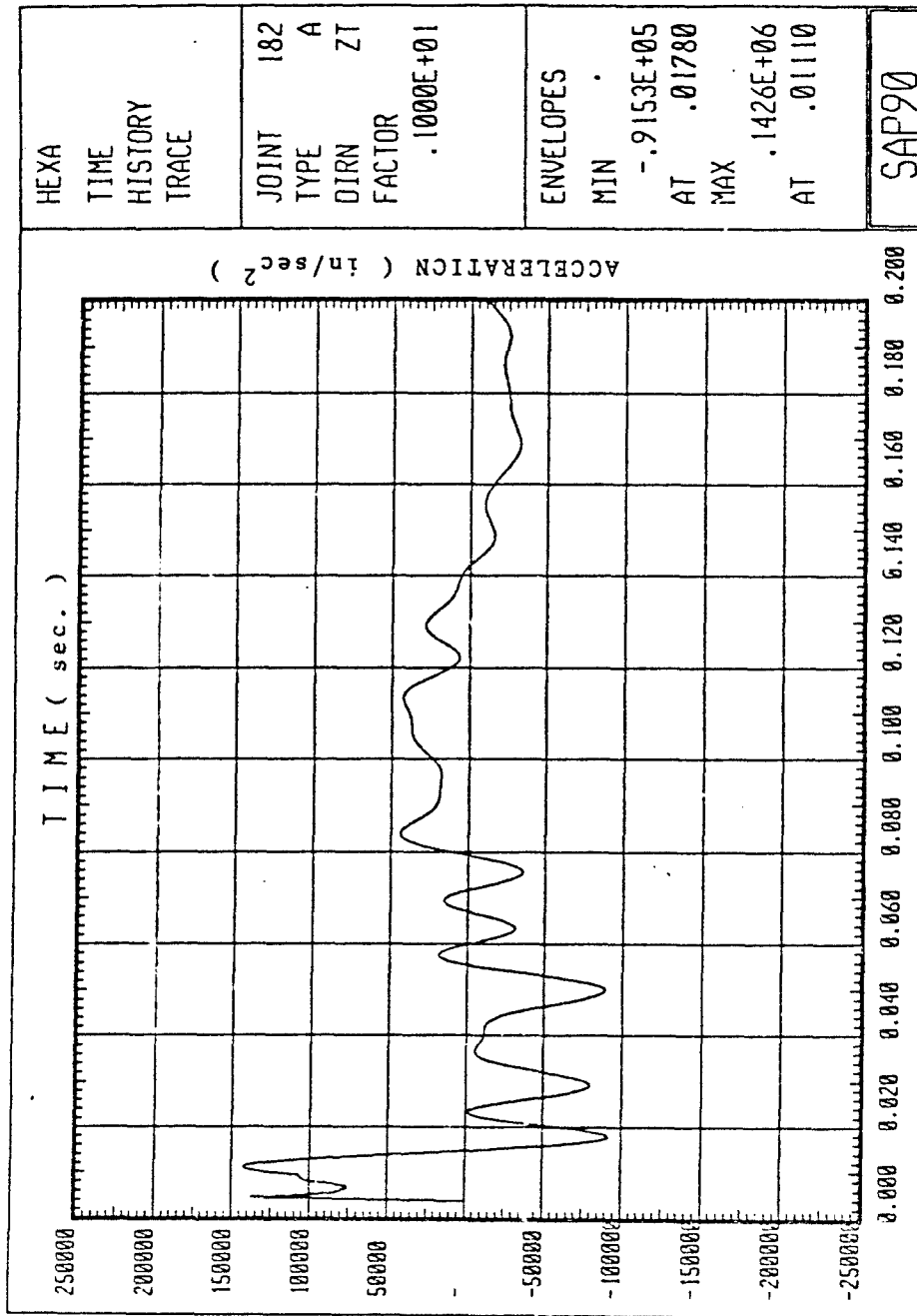
Figure 30. Acceleration Time-history at the Center of Hexagonal Wall Configuration

61

MASON
TIME
HISTORY
TRACE

JOINT 215
TYPE   0
DIRN   ZT
FACTOR .1000E+01

ENVELOPES
MIN   -.1045E+02
AT   .06860
MAX   .1206E+02
AT   .02630

SAP90

DISPLACEMENT (in.)

TIME (sec.)
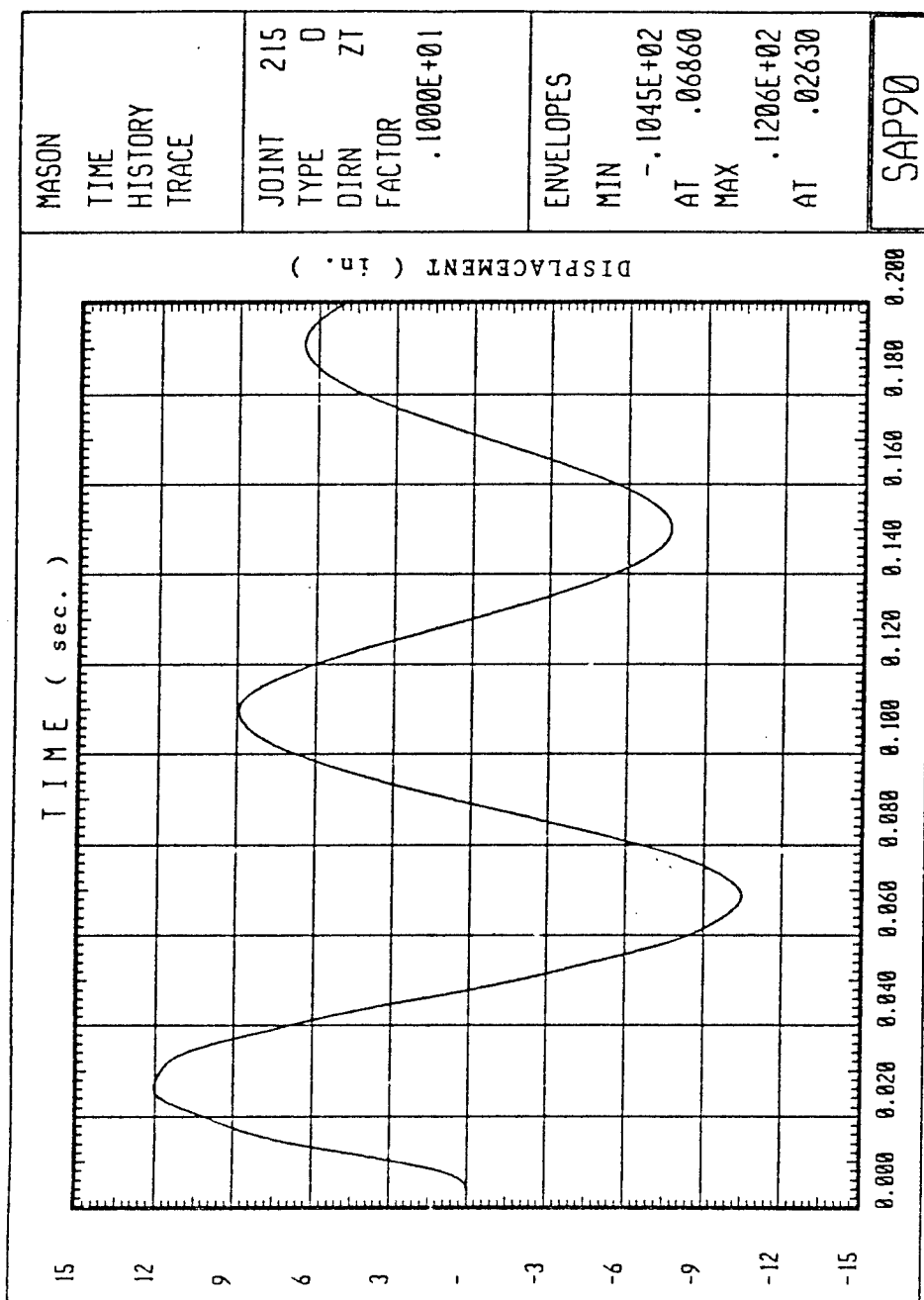
Figure 31. Displacement Time-history at the Center of MasonryWall Configuration

MASON
TIME
HISTORY
TRACE

JOINT 215 V
TYPE V
DIRN ZT
FACTOR .1000E+01

ENVELOPES
MIN -.9758E+03
AT .04620
MAX .1041E+04
AT .01190

SAP90

VELOCITY (in/sec)

TIME (sec.)

0.000 0.020 0.040 0.060 0.080 0.100 0.120 0.140 0.160 0.180 0.200

1200 960 720 480 240 - -240 -480 -720 -960 -1200
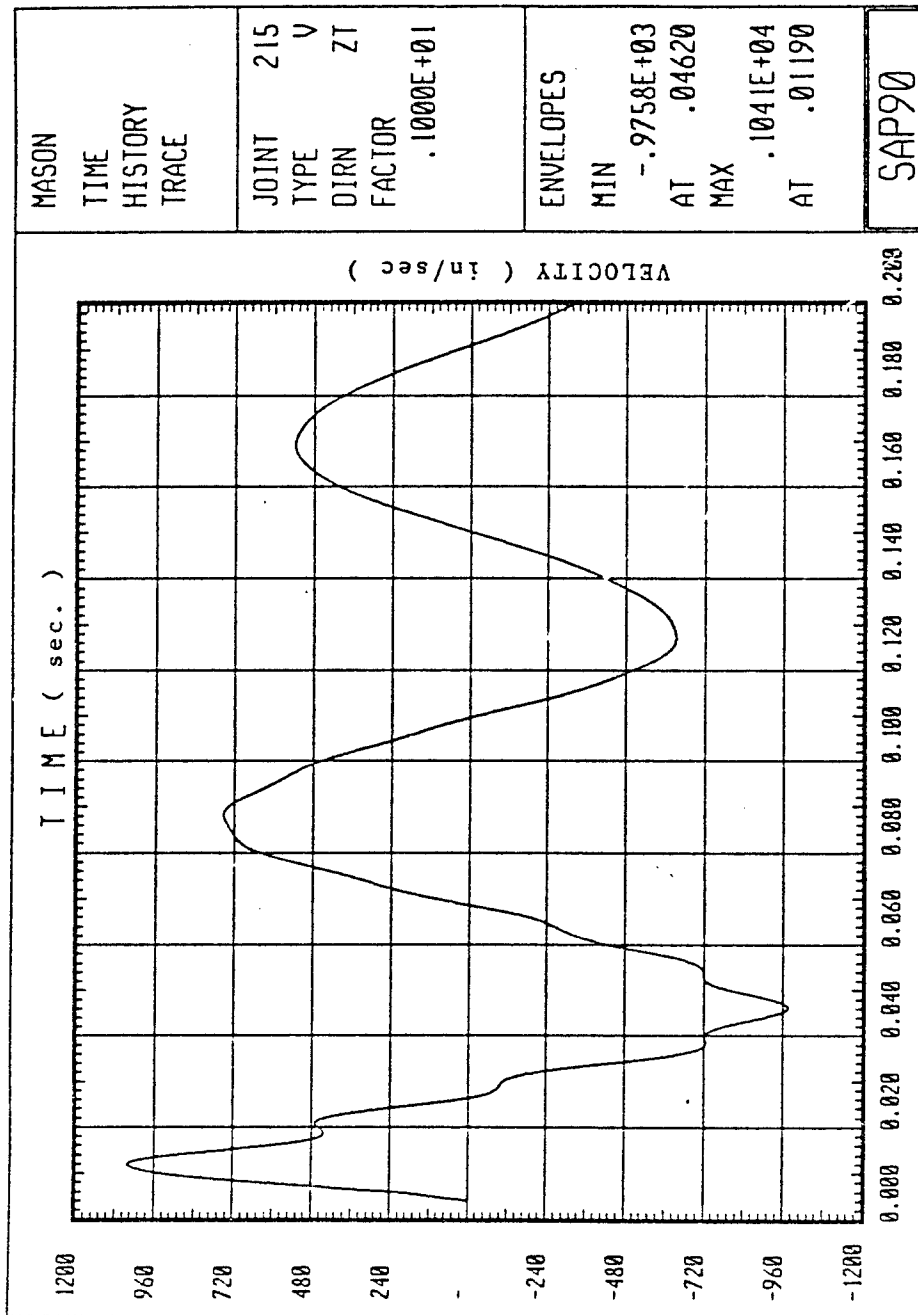
Figure 32. Velocity Time-history at the Center of Masonry Wall Configuration

63

MASON		
TIME		
HISTORY		
TRACE		
JOINT	215	
TYPE	A	
DIRN	ZT	
FACTOR	.1000E+01	
ENVELOPES		
MIN		
-.1490E+06		
AT	.01490	
MAX		
.2423E+06		
AT	.00630	
SAP90		

ACCELERATION (in/sec²)

TIME (sec.)
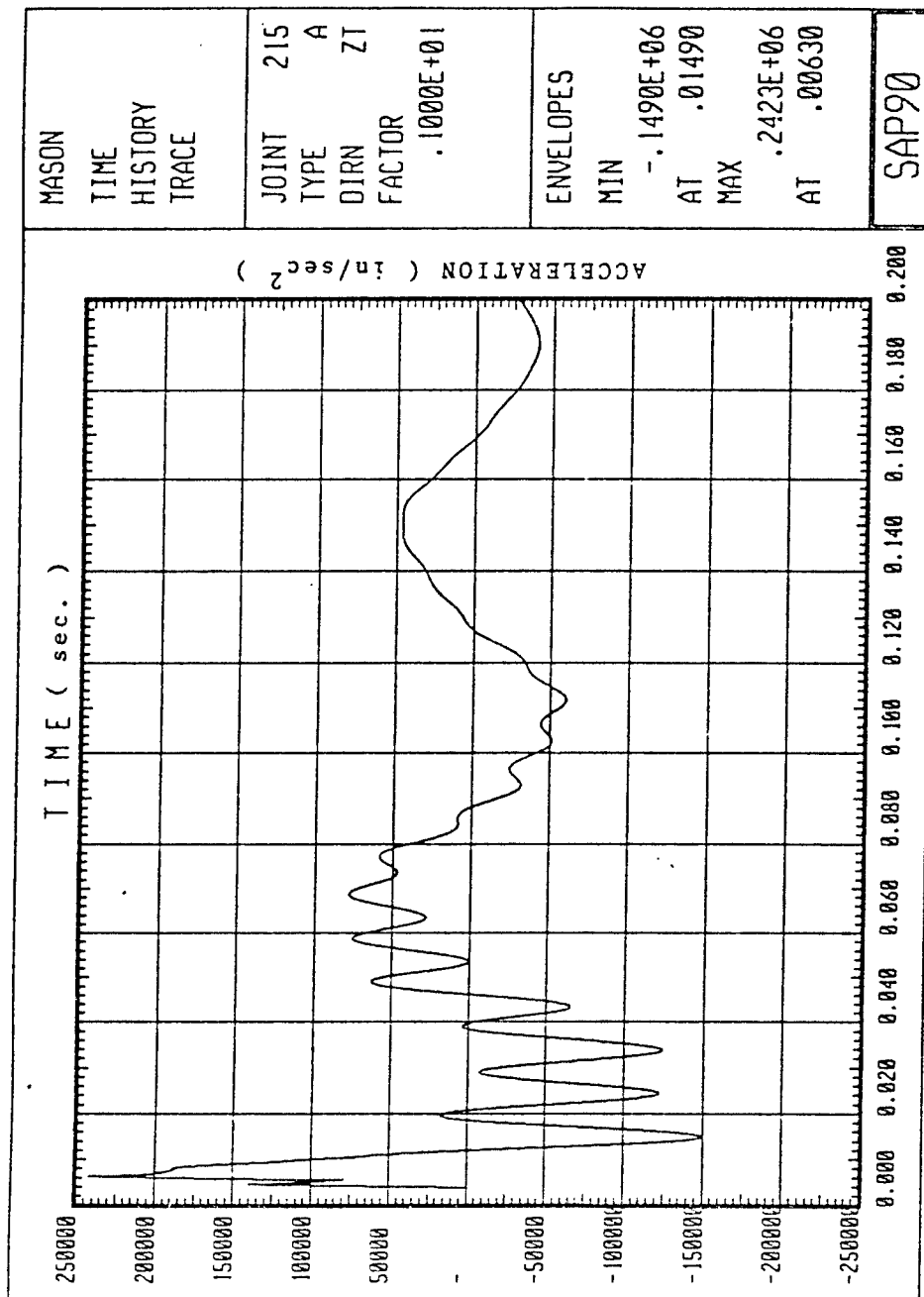
Figure 33. Acceleration Time-history at the Center of Masonry Wall Configuration

64

RECTA
DEFORMED
SHAPE
LOAD   1

MINIMA
X -.3128E-04
Y -.1413E-03
Z .0000E+00
MAXIMA
X .3128E-04
Y .0000E+00
Z .8951E+02

SAP90
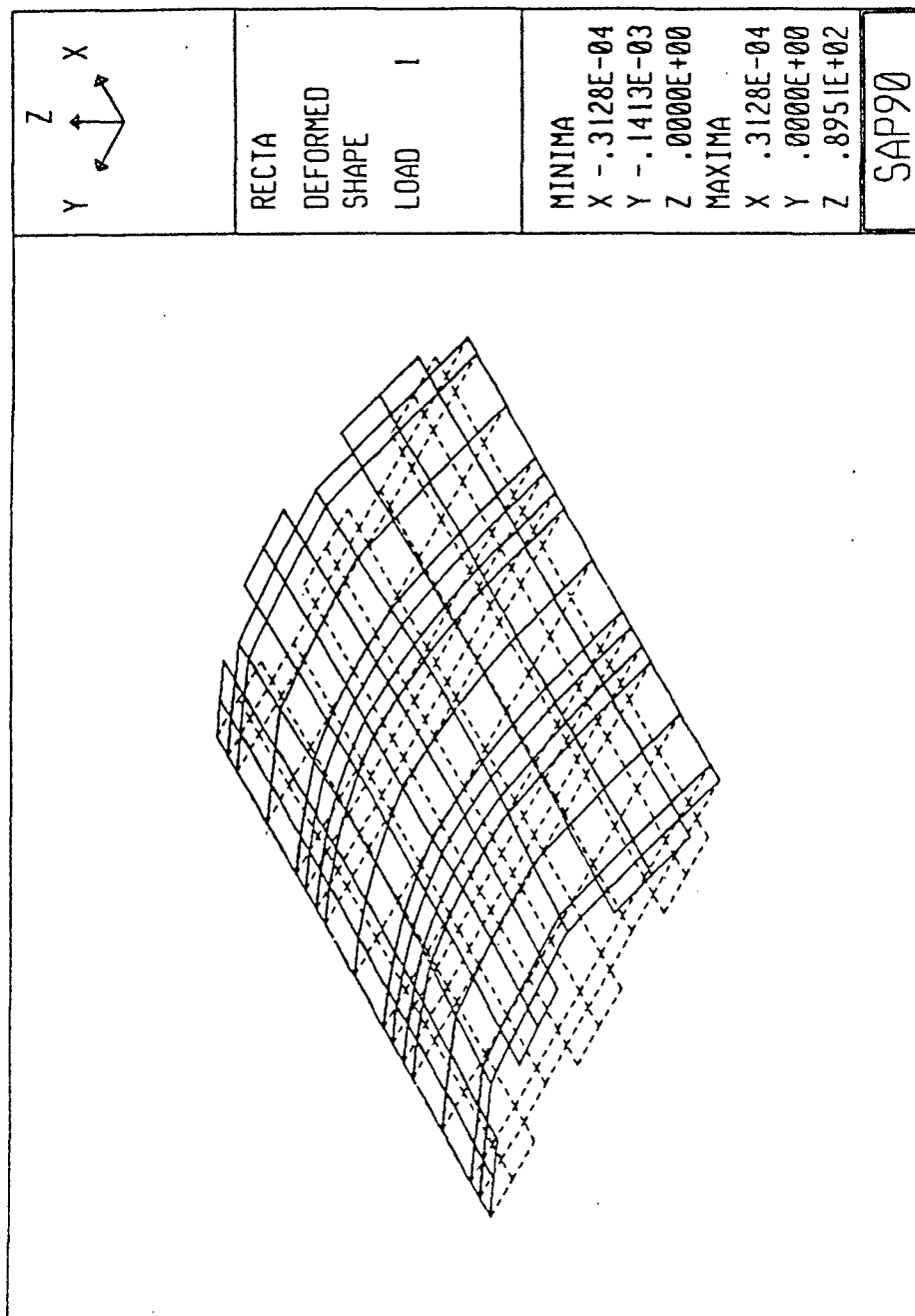
Figure 34.   Deformed Shape of Rectangular Wall Panel Configuration

Y	Z ↑ X

HEXA
DEFORMED
SHAPE
LOAD   1

MINIMA
X -.3316E-04
Y -.1720E-03
Z   .0000E+00
MAXIMA
X   .3312E-04
Y   .0000E+00
Z   .1251E+03

SAP90
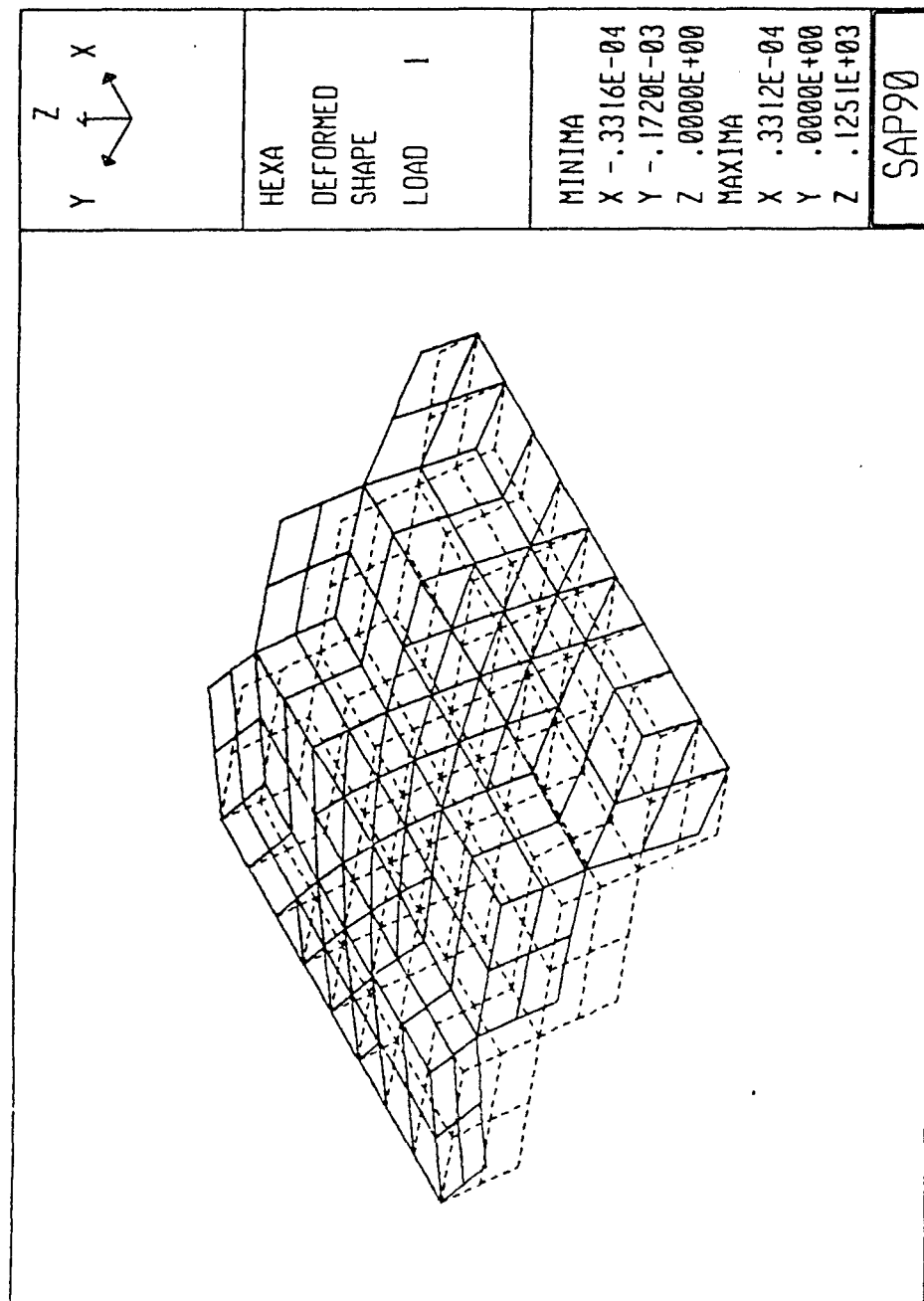
Figure 35. Deformed Shape of Hexagonal Wall Panel Configuration
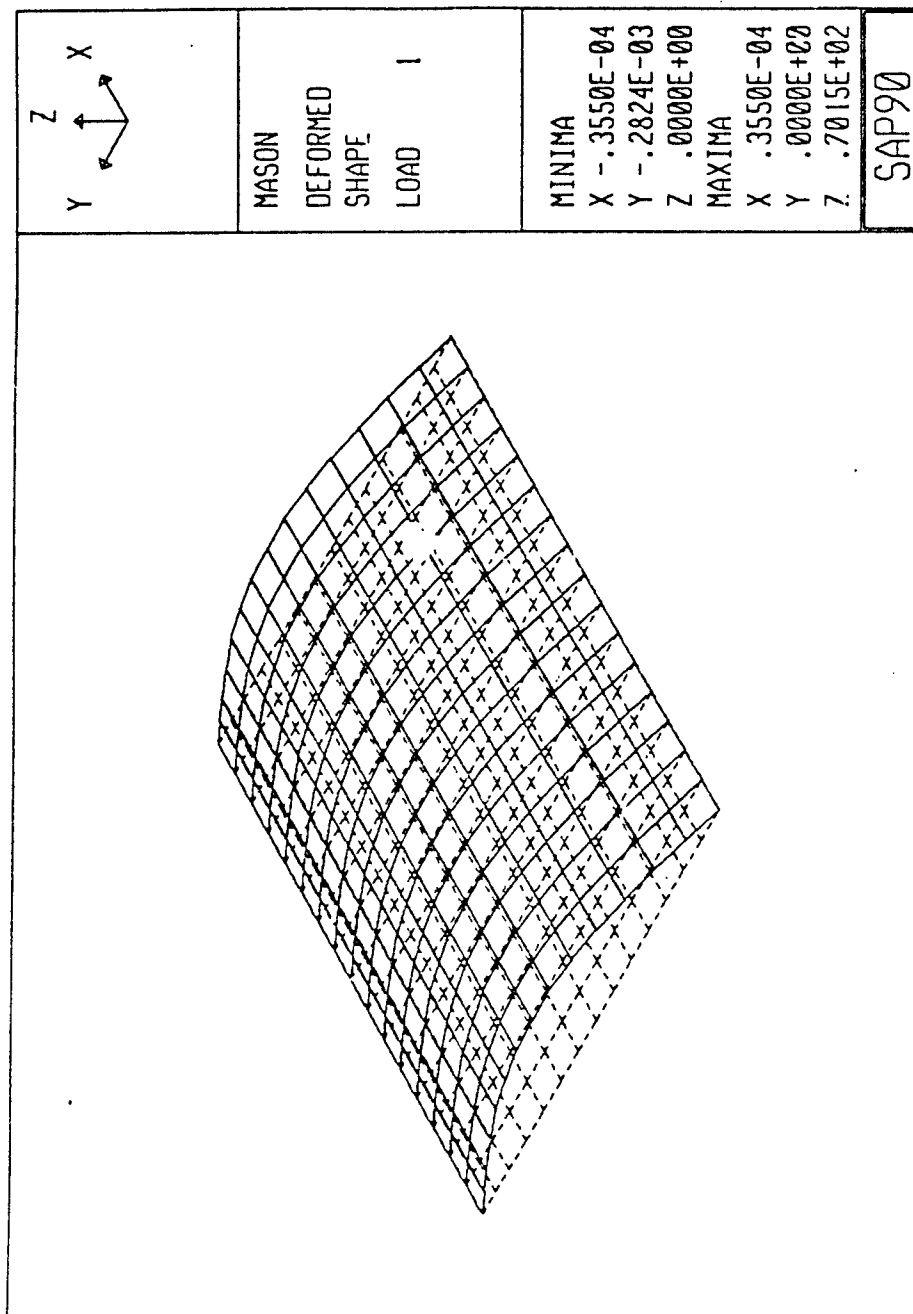
Figure 36. Deformed Shape of Masonry Wall Configuration

TABLE 3. COMPARISON OF EFFECTS DUE TO DIFFERENT PANEL CONFIGURATIONS

Panel Geometry

Parameters	Rectangular	Hexagonal	Masonry Blocks
Peak Panel Displacement (in.)	13.64	17.62	12.06
Peak Panel Velocity (fps)	96.33	87.92	86.75
Peak Panel Acceleration (g)	594.	369.	627.
Peak Joint Force (kips)	4940.	4510.	383.
Peak Moment (ft-kips)	2442.	5333.	1533.
Peak Panel Force (in-plane stretching) (lbs/in.)	91.4	128.	249.
Peak Panel Moment (out-of-plane bending and twisting) (ft-kips/in.)	187.5	685.8	257.5

Effects Due to Aspect Ratio and Panel Thickness
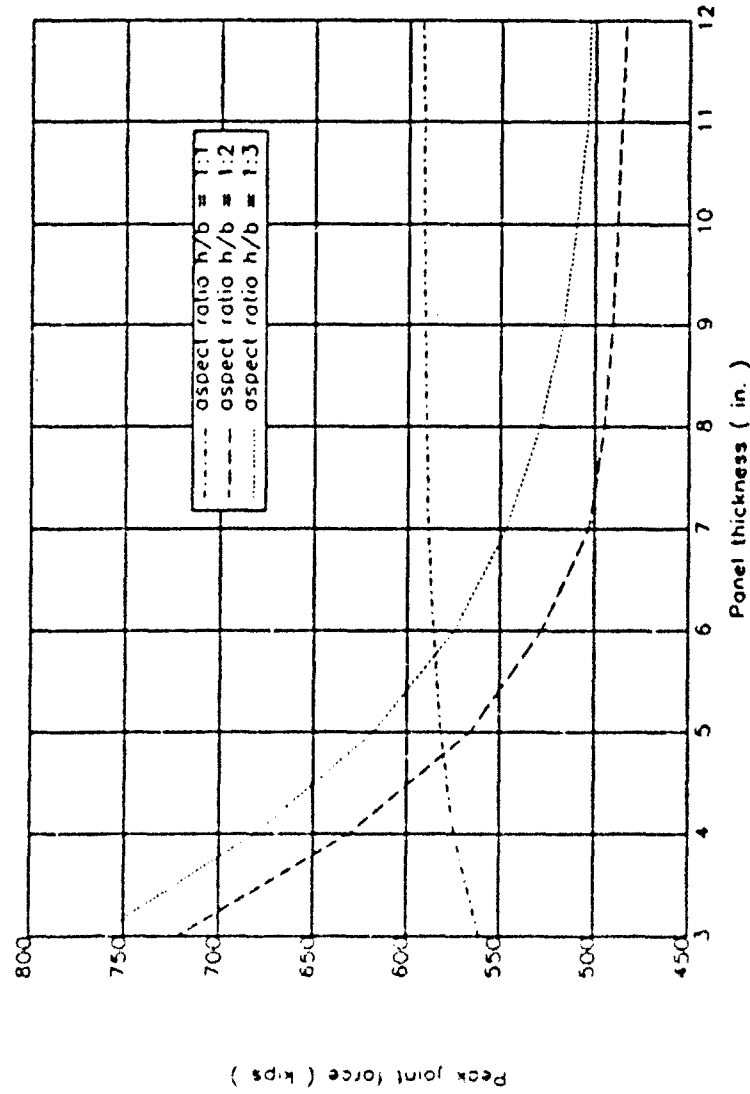
Figure 37. Effects on the Peak Connection Shear Force Due to Variation of Aspect Ratio and Panel Thickness

69

Effects Due to Aspect Ratio and Panel Thickness

Figure 38. Effects on the Peak Connection moment Due to Variation of Aspect Ratio and Panel Thickness

70

minimize the peak joint force and moment. The maximum panel displacement, velocity and acceleration of that configuration were predicted to be 13 inches, 83 fps and 370 g, respectively. Figures 39 to 41 show the influence on the maximum panel displacement, velocity and acceleration due to variations of panel's aspect ratio and thickness. A summary of the geometric effects of aspect ratio and panel thickness on the peak response parameters of a masonry wall configuration with 4-foot wide and 8-inch thick blocks is given in Table 4. It may be concluded from Table 3 that, among the geometries of wall panel, rectangular panels or blocks arranged in a masonry wall configuration would minimize the shear and moment at panel connections. In addition, it may be concluded from Table 4 that, rectangular panels or blocks, 4-foot wide, 2-foot high and 8-inch thick, are the most effective and practical configuration to minimize the shear and moment at panel connections.

Effects Due to Aspect Ratio and Panel Thickness
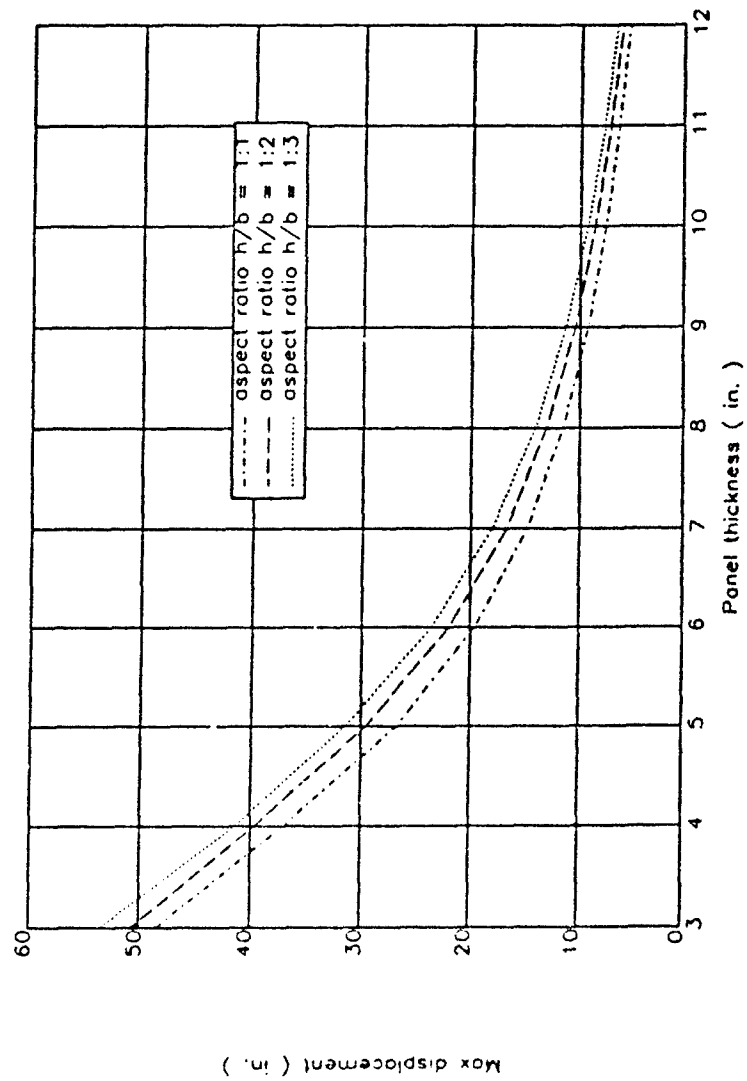
Figure 39. Effects on the Maximum Wall Panel Displacement Due to Variation of Aspect Ratio and Panel Thickness

Effects Due to Aspect Ratio and Panel Thickness
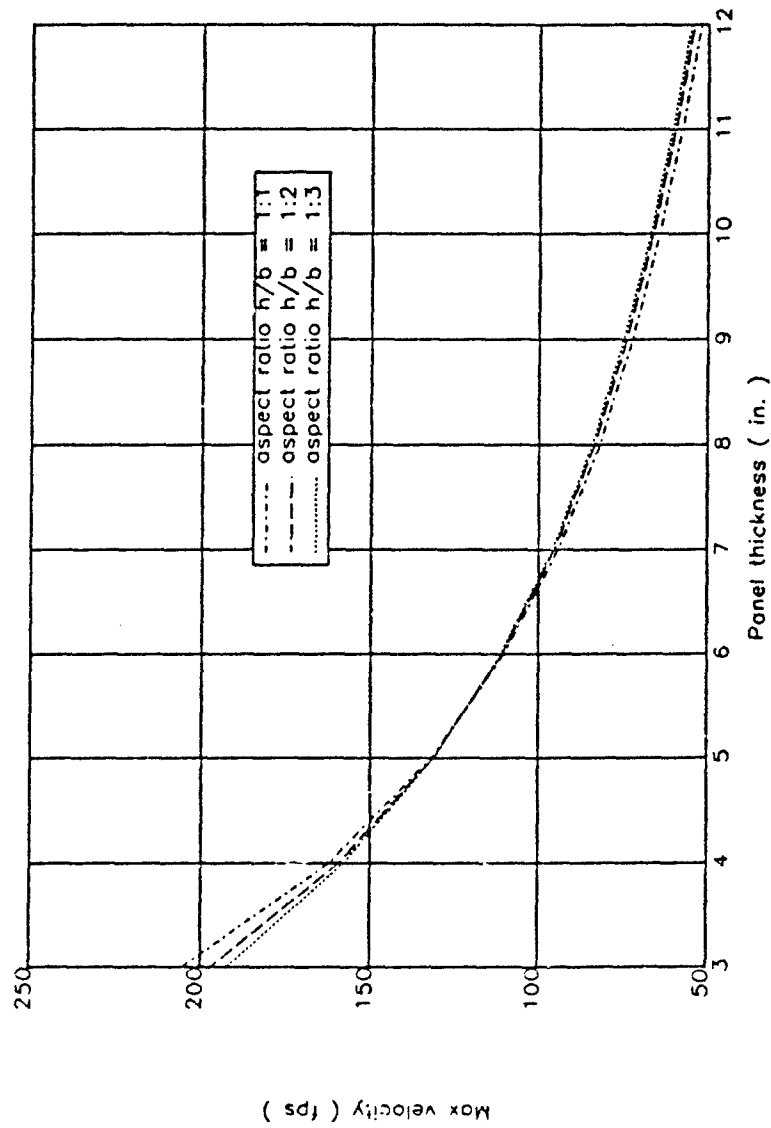
Figure 40. Effects on the Maximum Wall Panel Velocity Due to Variation of Aspect Ratio and Panel Thickness

73

Effects Due to Aspect Ratio and Panel Thickness
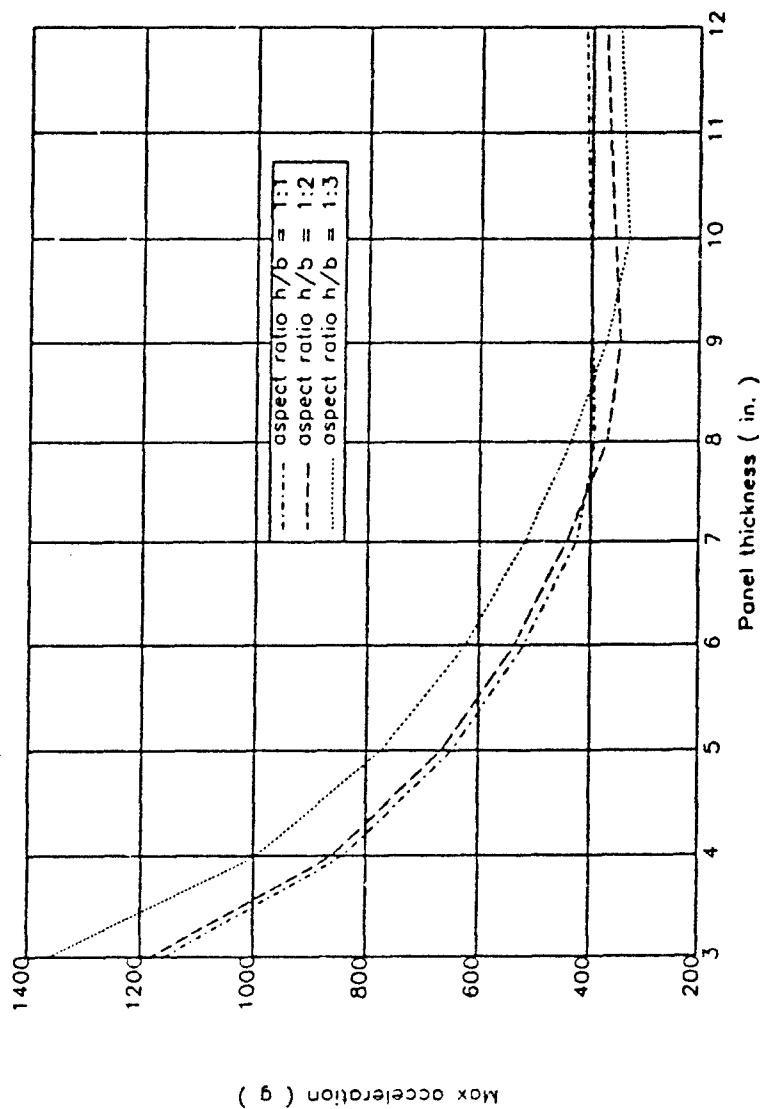
Figure 41. Effects on the Maximum Wall Panel Acceleration Due to Variation of Aspect Ratio and Panel Thickness

74

TABLE 4. COMPARISON OF EFFECTS DUE TO PANEL ASPECT RATIOS
(BLOCKS ARE 4-FOOT WIDE AND 8-INCH THICK)

	Aspect Ratio		
Parameters	1 to 1	1 to 2	1 to 3
Peak Panel Displacement (in.)	11.55	13.09	14.14
Peak Panel Velocity (fps)	81.9	83.4	84.2
Peak Panel Acceleration (g)	393.	370.	436.
Peak Joint Force (kips)	590.	495.	529.
Peak Moment (ft-kips)	2125.	2083.	2092.
Peak Panel Force (in-plane stretching) (lbs/in.)	199.	299.	399.
Peak Panel Moment (out-of-plane bending and twisting) (ft-kips/in.)	346.	344.	362.

SECTION VI

DESIGN PROCEDURES

A. DESIGN CONSIDERATIONS

Crawford, Higgins and Bultmann stated, in the 1974 version of the Air Force Design Manual, that the normal stress acting across the interface between soil and a buried structure due to ground shock can be expressed as

$$\sigma_i(t) = \sigma_{ff}(t) \pm \rho c \Delta V(t) \tag{49}$$

where $\sigma_i(t)$ is the stress acting on the structure surface perpendicular to the direction of incident wave propagation, $\sigma_{ff}(t)$ is the free-field incident stress produced by the explosion, $\Delta V(t)$ is the velocity differential between the free-field particle velocity at the location of structure surface and the velocity of the structure at the same point, and ρc is the soil acoustic impedance. The sign of the second term in Equation (49) is taken positive for incident faces and negative for reactive faces.

Drake and Rochefort(1987) showed that Equation (49) is actually a statement of continuity for both stress and displacement at the interface between the soil and structure, and the interface stress is

$$\sigma_i = \sigma_{ff} + \rho c_L (V_{ff} - \overset{\bullet}{u})$$

$$= 2\sigma_{ff} - \rho c_L \overset{\bullet}{u} \tag{50}$$

where ρ is the mass density and c_L the loading wave velocity of the soil, V_{ff} is the free-field particle velocity associated with σ_{ff}, and $\overset{\bullet}{u}$ is the velocity of the structure. They also derived the equation of motion for a single-degree-of-freedom(SDOF) structural system, and presented solutions for perfectly plastic and elastoplastic structural responses.

The one-dimensional (1D) mathematical model, described in detail in Section IV, is more general, and accommodates Equation (50) as a special case because the 1D model accounts for superposition of incident and reflected waves propagating between the explosion point and the

76

interface. The 1D model gives the same interface stress as that given by Equation (50), provided the wall panel stays in contact with the soil, and the soil medium is semi-infinite. Although the 1D model is more rigorous theoretically, it gains little advantage over Drake's model, since in reality stress waves decay rapidly with distance. Therefore, Drake's model has been adopted as the basis for guidelines and procedures for the design of modular wall panel and soil reinforcement connection systems.

Figure 42 shows the free-body diagram of a wall panel, typically attached to two layers of geogrid in a backfill. Also shown in Figure 42 are vertical reinforcing bars running through the wall panel to guide alignment of panels and to serve as shear connectors between panels. The interface pressure σ_i produced by the explosion is balanced by the inertia force of the wall panel, the tension developed in the soil reinforcement, T_g, and the shear forces developed in the reinforcing bars, F_v. Note that the confined stiffness or "pull-out resistance" of the geogrid should be used in the design calculations. Figure 43 shows different characteristics of the confined versus unconfined stiffnesses of CONWED Stratagrid^{TM} 9027(Farrag et al. 1991). The higher confined stiffness can be attributed to the composite action of geogrid with the surrounding soil.

Based on the free-body diagram, the equation of motion can be written as

$$(\rho_s Lbh)\, \ddot{u} + K(u)u = \sigma_i bh \tag{51}$$

where ρ_s is the mass density of the wall panel, b, h, and L are, respectively, the width, height, and thickness of the wall panel, and $u(t)$ is the horizontal displacement of the panel. $K(u)$ is the combined stiffness of the reinforced soil and shear connectors, which is generally a function of the wall panel displacement. Dividing both sides of Equation (51) by bh and combining it with Equation (50) yields

$$\rho_s L\, \ddot{u} + \rho c_L \dot{u} + R(u) = 2\sigma_{ff} \tag{52}$$

where $R(u)$ is the total structural resistance per unit area of wall panel, equal to $\dfrac{K(u)u}{bh}$.

Equation (52) is in the same form as the equation of motion of a damped SDOF system, except that the "damping" term results from imposing continuity of stress and displacement at the interface and not from viscous material damping. It is sometimes called radiation damping. It is
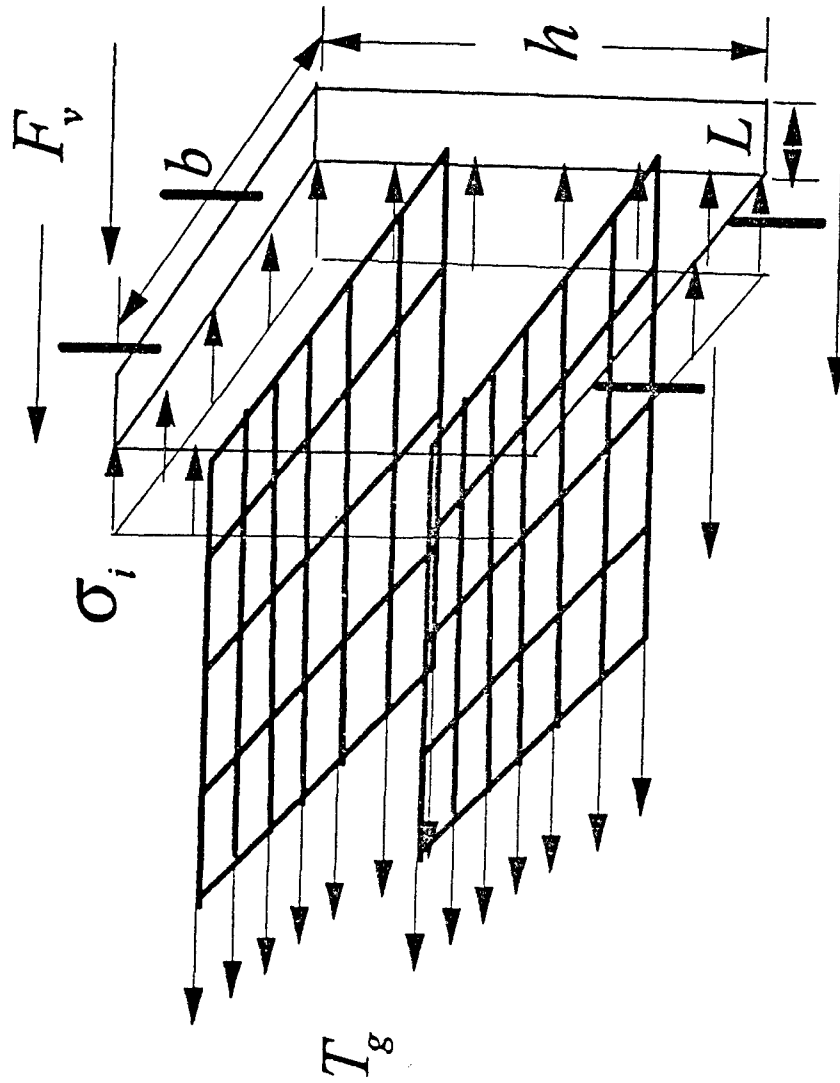
Figure 42.   Free-Body Diagram of Panel Connection System
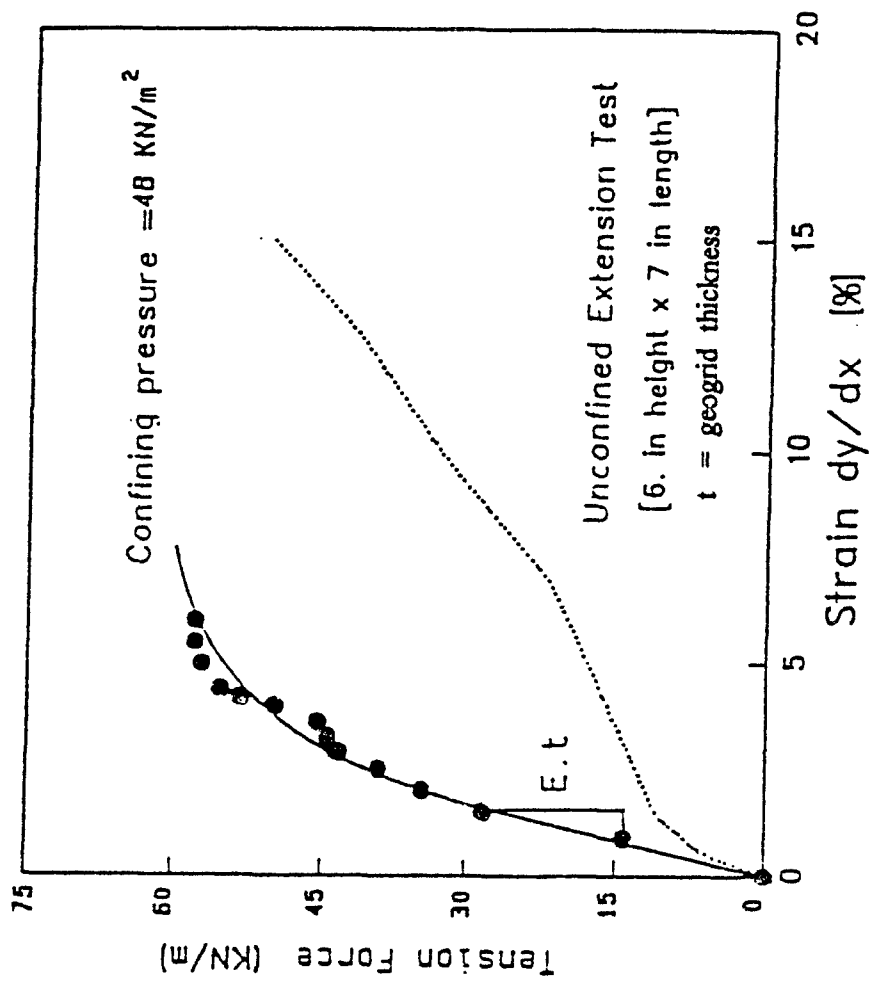
Figure 43. CONWED StratagridTM Characteristic

essential to realize that the wall panel may become separated from the soil when the deceleration of the panel caused by the structural resistance is less than the deceleration of the incident pulse. In this case, the interface stress in Equation (50) becomes zero, giving rise to a free vibration of the structural system, and Equation (52) reduces to

$$\rho_s L \ddot{u} + R(u) = 0 \tag{53}$$

The free-field normal stress in the soil, σ_{ff}, due to a given fully-contained, buried explosion at a certain standoff can be approximated by an exponentially decaying wave, such as

$$\sigma_{ff} = \sigma_o e^{-\alpha t} \tag{54}$$

where σ_o is the peak compressive normal stress and α is the normal stress decay rate. The Air Force Protective Construction Design Manual(Drake et al. 1989) contains formulas for computing these parameters for ground shocks propagating through homogeneous soil media.

The presence of geogrids in soil may significantly alter the soil's original mechanical properties. As discussed previously in Section IV, the mechanical properties of the reinforced soil can be expressed in terms of those of the soil and the geogrid, and the volume ratio of geogrid in the reinforced soil, defined as

$$V_g = \frac{A_g}{bh} \tag{55}$$

where A_g is the net cross-sectional area of geogrids attached to the wall panel. Based on the composite material assumption, the constrained modulus of the reinforced soil was shown to be

$$K_x = \frac{E_s(1-v_s)}{(1+v_s)(1-2v_s)}(1-V_g) + \frac{E_g(1-v_g)}{(1+v_g)(1-2v_g)}(V_g)$$

$$-V_g(1-V_g)\frac{\left[\dfrac{E_s v_s}{(1+v_s)(1-2v_s)} - \dfrac{E_g v_g}{(1+v_g)(1-2v_g)}\right]^2}{\dfrac{E_s(1-v_s)}{(1+v_s)(1-2v_s)}(V_g) + \dfrac{E_g(1-v_g)}{(1+v_g)(1-2v_g)}(1-V_g)} \tag{1 bis}$$

where E_s and E_g, and v_s and v_g, are, respectively, the Young's moduli and Poisson's ratios of the soil and the geogrid, and the mass density of the reinforced soil can be expressed as

$$\rho_o = \rho(1 - V_g) + \rho_g V_g \qquad (56)$$

where ρ_g is the mass density of the geogrid. Therefore, the loading wave velocity of the reinforced soil, approximated by its seismic velocity, is

$$c_L \approx \sqrt{\frac{K_x}{\rho_o}} \qquad (57)$$

The attenuation rate with range of the peak ground shock stress is controlled by irreversible crushing of the void volume within a soil matrix by the passage of the stress wave. The Air Force Protective Construction Design Manual (Drake et al. 1989) gives an estimate for this attenuation rate with range, n, in terms of the irreversible volumetric compaction behind the wave front, ε_o:

$$n = \frac{2 + \varepsilon_o}{1 - \varepsilon_o} \qquad (\text{ for most soils, } 0 < \varepsilon_o < 0.3) \qquad (58)$$

Since the irreversible compaction of soil would be reduced by the soil reinforcement, the attenuation rate with range would also be reduced and approach a limiting value of 2. These modified parameters for reinforced soil should be used to determine the peak normal stress σ_o and the decay rate α.

The structural resistance function $R(u)$ may be modeled as linearly elastic, elastoplastic, perfectly plastic or by some other appropriate model. In any event, the governing equation of motion, along with the associated interface stress expression can be solved numerically. However, the high strain rate of a structural system under a strong incident shock would produce perfectly plastic response, if the system were designed to be ductile. Furthermore, Drake and Rochefort (1987) presented a closed form solution for perfectly plastic structural response. This solution is briefly summarized herein:

The equation of motion, Equation (52), for perfectly plastic response with $R(u) = R_{max}$, becomes

$$\ddot{u} + \eta \dot{u} = \frac{1}{\rho_s L} (2\sigma_o e^{-\alpha t} - R_{max}) \qquad (59)$$

where

81

$$\eta = \frac{\rho c_L}{\rho_s L} \tag{60}$$

The velocity of the wall panel is

$$\dot{u}(t) = \frac{2\sigma_o}{\rho_s L}(\frac{1}{\eta - \alpha})(e^{-\alpha t} - e^{-\eta t}) - \frac{R_{max}}{\rho c_L}(1 - e^{-\eta t}) \tag{61}$$

the displacement of the wall panel is

$$u(t) = \frac{2\sigma_o}{\alpha \rho c_L}(1 + \frac{\alpha}{\eta - \alpha}e^{-\eta t} - \frac{\eta}{\eta - \alpha}e^{-\alpha t}) - \frac{R_{max}}{\rho c_L \eta}(\eta t - 1 + e^{-\eta t}) \tag{62}$$

and the interface stress is

$$\sigma_i(t) = 2\sigma_o(\frac{\eta}{\eta - \alpha}e^{-\eta t} - \frac{\alpha}{\eta - \alpha}e^{-\alpha t}) + R_{max}(1 - e^{-\eta t}) \tag{63}$$

Equations (61) through (63) are valid as long as the soil and the wall panel remain in contact. When the wall panel separates from the soil, the interface stress becomes zero and Equation (53) becomes effective and has to be solved numerically. If the wall panel stays in contact with soil, the connection system is termed "compression-controlled". If the wall panel separates from the soil, the connection system is termed "tension-controlled". Figure 44 shows the relationship between the ratio η / α and the ratio σ_o / R_{max}, which can be used to determine whether separation will occur.

The free-field soil displacement under the stress wave prescribed by Equation (54) is

$$u_{ff}(t) = \frac{\sigma_o}{\alpha \rho c_L}(1 - e^{-\alpha t}) \tag{64}$$

The maximum wall panel displacement, u_{max}, for a compression-controlled system is less than twice the peak free-field soil displacement. As can be deduced from Equation (62), this corresponds to the limiting case of a free soil boundary where $R_{max} \rightarrow 0$ and $\eta \rightarrow \infty$. However, a large wall panel displacement may occur for a tension controlled system. Figure 45 shows a normalized displacement envelope in terms of σ_o / R_{max} for both compression- and tension-controlled systems.

82

INTERFACE STRESS
(Perfectly plastic structural response)

Peak incident stress/Maximum resistance per unit area, σ_o/R_{max}
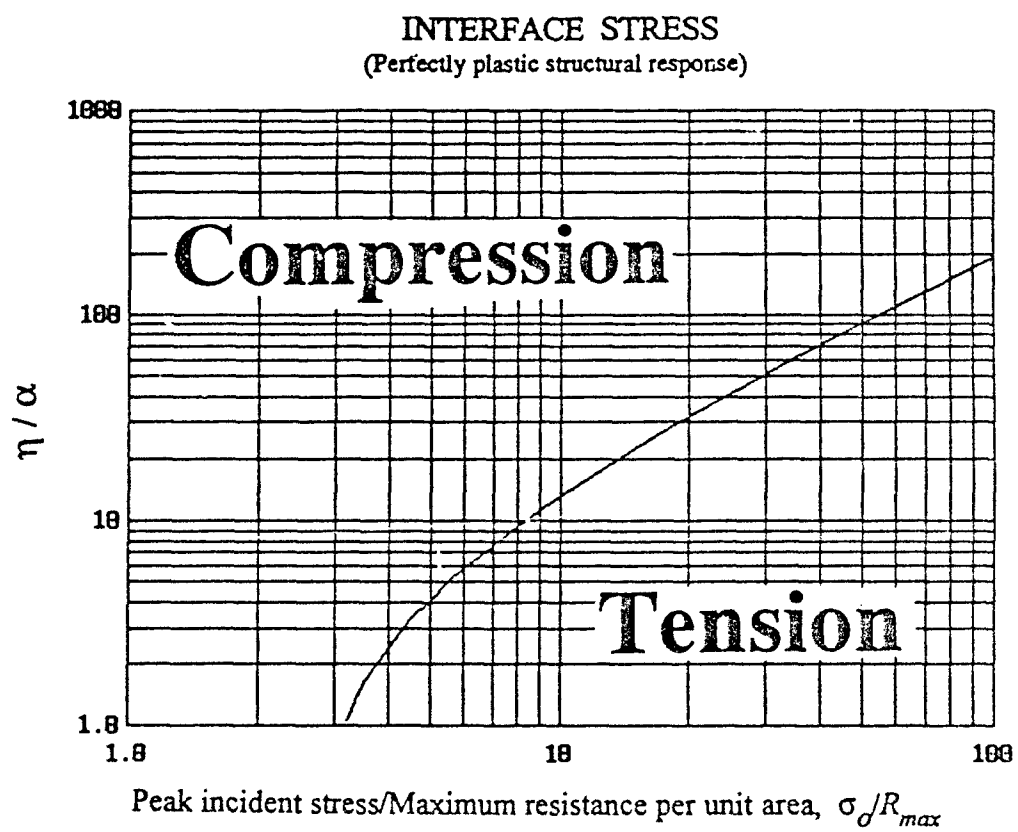
Figure 44.   Prediction of Tensile or Compressive Interface Stress

WALL PANEL DISPLACEMENT
(Perfectly plastic structural response)
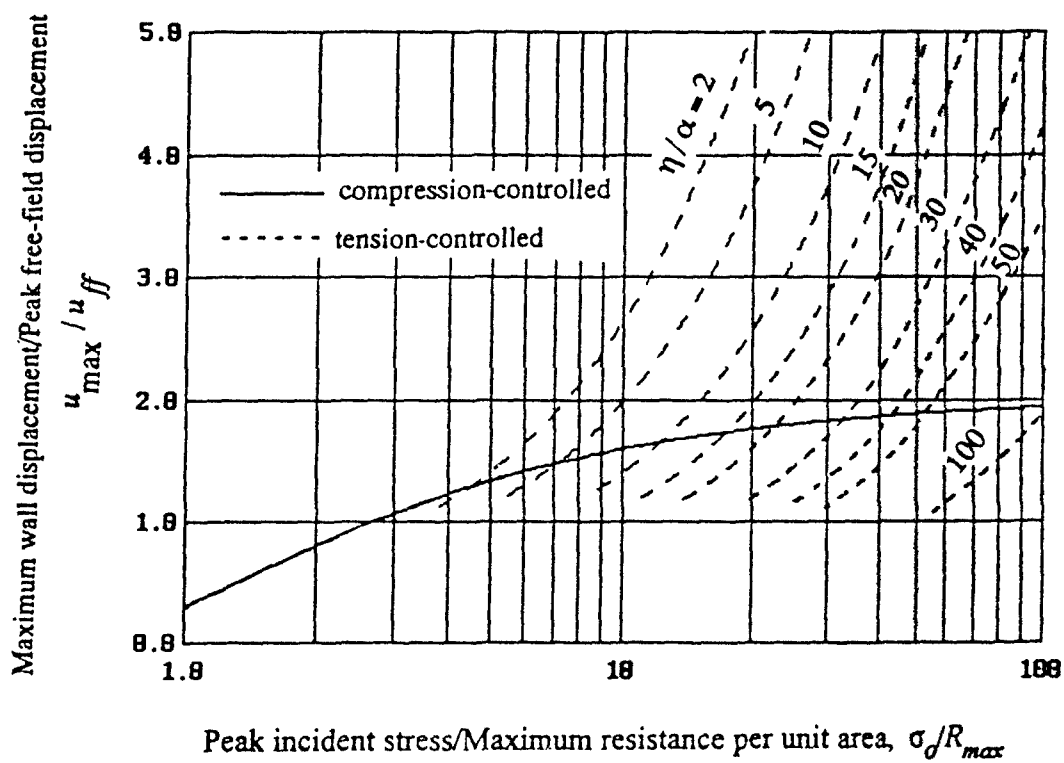
Figure 45. Ratio of Maximum Wall Displacement to Maximum
Free-field Soil Displacement

B. LIMIT ANALYSIS OF STRUCTURAL RESISTANCE

For perfectly plastic structural response, the maximum resistance per unit area of wall panel (or unit resistance), R_{max}, is the sum of the maximum unit resistance of the reinforced soil and that of the shear connectors. However, the resistance of the reinforced soil may become ineffective if sufficient embedment length is not provided to develop the required tensile force in the reinforcement. As illustrated in Figure 46(a), the interface pressure produced by the explosion is carried by both the pull-out resistance of soil reinforcement and the resistance of shear connectors; whereas in Figure 46(b), the interface pressure has to be carried entirely by the shear connectors. The maximum pull-out resistance of the reinforced soil is dictated by the following three modes of failure:

- soil shear failure in a zone away from the geogrid;
- tensile rupture in the geogrid; and
- bond failure between soil and geogrid.

The smallest value of these resistances is the maximum pull-out resistance of the reinforced soil.

Jewell et al.(1985) have identified two bond strength interaction mechanisms between soil and geogrid: skin friction on the plane surface area of the geogrid, and bearing on reinforcement surfaces normal to the direction of relative movement between the soil and the geogrid. The two effects are additive. In order to quantify the bond strength, the dimensions of a geogrid are shown in Figure 47. The width, length and thickness of a grid are denoted by b, l, and d, respectively. Discounting the aperture areas in a grid, the solid plane surface area of the grid, A_r, can be expressed as

$$A_r = \psi_s bl \tag{65}$$

where ψ_s is the solidity ratio. Similarly, the cross-sectional area available for bearing can be expressed as

$$A_b = \psi_b bd \tag{66}$$

where ψ_b is the bearing area ratio. The clear spacing between the members on which soil bearing may occur is denoted by S.

The shear stress due to skin friction depends upon the angle of skin friction, δ, and the effective normal stress between the soil and the geogrid, $\overline{\sigma}_n$. The ratio of skin friction to soil friction, δ/ϕ, for sands and silts acting on smooth metallic or concrete surfaces is typically in the

(a) Explosion within Reinforced Soil
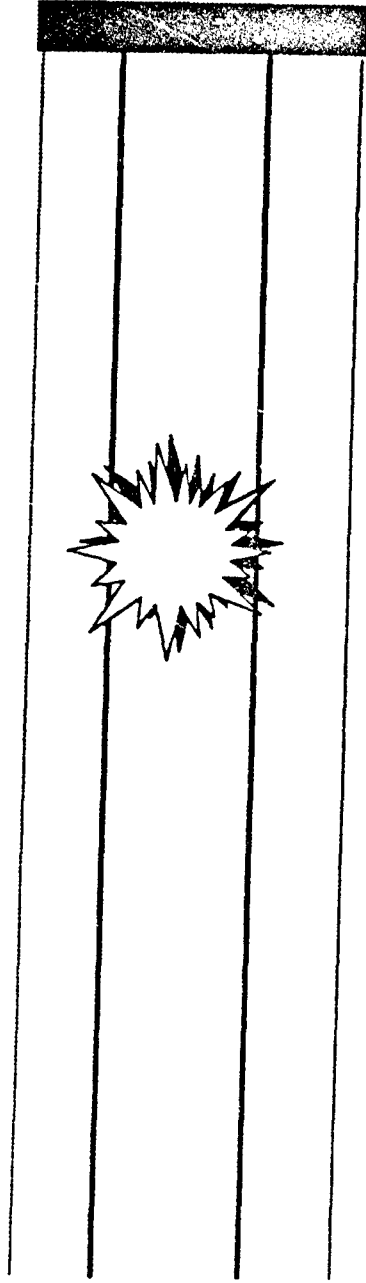
(b) Explosion beyond Reinforcement
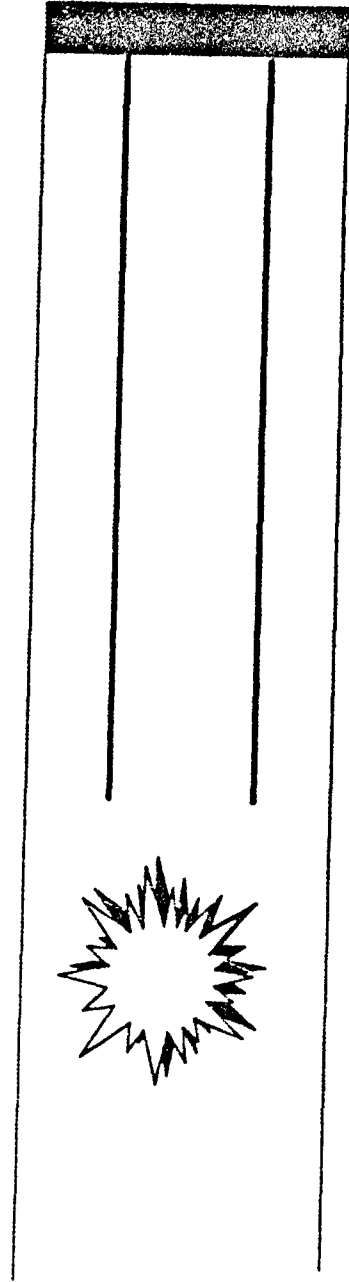
Figure 46. Explosion in a Reinforced Soil Berm

86
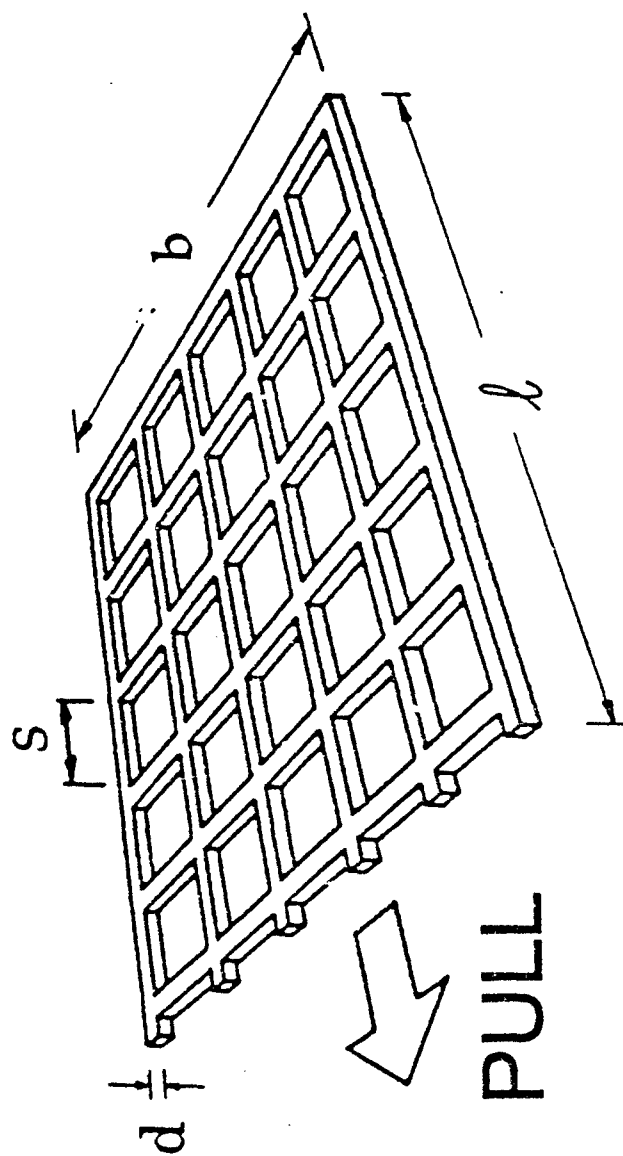
Figure 47   Geometric Parameters of a Geogrid

range of 0.5 to 0.8. The effective normal stress can be calculated from self-weight and external loadings. Therefore, the shearing resistance in double shear is

$$P_{shear} = 2(\psi_s bl)\overline{\sigma}_n \tan \delta \tag{67}$$

Jewell et al.(1985) proposed that the bearing members of a grid be modeled as a line of anchors at a spacing of S. Based on the results of an extensive investigation of horizontally loaded anchor plates by Rowe and Davis(1982), Jewell devised bounds for the effective bearing stress, $\overline{\sigma}_b$, in terms of the effective normal stress, $\overline{\sigma}_n$, and the soil friction angle, ϕ. The lower bound was derived from a punching shear failure mode of deep footings in soil,

$$\frac{\overline{\sigma}_b}{\overline{\sigma}_n} = e^{\left(\frac{\pi}{2}+\phi\right)\tan\phi} \tan\left(\frac{\pi}{4}+\frac{\phi}{2}\right) \tag{68}$$

and the upper bound is the conventional bearing stress for a footing,

$$\frac{\overline{\sigma}_b}{\overline{\sigma}_n} = e^{\pi\tan\phi} \tan^2\left(\frac{\pi}{4}+\frac{\phi}{2}\right) \tag{69}$$

It was shown that data from many pullout tests of grids and anchor plates are closely bounded by Equations (68) and (69).

Summing up the resistance from all bearing members, the total resistance can be expressed as

$$P_{bearing} = \left(\frac{l}{S}\right)\overline{\sigma}_b (\psi_b bd) \tag{70}$$

It is desirable to express the bond strength of a geogrid in terms of its gross surface area and the friction angle of the soil. Using Equations (67) and (70), the bond strength can be expressed as

$$P_{bond} = P_{shear} + P_{bearing}$$
$$= f_{bond} \times (2bl)\overline{\sigma}_n \tan \phi \tag{71}$$

where the coefficient of bond is

$$f_{bond} = \psi_s\left(\frac{\tan\delta}{\tan\phi}\right)+\left(\frac{\overline{\sigma}_b}{\overline{\sigma}_n}\right)\left(\frac{d}{S}\right)\left(\frac{\psi_b}{2\tan\phi}\right) \tag{72}$$

Soil particle size is likely to affect the bond strength for a geogrid. However, there is no test data for the influence of soil particle size on the bond strength of a grid. Jewell et al.(1985) stated

88

that, as long as the minimum aperture width of the grid is at least three times the average soil particle size, Equations (71) and (72) should provide a reasonably conservative value for design. They also suggested that the ratio of bearing spacing to grid thickness, S/d, be in the range of 10 to 20 in order to develop full bearing capacity.

C. DESIGN EXAMPLE

Given:

A bermed, aboveground shelter has an internal space 50-foot long, 22-foot wide and 16-foot high. The berm is to be built around three sides of the shelter with 1:3 slopes. The retaining walls are to be built with precast concrete panels connected to geosynthetic grids in the soil backfill. Soil backfill is dry sand with the following properties:

Dry unit weight = 105 pcf

Seismic velocity = 1600 fps

A weapon having a net explosive weight of 242 pounds of TNT is assumed to be detonated at a distance of 10 feet from a side wall, at a depth of burial of 8 feet in a berm.

Required:

Design a reinforced soil system, using wall panels with geogrids and shear connectors, to survive the given threat. Assume the failure criterion for the connection system is 12 inches of wall panel displacement.

Design procedures:

Extensive three-dimensional (3D) finite element analyses using SAP90^{TM} have been conducted to study the geometric effects of different wall panel configurations on the structural behavior of the connection system. Rectangular and hexagonal wall panels commonly used in highway construction, and a "masonry wall" type of construction were studied in detail. A wall segment, 16-foot high by 16-foot wide, built with different wall panel configurations but with the same soil reinforcement was employed for the parametric studies. The results of these parametric studies were summarized in Section V. It was concluded that using 4-foot wide, 2-foot high, 8-inch thick wall panels or blocks, arranged in a masonry wall configuration, would minimize the joint forces and consequently maximize the survivability of the wall.

89

Due to the high strain rate from a ground shock, an ideal geogrid should posses high tensile modulus, high tensile and impact strength, but most importantly, high ductility. Most commercially available geogrids are made of either high-density polyethylene (HDPE) or polyprepylene (PP). Some mechanical properties of several polymers at room temperature are given in Table 5.

McGown et al.(1985) conducted constant strain rate tests to determine the load-strain-time behavior of TENSAR™ geogrids. The influence of temperature on the strength parameters of these geogrids was also evaluated. Based on the test data, TENSAR™ SR2 was chosen for this design example. Some dimensional terminology for this geogrid is shown in Figure 48 with numerical values given in Table 6. In field practice, the geogrids are rolled in a direction parallel to the ribs. The bars provide the anchorage when the geogrid is placed in the backfill.

Using the above information, a step-by-step design methodology is illustrated herein:

Step 1. Determine the volume ratio of geogrid in the reinforced soil.

The dimensions of wall panels are: $b = 4$ feet, $h = 2$ feet and $L = 8$ inches. There are 44 ribs per meter along the width of geogrids. If each panel is connected to two layers of geogrids, the net cross-sectional area of the geogrids per panel, considering only the ribs, is

$$A_g = 2 \times \frac{(5.72 \times 1.34)}{(25.4)^2} \times \left(\frac{44}{100} \times 30.48 \times 4 \right)$$

$$= 1.27 \text{ in.}^2$$

The volume ratio of geogrids in the reinforced soil is

$$V_g = \frac{1.27}{4 \times 2 \times (12)^2} = 0.0011 = 0.11\%$$

Step 2. Determine the peak value σ_o and the decay rate α of the free-field normal stress in the reinforced soil due to the given explosion.

Since the soil is very lightly reinforced, the mass density and the loading wave velocity of the soil are not affected by the presence of the geogrids. Using Equation (V-7) in Section V of the 1989 version of the Air Force Protective Construction Design Manual:

90

TABLE 5. ROOM TEMPERATURE MECHANICAL PROPERTIES OF SOME COMMON POLYMERS

Material	Specific Gravity	Tensile Modulus [psi × 10^5 (MPa × 10^2)]	Tensile Strength [psi × 10^3 (MPa)]	Elongation at Break (%)	Impact Strength (ft-lb/in.)[a]
Polyethylene (low density)	0.917–0.932	0.25–0.41 (1.7–2.8)	1.3–2.1 (9.0–14.5)	100–650	No break
Polyethylene (high density)	0.952–0.965	1.55–1.58 (10.6–10.9)	3.2–4.5 (22–31)	10–1200	0.4–4.0
Polyvinyl chloride	1.30–1.58	3.5–6.0 (24–41)	6.0–7.5 (41–52)	40–80	0.4–20
Polytetrafluoroethylene	2.14–2.20	0.58–0.80 (4.0–5.5)	2.0–5.0 (14–34)	200–400	3
Polypropylene	0.90–0.91	1.6–2.3 (11–16)	4.5–6.0 (31–41)	100–600	0.4–1.0
Polystyrene	1.04–1.05	3.9–4.8 (23–33)	5.2–7.5 (36–52)	1.0–2.5	0.35–0.45
Polymethyl methacrylate	1.17–1.20	3.5–4.5 (22–31)	7.0–11.0 (48–76)	2–10	0.3–0.6
Phenol-formaldehyde	1.24–1.32	4.0–7.0 (28–48)	5.0–9.0 (34–62)	1.5–2.0	0.24–4.0
Nylon 6,6	1.13–1.15	—	11.0–12.0 (76–83)	60–300	0.8–2.1
Polyester (PET)	1.34–1.39	4.0–6.0 (28–41)	8.5–10.5 (59–72)	50–300	0.25–0.65
Polycarbonate	1.20	3.5 (24.0)	9.5 (66)	110	16

[a] 1/8 in. (3.2mm) thick specimen.
Source: Modern Plastics Encyclopedia 1985–1984. Copyright 1985, McGraw-Hill Inc. Reprinted with permission.
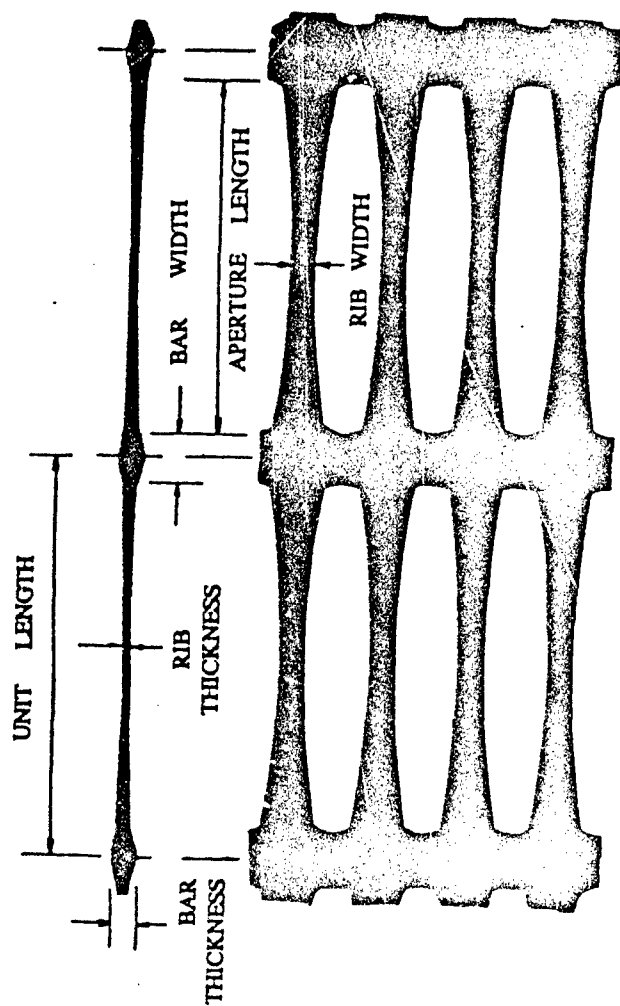
Figure 48. Dimensional Terminology for TENSAR™ SR2

92

TABLE 6. DIMENSIONS OF TENSAR™ SR2

Product Width	1000 mm
Number of Ribs	44 per meter
Aperture Length	90.73 mm
Bar Width	12.69 mm
Bar Thickness (max.)	4.56 mm
(min.)	4.36 mm
Rib Thickness	1.34 mm
Rib Width	5.72 mm
Mass per unit area	971.6 g/m^2

$$\alpha \approx \frac{c}{R} = \frac{1600}{10} = 160 \ sec.^{-1}$$

$$\rho_o = \frac{\gamma_s}{g} = \frac{105}{32.2} = 3.26 \ \frac{lb \cdot sec^2}{ft^4}$$

$W = (242)(0.73) = 177$ *pounds of C-4* (from Table V-2 of the Air Force Design Manual)

The ground shock coupling factor $f = 1$ for $\dfrac{d}{W^{1/3}} = \dfrac{8}{(177)^{1/3}} = 1.42$ ft/lb$^{1/3}$. The

attenuation coefficient n is estimated to be 2.3. The particle velocity is computed according to Equation (V-11),

$$V_o = f \times 160 \times \left(\frac{R}{W^{1/3}} \right)^{-n} = 1 \times 160 \times \left(\frac{10}{177^{1/3}} \right)^{-2.3} = 42 \ fps$$

For sand, $k = 1$, and from Table V-1 of the Air Force Design Manual, $S = 3$. The loading wave velocity of the reinforced soil is computed according to Equation (V-9),

$$c_L = kc + SV_o = 1 \times 1600 + 3 \times 42 = 1726 \ fps$$

and the peak free-field normal stress is computed according to Equation (V-10),

$$\sigma_o = \rho_o c_L V_o = f \times \rho_o c_L \times \frac{160}{144} \times \left(\frac{R}{W^{1/3}} \right)^{-n}$$

$$= 1 \times 3.26 \times 1726 \times \frac{160}{144} \times \left(\frac{10}{177^{1/3}} \right)^{-2.3} = 1657 \ psi$$

Step 3. Conduct limit analyses of the maximum pull-out resistance of reinforced soil.

Requirements for minimum embedment length and maximum vertical spacing of geogrid layers have been developed based on slope stability by Christopher et al. (1990) and Jewell (1990). However, a simple and conservative rule-of-thumb is that the minimum embedment length of geogrid layers equals the wall height, so $l = 16$ feet is used for preliminary design. The

vertical spacing between geogrid layers is 1 foot. The maximum pull-out resistance is the smallest of the following three values:

3(a) Shear failure in soil in a zone away from the geogrids

There are two planes of direct shear failure associated with each wall panel, extending from the wall panel surface to the end of the geogrid. Assuming the critical friction angle of the soil to be 32.5^o, the ultimate shear resistance is

$$P_{soil} = 2 \times bl \times \overline{\sigma}_n \tan \phi = 2 \times 4 \times 16 \times (105 \times 8) \times \tan(32.5^o) = 68500 \ pounds$$

3(b) Tensile rupture in the geogrids

McGown et al.(1985) reported that at a temperature of 20^oC, and a strain rate of 20% per minute, the tensile strength of SR2 is 84 kN/m (5760 lb/ft). Thus, the ultimate tensile strength of the two geogrids is

$$T_g = 2 \times 4 \times 5760 = 46000 \ pounds$$

3(c) Bond Failure between soil and geogrid

In order to use Equations (71) and (72) to determine the bond strength between soil and geogrids, some geometric parameters of the geogrids need to be determined using Table 6 and Figure 48. The bearing spacing between the bars, S, is equal to the aperture length:

$$S = 90.73 \ mm$$

and the ratio of bearing spacing to average bar thickness is

$$\frac{S}{d} = \frac{90.73}{4.46} = 20.34, \ \text{which would allow full development of the geogrid's bearing capacity.}$$

The clear spacing between the ribs can be computed as

$$\frac{1000 - 44 \times 5.72}{44} = 17 \ mm$$

The unit length of this geogrid is 90.73 + 12.69 = 103.42 mm, and the solidity ratio of the geogrid can be determined based on a unit length,

$$\psi_s = 1 - \frac{44 \times 17 \times 90.73}{1000 \times (12.69 + 90.73)} = 0.34$$

The bearing ratio is determined from the rib clear spacing and the bar thickness,

95

$$\psi_b = \frac{4.46 \times (44 \times 17)}{4.46 \times 1000} = 0.748$$

The ratio of the geogrid skin friction angle to the soil internal fricition angle is approximately $\delta/\phi \approx 0.6$, which is insensitive to soil reinforcement type and the overburden stress. Using Equation (68) along with the geometric parameters, the coefficient of bond given by Equation (72) is

$$f_{bond} = 0.34 \left(\frac{\tan 19.5^o}{\tan 32.5^o} \right) + 7.12 \times \frac{1}{20.34} \times \left(\frac{0.748}{2 \tan 32.5^o} \right) = 0.39,$$

and the bond strength given by Equation (71) is

$$P_{bond} = 0.39 \times (2 \times 4 \times 16) \times (105 \times 8) \times \tan 32.5^o = 26700 \ pounds$$

The smallest value obtained from steps 3(a), 3(b) and 3(c), 26700 *pounds*, is the maximum pull-out resistance of the reinforced soil.

Step 4. Conduct limit analyses of the maximum resistance of shear connectors.

Vertical steel reinforcing bars should run continuously from floor to roof through the wall panels. These reinforcing bars will serve as guides for wall panel alignment and as shear connectors. The ground shock pressure on a wall panel would be resisted by the "dowel action" of the reinforcing bars. The shear forces developed in the reinforcing bars will transmit into bearing pressure in the concrete wall panel, causing tensile and shear stresses in the concrete and subsequent splitting of the concrete along the bars. As a result, the maximum resistance of the reinforcing bars is the smaller of the following two modes of failure:

4(a) Shear failure of reinforcing bars around the perimeter of wall panel

If each wall panel is reinforced with two #5 bars having a minimum yield strength of 40,000 psi, the maximum shear resistance can be estimated using the "shear-friction" concept developed in reinforced concrete design (ACI 318-88):

$$F_v = A_{vf} f_y \mu = (4 \times 0.31) \times 40000 \times 0.6 = 29800 \ pounds$$

4(b) Failure of concrete wall panel

Assuming the concrete strength is $f_c' = 5000$ psi, the dowel force which would cause tearing in the concrete along the reinforcing bar is

$$F_d = 2Lhv_c = 2 \times 8 \times (2 \times 12) \times (2 \times \sqrt{5000}) = 54300 \ pounds$$

where v_c, the nominal shear strength of the concrete, is $2\sqrt{f_c'}$.

Therefore, the maximum shear resistance of the reinforcing bars is 29800 *pounds*.

Step 5. Determine the maximum wall panel displacement due to the given threat

The maximum wall panel displacement due to the given explosion can be easily determined using Figures 44 and 45 along with the value of η / α and σ_o / R_{max}. If the unit weight of the concrete wall panels is $\gamma_c = 145$ *pcf*, η is computed using Equation (60),

$$\eta = \frac{\rho c_L}{\rho_s L} = \frac{105 \times (1726 \times 12)}{145 \times 8} = 1875 \ sec^{-1}$$

and

$$\frac{\eta}{\alpha} = \frac{1875}{160} \approx 12$$

The maximum unit resistance of the wall panel and geogrid connection system is

$$R_{max} = \frac{P_{bond} + F_v}{bh} = \frac{26700 + 29800}{(4 \times 12) \times (2 \times 12)} = 49 \ psi$$

and

$$\frac{\sigma_o}{R_{max}} = \frac{1657}{49} = 34$$

Entering Figure 44, this connection system design is located in the tension-controlled zone. This means that, during the loading phase, the soil will separate from the wall panel. Using Figure 45, the ratio of maximum wall panel displacement to the peak free-field displacement is found to be approximately 3.8. The peak free-field displacement is determined using Equation (64),

$$u_{ff} = \frac{\sigma_o}{\alpha \rho c_L} = \frac{1657}{160 \times 0.000157 \times (1726 \times 12)} = 3.18 \ inches$$

97

and the maximum wall displacement is $3.8 \times 3.18 \approx 12$ *inches*

Since the maximum wall displacement is no greater than the 12-inch failure criterion, the current connection system design is acceptable. Had the maximum wall displacement exceeded 12 inches, the design would have been altered through iterations of the above steps until the design met the requirements.

Step 6. Design against breaching of reinforced concrete

Section IX of the 1989 version of the Air Force Protective Design Manual provides guidelines for determining structural element thickness and minimum standoff distance to prevent localized breaching. McVay(1988) reported that breaching is likely to occur when the scaled range, $R/W^{1/3}$, is less than 1.3 ft/lb$^{1/3}$, where R is the standoff in feet and W is the net explosive weight in pounds of TNT. The scaled range of this design example is 1.6 ft/lb$^{1/3}$.

In general, the concrete wall panels are reinforced with welded wire fabric(WWF), which is also called "mesh," made of A82 steel with a minimum yield strength of 64000 *psi*. These reinforcements are placed in the concrete parallel to the reinforcing bars and close to the concrete surface. For close-in and contact explosions, fibrous concrete may be used as an alternative.

SECTION VII

CONCLUSIONS AND RECOMMENDATIONS

A. CONCLUSIONS

Based on the results of extensive numerical analyses, a step-by-step procedure has been proposed for designing a reinforced soil and modular wall panel connection system to withstand the ground shock from a buried explosion. The design procedure consists of six major steps: (1) determine the geogrid volume ratio in the reinforced soil; (2) determine the peak value and time decay rate of the free-field normal stress in the reinforced soil due to a given explosion; (3) conduct limit analyses of the maximum pull-out resistance of the soil reinforcement; (4) conduct limit analyses of the maximum resistance of wall panel shear connectors; (5) determine the maximum wall panel displacement due to the given threat; and (6) design against breaching of a reinforced concrete wall panel. The preliminary design for an anchored wall panel and soil reinforcing system was prepared using this proposed procedure in Section VI.

The design procedure was based on the "limit state" concept, which requires determination of the peak ground shock loading as well as the ultimate resistance of the structural system. It was illustrated in Section V that no single algorithm would provide accurate ground shock predictions for homogeneous soils, let alone reinforced soil. A number of algorithms have been used to predict the peak ground shock through a reinforced sandy soil for the given design threat. The Air Force Design Manual predicted a peak free-field normal stress of 1520 psi, while the hydrodynamic code SABER-PC predicted 670 psi. For the peak wall/soil interface stress in the wall panel and reinforced soil system described in Figures 7 and 8, the 1D mathematical model predicted 1340 psi and the DYNA2D finite element model predicted 710 psi. There is significant scatter in these values. If the ground shock parameters in a homogeneous soil could be predicted accurately, however, the corresponding values for the soil with reinforcement could be derived according to stress and strain compatibility assumptions. Jewell et al.(1985) proposed a rational method to determine the ultimate pull-out resistance of a geogrid under static loading, based on the frictional and bearing interaction between the soil and the geogrid. This method has been adopted in the FHWA design guidelines for reinforced soil structures and is used herein as Step 3 of the design procedure.

99

Extensive three-dimensional (3D) finite element analyses using SAP90^{TM} have been conducted to study the geometric effects of different wall panel configurations on the structural behavior of the connection system. Rectangular and hexagonal wall panels commonly used in highway construction, and a "masonry wall" type of construction were studied in detail. A segment of a wall, 16 feet high by 16 feet wide, built with different wall panel configurations but with the same soil reinforcement was employed for the parametric studies. The results of these parametric studies were summarized in Section V. It was concluded that using 4-foot wide, 2-foot high, 8-inch thick wall panels or blocks, arranged in a masonry wall configuration, would minimize the joint forces and consequently maximize the wall's survivability. It is interesting to note that SAP90^{TM} predicted a maximum wall panel displacement of 13 inches, DYNA2D predicted 7 inches and the simplified design procedure predicted 11 inches SAP90^{TM} predicted a maximum geogrid tension of 13000 pounds and the design procedure predicted the maximum tension in each layer of geogrid to be 16750 pounds. Because of the impulsive nature of ground shock, the maximum response of the wall panel and reinforced soil system depends mainly on the capacity and rate of energy absorption and dissipation of the system. Therefore, the connection between wall panels and soil reinforcement, and soil reinforcement itself should be ductile beyond the proportional limit. Furthermore, the soil reinforcement should possess a high elastic tensile modulus to minimize the wall panel displacement.

B. RECOMMENDATIONS

The simplified design procedure proposed herein for a modular wall panel and reinforced soil connection system should be validated by conducting full-scale explosive tests or small-scale centrifuge tests. The design parameters to be varied in the tests should include panel geometry, geogrid mechanical properties, and shear connector design. These tests should be fully instrumented to provide data for design guidance. The transducers should include free-field pressure gages in soil, strain (or stress) gages on the geogrid, interface stress gages on wall panels, accelerometers on wall panels, and LVDTs to measure instantaneous, as well as permanent displacement of wall panels.

100

SECTION VIII

REFERENCES

Al-Hussaini, M., and Perry, E.B., "Field Experiment of Reinforced Earth Wall," J. of the Geotechnical Engrg. Div., ASCE, Vol.104, No.GT3, March 1978, pp.307-322.

American Concrete Institute, Building Code Requirements for Reinforced Concrete, ACI 318-88, Detroit, MI, 1988.

Andrawes, K.Z., et al., "Tension Resistant Inclusions in Soils," J. of the Geotechnical Engrg. Div., ASCE, Vol.106, No.GT12, Dec. 1980, pp.1313-1326.

Chang, J.C., and Forsyth, R.A., "Design and Field Behavior of Reinforced Earth Wall," J. of the Geotechnical Engrg. Div., ASCE, Vol.103, No.GT7, July 1977, pp.677-692.

Chang, J.C., and Forsyth, R.A., "Finite Element Analysis of Reinforced Earth Wall," J. of the Geotechnical Engrg. Div., ASCE, Vol.103, No.GT7, July 1977, pp.711-724.

Christopher, B.R., et al., Reinforced Soil Structures: Volume I. Design and Construction Guidelines, FHWA-RD-89-043, U.S. Department of Transportation, Federal Highway Administration, McLean, VA, 1990.

Crawford, R.E., Higgins, C.J., and Bultmann, E.H., The Air Force Manual for Design and Analysis of Hardened Structures, AFWL-TR-74-102, Air Force Weapons Laboratory, Kirtland AFB, NM, 1974.

de Buhan, P., et al., "Yield Design of Reinforced Earth Walls by a Homogenization Method," Geotechnique, Vol.39, No.2, 1989, pp.189-201.

Drake, J.L., and Rochefort, M.A., "Response of Buried Structure Walls to Earth Penetrating Conventional Weapons," Dynamics of Structures, ASCE, August 1987, pp.455-468.

Drake, J.L., et al., "A Simplified Method for the Prediction of the Ground Shock Loads on Buried Structures," Proc. of the 3rd Int. Symp. on the Interaction of Conventional Weapons with Structures, Manheim, W. Germany, March 9-13, 1987, pp.3-14.

Drake, J.L., et al., "Backfill Effects on Buried Structure Response," Proc. of the 4th Int. Symp. on the Interaction of Non-nuclear Munitions with Structures, Vol.2, Panama City Beach, FL, April 17-21, 1989, pp.38-43.

Drake, J.L., et al., Protective Construction Design Manual: Groundshock and Cratering, (Section V), ESL-TR-87-57, Tyndall AFB, FL, 1989.

Drake, J.L., et al., Protective Construction Design Manual: Resistance of Structural Elements, (Section IX), ESL-TR-87-57, Tyndall AFB, FL, 1989.

Farrag, K.A., Acar, Y.B., and Juran, I., In-Soil Characteristics and Interface Properties of STRATAGRID 9027, Technical Bulletin GS 101, CONWED Plastics, Roseville, MN, 1991.

Gerrard, C.M., "Reinforced Soil: An Orthorhombic Material," J. of the Geotechnical Engrg. Div., ASCE, Vol.108, No.GT11, Nov. 1982, 1460-1474.

Giroud, J.P., and Noiray, L., "Geotextile-Reinforced Unpaved Road Design," J. of the Geotechnical Engrg. Div., ASCE, Vol.107, NO.GT9, Sept. 1981, pp.1233-1254.

Goodings, D.J., and Santamarina, J.C., "Reinforced Earth and Adjacent Soils: Centrifuge Modeling Study," J. of Geotechnical Engrg., ASCE, Vol.115, No.7, July 1989, pp.1021-1025.

Haliburton, T.A., et al., "Testing of Geotechnical Fabric for Use as Reinforcement," Geotechnical Testing Journal, GTJODJ, Vol.1, Dec. 1978, pp.203-212.

Harrison, W.J., and Gerrard, C.M., "Elastic Theory Applied to Reinforced Earth," J. of the Soil Mechanics and Foundations Div., ASCE, Vol.98, No.SM12, Dec. 1972, 1325-1345.

Ingold, T.S., "Reinforced Clay Subject to Undrained Triaxial Loading," J. of Geotechnical Engrg., ASCE, Vol.109, No.5, May 1983, pp.738-744.

102

Ingold, T.S., and Miller, K.S., "Drained Axisymmetric Loading of Reinforced Clay," J. of Geotechnical Engrg., ASCE, Vol.109, No.7, July 1983, pp.883-898.

Jewell, R.A., Milligan, G.W.E., Sarsby, R.W., and DuBois, D., "Interaction Between Soil and Geogrids," Polymer Grid Reinforcement, Proceedings of a Conference sponsored by the Science and Engineering Research Council and Netlon Ltd, London, March 1984, pp.18-30.

Jewell, R.A., "Revised Design Charts for Steep Reinforced Slopes," Proceedings of a Symposium on Reinforced Embankments, Cambridge University, U.K., 1990.

Jones, R.M., Mechanics of Composite Materials, McGraw-Hill Book Company, New York, N.Y., 1975, pp.31-84.

Juran, I., and Chen, C.L., "Strain Compatibility Design Method for Reinforced Earth Walls," J. of Geotechnical Engrg., ASCE, Vol.115, No.4, April 1989, pp.435-456.

Juran, I., and Christopher, B., "Laboratory Model Study on Geosynthetic Reinforced Soil Retaining Walls," J. of Geotechnical Engrg., ASCE, Vol.115, No.7, July 1989, pp.905-926.

Juran, I., et al., "Strain Compatibility Analysis for Geosynthetics Reinforced Soil Walls," J. of Geotechnical Engrg., ASCE, Vol.116, No.2, Feb. 1990, pp.312-329.

Juran, I., et al., "Modeling and Simulation of Load Transfer in Reinforced Soils: Part 1," Int. J. of Numerical and Analytical Methods in Geomechanics, Vol.12, 1988, pp.141-155.

Juran, I., et al., "Numerical Analysis of the Response of Reinforced Soils to Direct Shearing: Part 2," Int. J. of Numerical and Analytical Methods in Geomechanics, Vol.12, 1988, pp.157-171.

Lee, K.L., et al., "Reinforced Earth Retaining Walls," J. of the Soil Mechanics and Foundation Div., ASCE, Vol.99, No.SM10, Oct. 1973, pp.745-764.

Leshchinsky, D., and Reinschmidt, A.J., "Stability of Membrane Reinforced Slopes," J. of Geotechnical Engrg., ASCE, Vol.111, No.11, Nov. 1985, pp.1285-1300.

Leshchinsky, D., and Boedeker, R.H., "Geosynthetic Reinforced Soil Structures," J. of Geotechnical Engrg., ASCE, Vol.115, No.10, Oct. 1989, pp.1459-1478.

McGown, A., Andrawes, K.Z., Yeo, K.C., and DuBois, D., "The Load-strain-time Behavior of Tensar Geogrids," Polymer Grid Reinforcement, Proceedings of a Conference sponsored by the Science and Engineering Research Council and Netlon Ltd, London, March 1984, pp.11-17.

McVay, M.K., "Spall Damage of Concrete Structures," Technical Report SL-88-22, U.S. Army Waterways Experiment Station, Vicksburg, MS, 1988.

O'Rourke, T.D., et al., "Shear Strength Characteristics of Sand-Polymer Interfaces," J. of Geotechnical Engrg., ASCE, Vol.116, No.3, March 1990, pp.451-469.

Palmeira, E.M., and Milligan, G.W.E., "Scale and Other Factors Affecting the Results of Pull-out Tests of Grids Buried in Sand," Geotechnique, Vol.39, No.3, 1989, pp.511-524.

Raudanski, E., Eytan, R., and Sweiry, G.(1990), "Reinforced Soil Ammunition Magazine, Full-scale Tests-1990, Testing Program," Headquarters Israeli Air Force Civil Engineering Division, Engineering and Products Branch.

Reid, R.A., "Reinforced-Soil Munition Bunker Test," The Military Engineer, Vol.82, No.537, August 1990, pp.51-52.

Reid, R.A., "Full-scale Test of a Reinforced Soil Bunker," Proceedings of the Fifth International Symposium on the Interaction of Non-nuclear Munitions with Structures, Mannheim, Germany, April 22-26, 1991, pp.12-16.

Richardson, G.N., and Lee, K.L., "Seismic Design of Reinforced Earth Walls," J. of the Geotechnical Engrg. Div., ASCE, Vol.101, No.GT2, Feb. 1975, pp.167-188.

Richardson, G.N., et al., "Seismic Testing of Reinforced Earth Walls," J. of the Geotechnical Engrg. Div., ASCE, Vol.103, No.GT1, Jan. 1977, pp.1-17.

Romstad, K.M., et al., "Integrated Study of Reinforced Earth - I: Theoretical Formulation," J. of the Geotechnical Engrg. Div., ASCE, Vol.102, No.GT5, May 1976, pp.457-471.

Rowe, R.K., and Davis, E.H., "The Behavior of Anchor Plates in Sand," Geotechnique, 32, No.1, pp.25-41, 1982.

Rowe, R.K., "Reinforced Embankments: Analysis and Design," J. of Geotechnical Engrg., ASCE, Vol.110, NO.2, Feb. 1984, pp.231-246.

Salamon, M.D.G., "Elastic Moduli of a Stratified Rock Mass," Int. J. of Rock Mechanics and Mineral Sciences, Vol.5, pp.519-527, 1968.

Sawicki, A., "Plastic Limit Behavior of Reinforced Earth," J. of Geotechnical Engrg., ASCE, Vol.109, No.7, July 1983, pp.1000-1005.

Schlosser, F., and Long, N.T., "Recent Results in French Research on Reinforced Earth," J. of the Construction Div., ASCE, Vol.100, No.CO3, Sept. 1974, pp.223-237.

Seed, H.B., and Idriss, I.M., "Soil Moduli and Damping Factors for Dynamic Response Analyses," Report No. EERC 70-10, Univ. of Calif., Berkeley, CA, Dec. 1970.

Segrestin, P., and Bastick, M.J., "Seismic Design of Reinforced Earth Retaining Walls - The Contribution of Finite Elements Analysis," Int. Geotechnical Symposium on Theory and Practice of Earth Reinforcement, Fukuoka, Japan, Oct. 5-7, 1988, pp.577-582.

Shen, C. K., et al., "Integrated Study of Reinforced Earth - II: Behavior and Design," J. of the Geotechnical Div., ASCE, Vol.102, No.GT6, June 1976, pp.577-590.

Tumay, M.T., "Metal Versus Nonwoven Fiber Fabric Earth Reinforcement in Dry Sands: A Comparative Statistical Analysis of Model Tests," Geotechnical Testing Journal, GTJODJ, Vol.2, No.1, March 1979, pp.44-56.

Westergaard, H.M., "A Problem of Elasticity Suggested by a Problem in Soil Mechanics," Mechanics of Solids, Timoshenko 60th Anniversary Vol.1, MacMillan & Co., New York, N.Y., 1938, pp.268-277.

Westine, P.S., "Ground Shock from the Detonation of Buried Explosives," Journal of Terramechanics, Vol.15, No.2, 1978, pp. 69-79.

Westine, P.S., and Friesenhahn, G.J., "Ground Shock Loads from Buried Bomb and Ordnance Detonations," AFATL-TR-82-19, Air Force Armament Laboratory, Armament Division, Eglin Air Force Base, FL , 1982.

Williams, N.D., and Houlihan, M.F., "Evaluation of Interface Friction Properties Between Geosynthetics and Soils," a paper presented at Geosynthetics '87 Conference, New Orleans, LA, 1987, pp.616-627.

Windham, J.E., Zimmerman, H.D., and Ito, Y.M., "Analysis of Ground Shock Measurements from Shallow-Buried MK83 Bombs," Headquarters, U.S. Army Corps of Engineers, Washington, D. C., April 1991.

Wu, J.T.H., "Measuring Inherent Load-Extension Properties of Geotextiles for Design of Reinforced Structures," Geotechnical Testing Journal, GTJODJ, Vol.14, No.2, June 1991, pp.157-165.

Yang, Z., "Strength and Deformation Characteristics of Reinforced Sand," A Ph.D. Dissertation, Univ. of California, Los Angeles, 1972.

Yogendrakumar, M., et al., "Dynamic Response Analysis of Reinforced-Soil Retaining Wall," J. of Geotechnical Engrg., ASCE, Vol.118, No.8, August 1992, pp.1158-1167.